



**NTNU – Trondheim**  
Norwegian University of  
Science and Technology

# Consolidation Settlement of Suction Caissons

**Anders Ulvestad**

Civil and Environmental Engineering

Submission date: June 2012

Supervisor: Steinar Nordal, BAT

Norwegian University of Science and Technology  
Department of Civil and Transport Engineering





Report Title: <b>Consolidation Settlement of Suction Caissons</b>	Date: 11.06.12		
	Number of pages (incl. appendices): 119		
	Master Thesis	x	Project Work
Name: Anders Ulvestad			
Professor in charge/supervisor: Steinar Nordal			
Other external professional contacts/supervisors: Erik Tørum, Joar S. Gloppestad			

Abstract:

Consolidation settlement analysis is an essential part of the design process for suction caissons. However it is a complex task since soil volume important for settlement analyses is directly affected by the installation process. Consolidation settlements have been found to be the critical design criterion in several subsea developments, adequate and correct analysis is therefore vital.

The FEM code PLAXIS has been used to evaluate the reconsolidation process after completed installation of the suction caisson. Emphasize has been placed on studying the shear strength increase with time along the skirt walls. During consolidation dissipation of excess pore pressures result in higher effective stresses. Consequently the modeled undrained shear strength increases. However the increase is small compared to the expected increase in shear strength due to the set-up phenomenon. To account for the deviation an adjusted simulation procedure incorporating incremental increase of friction angle in the interface zones has been suggested. The results were found to be reasonable with respect to final consolidation settlements and development of mobilized shear strength with time.

Adequate modeling of the changes in the interface zones adjacent to the caisson walls during consolidation is vital for correct prediction of long term settlements. Modeled undrained shear strength with time have huge impact on the analysis results due to different mobilization of the surrounding soil. Appropriate evaluation of soil structure interaction is essential to assess the reliability of the analysis. Taking into account changes to the soil volume important for settlement analysis is also vital.

A simple physical model test has been performed. Due to delays and relatively short test period the results were inconclusive. However the importance of considering short term set-up effects has been underlined by recorded resistance and physical observations in the field.

Keywords:

1. Suction caissons
2. Consolidation
3. Undrained shear strength
4. Model test

\_\_\_\_\_  
(signature)



## Geotechnical Engineering Master Thesis, Spring 2012

### Master thesis description for **Anders Ulvestad**

#### Master thesis title: **Consolidation Settlement of Suction Caissons**

##### **Background**

Suction caissons are an important foundation solution in several offshore projects. Skirted foundations deliver viable and attractive qualities with respect to capacity and cost efficiency.

Finite element analysis for design of suction caissons has become an important tool in later years. Consolidation settlement analysis is an essential part of the design process. However, evaluating consolidation settlements for suction caissons is a complex task since some of the soil volume important for settlement analyses are directly affected by the installation process. Soil strength and stiffness are changed by self-weight penetration and penetration by suction and possibly also by irregular skirt geometries with inside stiffeners. Additionally, there is a general lack of in-situ monitoring records from installed suction caissons which could be used for calibration purposes and comparison with numerical calculations. The fact that consolidation settlements have been the critical design criterion for several subsea developments underlines the importance of adequate and correct analysis. The topic studied in this MSc thesis was suggested by Multiconsult AS, represented by Erik Tørum and Joar Gloppestad, based on challenges met in designing offshore templates with suction caissons.

##### **Task**

The candidate shall study the principles of consolidation settlement analyses of suction caissons. Further the candidate shall incorporate this into a finite element model using the FEM code PLAXIS and procedures proposed in the literature. Focus should be on understanding the installation and reconsolidation process and evaluating the FEM results. In particular the candidate should use the FEM analyses to look into the undrained shear strength increase with time along the foundation skirts. General evaluation of model applicability and reliability with respect to final consolidation settlement is important.

If possible the candidate shall consider doing some simple physical model tests regarding reconsolidation and increase in shear strength with time around a penetrated body.

##### **Delivery**

The master thesis shall be documented in a report delivered no later than 11<sup>th</sup> of June 2012. Three bounded B5 paper copies shall be handed in together with a digital version including all work related files.

Steinar Nordal  
Professor, NTNU



# I Preface

This master thesis is submitted as the final contribution to my MSc in civil and environmental engineering at the Geotechnical Division in the Department of Civil and Transport Engineering at the Norwegian University of Science and Technology.

To begin with I would like to thank Multiconsult AS represented by Signe G. Hovem, Erik Tørum and Joar S. Gloppestad for suggesting an intriguing topic for this MSc thesis. I really appreciate the follow-up on practical issues (e.g. soil investigation data) and introductory discussions related to the topic with Joar and Erik respectively.

There are several people who have been involved in the manufacturing of model test equipment and guidance related to practical aspects in the field and laboratory work. In despite of some unforeseen challenges and delays much effort has been put into realizing the simple model test. I would like to thank Jan Jønland for guidance in the laboratory and Gunnar Winther for helping out with accomplishing the field work. Additionally I thank MSc student Tommy H. Sjødis for excellent collaboration with the soil investigation.

Finally I would like to express my gratitude to the professor in charge and main supervisor Steinar Nordal for many great discussions, always with positive attitude and constructive suggestions for my MSc thesis. I have learned a lot with respect to understanding the relation between soil behavior, the soft soil material model and FEM analysis.

Trondheim 11.06.12

-----  
Anders Ulvestad





## II Abstract

### English version:

Consolidation settlement analysis is an essential part of the design process for suction caissons. However it is a complex task since soil volume important for settlement analyses is directly affected by the installation process. Consolidation settlements have been found to be the critical design criterion in several subsea developments, adequate and correct analysis is therefore vital.

The FEM code PLAXIS has been used to evaluate the reconsolidation process after completed installation of the suction caisson. Emphasize has been placed on studying the shear strength increase with time along the skirt walls. During consolidation dissipation of excess pore pressures result in higher effective stresses. Consequently the modeled undrained shear strength increases. However the increase is small compared to the expected increase in shear strength due to the set-up phenomenon. To account for the deviation an adjusted simulation procedure incorporating incremental increase of friction angle in the interface zones has been suggested. The results were found to be reasonable with respect to final consolidation settlements and development of mobilized shear strength with time.

Adequate modeling of the changes in the interface zones adjacent to the caisson walls during consolidation is vital for correct prediction of long term settlements. Modeled undrained shear strength with time have huge impact on the analysis results due to different mobilization of the surrounding soil. Appropriate evaluation of soil structure interaction is essential to assess the reliability of the analysis. Taking into account changes of the soil volume important for settlement analysis is also vital.

A simple physical model test has been performed. Due to delays and relatively short test period the results were inconclusive. However the importance of considering short term set-up effects has been underlined by recorded resistance and physical observations in the field.

### Norwegian version:

Setningsberegning utgjør en viktig del av prosjekteringen av bøttefundamenter. Korrekt beregning av endelige langtidssetninger er spesielt viktig da dette ved flere anledninger har vist seg å være det kritiske dimensjoneringskriteriet. Tilstrekkelige analyser er derfor nødvendig, men det er en kompleks oppgave blant annet fordi viktige styrke og stivhetsparametre i jorden blir direkte berørt under installasjon av fundamentet.

I denne oppgaven har elementmetodeprogrammet Plaxis vært benyttet for å studere rekonsolideringsfasen i etterkant av installasjonen av et bøttefundament. Det er lagt vekt på

å studere utviklingen av skjærstyrke med tid, spesielt med tanke på hvordan dette påvirker de dimensjonerende langtidssetningene. Grunnet dissipasjon av poreovertrykk øker effektivspenningene langs skjørtet på bøttefundamentet med tiden. Dette medfører en økning i skjærstyrke, men økningen samsvarer ikke nødvendigvis med forventet kapasitet over tid i henhold til set-up tankegangen. En alternativ modelleringsprosess som inkluderer periodisk økning av friksjonsvinkelen i grensesonene langs skjørtet er foreslått. Ut i fra de resultatene som foreligger virker det som om den justerte modelleringsprosessen tar bedre hensyn til økningen av skjærstyrke med tid. De tilhørende endelige langtidssetningene virker å ligge innenfor forventet område.

Den modellerte udrenerte skjærstyrken påvirker langtidssetningene i stor grad. Over- eller underestimering av styrken medfører feilaktig mobilisering av omliggende havbunn. Dette gjenspeiler seg igjen i langtidssetningene. Det er viktig å vurdere forholdet mellom jord og konstruksjon med tanke på å modellere en realistisk oppførsel. I tillegg er det svært viktig å ta hensyn til endringen i styrke og stivhet som konsekvens av installasjonen av bøttefundamentet.

I denne masteroppgaven er det også gjennomført et enkelt modellforsøk i felt. På grunn av utsettelse og uforutsette hendelser lar det seg ikke gjøre å trekke slutninger ut i fra resultatene. På en annen side viser observasjoner av påbygning av leire på stålplatene, samt tendensene i utvikling av motstand at det er viktig å ta hensyn til økning av skjærstyrken selv etter kort tid med konsolidering.

### III Table of contents

<b>I</b>	<b>PREFACE</b>	<b>1</b>
<b>II</b>	<b>ABSTRACT</b>	<b>2</b>
<b>III</b>	<b>TABLE OF CONTENTS</b>	<b>4</b>
<b>A</b>	<b>LIST OF FIGURES</b>	<b>6</b>
<b>B</b>	<b>LIST OF TABLES</b>	<b>8</b>
<b>C</b>	<b>NOTATIONS</b>	<b>9</b>
<b>D</b>	<b>ABBREVIATIONS</b>	<b>11</b>
<b>1</b>	<b>INTRODUCTION</b>	<b>12</b>
<b>2</b>	<b>LITERATURE REVIEW</b>	<b>14</b>
2.1	IMPACT OF INSTALLATION ON THE SOIL OUTSIDE THE SUCTION CAISSON	15
2.2	IMPACT OF INSTALLATION ON THE SOIL INSIDE THE SUCTION CAISSON	16
2.3	SET-UP EFFECT ON STEEL SKIRTS IN SOFT CLAY	19
2.4	CALCULATION PROCEDURE	23
<b>3</b>	<b>PROBLEM</b>	<b>28</b>
<b>4</b>	<b>APPROACH</b>	<b>30</b>
4.1	FEM MODEL OF SUCTION CAISSON	30
4.2	MODEL TEST	37
4.2.1	SOIL INVESTIGATION	40
4.2.2	THIXOTROPY TEST	42
<b>5</b>	<b>RESULTS AND EVALUATION</b>	<b>44</b>
5.1	FEM ANALYSES	44
5.1.1	INITIAL STRESS GENERATION	45
5.1.2	UNDRAINED LOADING AND CONSOLIDATION	50
5.1.3	UNDRAINED SHEAR STRENGTH	59
5.1.4	COHESION ( $C'$ )	63
5.2	ADJUSTED FEM ANALYSIS	65

---

<b>5.3</b>	<b>MODEL TEST</b>	<b>68</b>
5.3.1	THIXOTROPY TEST	70
<b>6</b>	<b>SUMMARY AND FUTURE WORK</b>	<b>72</b>
<b>7</b>	<b>BIBLIOGRAPHY</b>	<b>74</b>
<b>APPENDIX</b>		<b>76</b>
<b>APPENDIX A.</b>	<b>SOIL INVESTIGATION DATA (WEST COAST OF AFRICA)</b>	<b>76</b>
<b>APPENDIX B.</b>	<b>INPUT DATA FEM MODEL</b>	<b>85</b>
<b>APPENDIX C.</b>	<b>PENETRATION ANALYSIS</b>	<b>88</b>
<b>APPENDIX D.</b>	<b>INPUT DATA FEM MODEL (SELF-WEIGHT PENETRATION)</b>	<b>89</b>
<b>APPENDIX E.</b>	<b>MATHEMATICAL DERIVATIONS</b>	<b>91</b>
<b>APPENDIX F.</b>	<b>SOIL INVESTIGATION TILLER</b>	<b>93</b>
<b>APPENDIX G.</b>	<b>MODEL TEST DESIGN</b>	<b>110</b>
<b>APPENDIX H.</b>	<b>THIXOTROPY TEST RESULTS</b>	<b>111</b>

## A List of figures

Figure 1 Left hand side: suction caisson with forces during installation. Right hand side: caisson with installed manifold and forces acting on the skirted foundation .....	14
Figure 3 Incremental soil displacements during self-weight penetration of skirt tip .....	15
Figure 4 Incremental soil displacements during penetration by self-weight and suction of skirt tip... ..	16
Figure 5 Longitudinal section of a clay sample inside a soils sampling tube.....	17
Figure 6 Soil displacement during installation of suction caisson with applied underpressure .....	17
Figure 7 Measured pore pressure normalized by undrained shear strength versus overconsolidation ratios (OCR) along the shaft of a CPTU test device .....	19
Figure 8 Suggested values for shear strength in remolded zone inside skirt wall after 3 months of horizontal pore pressure distribution and thixotropy effect .....	19
Figure 9 Correction of set-up factor ( $\alpha$ ) as a function of overconsolidation ratio .....	20
Figure 10 Final radial effective stress ratio $K_c$ ( $K_c = \sigma'_{rc} / \sigma'_{v0}$ ) versus OCR for piles.....	22
Figure 11 Suggested increase in ultimate shaft friction during re-consolidation ("set-up" effect) .....	23
Figure 12 Connectivity plot and dimensions complete FEM model and detailed cut of the suction caisson .....	31
Figure 13 Constant rate of strain consolidation test correlation from PLAXIS soil test.....	32
Figure 14 Undrained shear strength values from TxCuD in soil test plotted versus suggested undrained shear strength profile .....	33
Figure 15 Model test equipment design .....	38
Figure 16 Model test equipment pre-assembled (left hand side), ready for installation (in the middle) and ready for testing (right hand side).....	39
Figure 17 Model test installation pattern and detailed map indicating model test installaiton site....	39
Figure 18 Overview of Trondheim marked with test area at Tiller .....	41
Figure 19 Detailed map with coordinates of soil investigation area.....	41
Figure 20 Remolded sample stored in plastic cup prepared for thixotropy fall cone test.....	43
Figure 21 Settlement of suction caisson center point for the initial FEM analyses .....	45
Figure 22 Pore pressure ( $U_{active}$ ), vertical ( $\sigma_v$ ) and radial total stresses ( $\sigma_r$ ) after initial stress generation .....	47
Figure 23 Excess pore pressures from initial stress generation .....	47
Figure 24 Vertical and horizontal displacement during initial stress generation .....	48
Figure 25 Yield surface of the Soft Soil model in $p'$ - $q$ -plane including Mohr-Coulomb failure criterion (PLAXIS Manual) .....	48
Figure 26 Undrained shear strength calculated from effective stresses during initial stress generation .....	49
Figure 27 Excess pore pressure ( $U_{excess}$ ) after undrained loading and at the end of consolidation .....	50
Figure 28 Horizontal cross section of normalized active pore pressure in the interface zones at depth = 10 m and different time intervals.....	51
Figure 29 Horizontal cross section of normalized active pore pressure in the clay plug, interface zones and surrounding soil at depth = 10 m and different time intervals .....	51
Figure 30 Radial effective stress ( $\sigma'_r$ ) after undrained loading and at the end of consolidation.....	52
Figure 31 Tangential effective stress ( $\sigma'_\theta$ ) after undrained loading and at the end of consolidation ..	52
Figure 32 Horizontal cross section of normalized horizontal radial stress in the interface zones at depth = 10 m and different time intervals .....	53
Figure 33 Horizontal cross section of normalized horizontal radial stress in the clay plug, interface zones and surrounding soil at depth = 10 m and different time intervals.....	53
Figure 34 Radial strains after undrained loading and at the end of consolidation.....	54
Figure 35 Horizontal cross section of radial strains in the interface zones.....	54

Figure 36 Horizontal cross section of radial strain in the clay plug, interface zones and surrounding soil at depth = 10 m and different time intervals.....	55
Figure 37 Vertical effective stress ( $\sigma'_v$ ) after undrained loading and at the end of consolidation .....	55
Figure 38 Horizontal cross section of normalized effective vertical stress in the interface zones at depth = 10 m and different time intervals .....	56
Figure 39 Horizontal cross section of normalized vertical effective stress in the clay plug, interface zones and surrounding soil at depth = 10 m and different time intervals.....	56
Figure 40 Mobilized shear stress ( $\tau_{mob}$ ) after undrained loading and at the end of consolidation.....	57
Figure 41 Relative mobilized shear stress ( $\tau_{mob}/\tau_{max}$ ) after undrained loading and at the end of consolidation .....	57
Figure 42 Vertical displacement after undrained loading and at the end of consolidation .....	58
Figure 43 Final effective radial stress ratio ( $K_c$ ) versus depth in the outer interface zone and surrounding soil.....	59
Figure 44 Maximal shear strength, mobilized shear strength and relative mobilized shear strength at different time intervals in the outer interface zone ( $x = 2.52$ m) for Case 5 .....	60
Figure 45 Plastic points after updating friction angle in the remolded zones ( $t = 100$ days) .....	61
Figure 46 Relative mobilized shear strength after updating friction angle in the remolded zones and further development .....	61
Figure 47 Maximal shear strength, mobilized shear strength and relative mobilized shear strength at different time intervals in the outer interface zone ( $x = 2.52$ m) for Case 5 with updated friction angle and $K_0^{NC}$ .....	62
Figure 48 Development of consolidation settlements with time for different cohesion values in the interface zones (Case 5) .....	63
Figure 49 Vertical displacement profile after consolidation ( $t = 20$ years, depth = 0.1 m) .....	64
Figure 50 Mobilized friction in the interface zones after equilibrium phase (phase 2) for $c' = 1$ and $c' = 10$ .....	64
Figure 51 Maximal shear strength, mobilized shear strength and relative mobilized shear strength at different time intervals in the outer interface zone ( $x = 2.52$ m) for Case 6 .....	66
Figure 52 Maximal shear strength, mobilized shear strength and relative mobilized shear strength at different time intervals in the inner interface zone ( $x = 2.48$ m) for Case 6.....	67
Figure 53 Consolidation settlement development for adjusted FEM analysis (Case 6) compared with initial analyses .....	68
Figure 54 Model test results.....	69
Figure 55 Deep-seated clay on steel plate (left hand side) and clay behavior in the transition zone from plate to rod (right hand side).....	70
Figure 56 Thixotropy test results.....	71

## B List of tables

Table 1 Outside set-up factor ( $\alpha$ ) for suction caissons penetrated by underpressure .....	20
Table 2 Inside set-up factor ( $\alpha$ ) for suction caissons penetrated by underpressure .....	20
Table 3 Material parameters suction caisson (plate elements) .....	31
Table 4 Clay input parameters for the soft soil material model .....	34
Table 5 Input data for adjusted initial stress generation calculation.....	35
Table 6 Updated parameters for the different zones .....	35
Table 7 Simulation procedure in FEM (PLAXIS) .....	36
Table 8 Aberration from original updates for the initial simulation cases.....	45
Table 9 Set-up factor and corresponding updated friction angle for the interface zones.....	60
Table 10 Adjusted FEM analysis procedure .....	65
Table 11 Executed installation and test procedure.....	68





## C Notations

- $S_{u,rem}$  – remolded undrained shear strength  
 $d$  – caisson diameter  
 $t$  – caisson wall thickness  
 $K_c$  – final radial effective stress ratio  
 $\sigma'_{rc}$  – radial effective stress  
 $\sigma'_{v0}$  – initial effective vertical stress  
 $I_p$  – plasticity index  
 $Q_{tot}$  – total penetration resistance  
 $Q_{side}$  – shear force along the skirt wall  
 $Q_{tip}$  – bearing capacity at the skirt tip  
 $A_{wall}$  – skirt wall area (sum of inside and outside contribution)  
 $A_{tip}$  – skirt tip area  
 $\alpha$  – shear strength factor (normally assumed equal to the inverse of the sensitivity)  
 $S_{u,D}^{av}$  – average DSS shear strength over penetration depth  
 $S_{u,tip}^{av}$  – average undrained shear strength at skirt tip level (average of triaxial compression, triaxial extension and DSS shear strengths)  
 $\gamma'$  – effective unit weight of soil  
 $N_c$  – bearing capacity factor, plane strain condition  
 $Z$  – skirt penetration depth  
 $W'$  – submerged weight of suction caisson during installation  
 $A_{in}$  – plan view inside area where underpressure is applied  
 $A_{inside}$  – inside skirt wall area  
 $S_{u,tip}^{LB}$  – 2/3 of the average of compression, extension and DSS shear strengths at skirt tip level  
 $t$  – skirt wall thickness  
 $R$  – radius of skirt compartment (inner radius suction caisson)  
 $\epsilon_v$  – vertical strain  
 $\epsilon_r$  – radial (horizontal) strain  
 $z$  – depth in clay plug  
 $S_u^{DSS}$  – average undrained direct simple shear strength over the penetration depth  
 $S_t$  – sensitivity of the clay  
 $\Delta U_{top}$  – applied underpressure (relative to hydrostatic) at the top of the clay plug  
 $\Delta \sigma_{oct}$  – change in octahedral total stress in the clay plug  
 $\Delta u_\gamma$  – generated pore pressure due to shear strains  
 $\sigma_v$  – vertical total stress  
 $\sigma_h$  – horizontal total stress  
 $K'_0$  – lateral earth pressure coefficient  
 $\sigma_{vc}'$  – initial vertical in situ effective stress  
 $c'$  – effective cohesion

L	– design load
D	– suction caisson diameter
EA	– axial modulus
EI	– rigidity modulus
w	– distributed weight of plate elements
A-A	– distributed load at suction caisson top
$\lambda^*$	– virgin compression ratio soft soil model
$\kappa^*$	– recompression ratio soft soil model
$\phi'$	– friction angle
$\psi$	– dilation angle
$\nu'_{ur}$	– poisson ratio unloading-reloading
$K_0^{NC}$	– lateral earth pressure coefficient normally consolidated clay
$k_x$	– horizontal permeability
$k_y$	– vertical permeability
$K'_{0,up}$	– updated lateral earth pressure coefficient
$OCR_{up}$	– updated overconsolidation ratio
$\tau/\sigma'_{v,0}$	– normalized shear stress at maximum vertical strain
$U_\gamma/\sigma'_{v,0}$	– normalized shear strain induced pore pressure
$\Delta U/\sigma'_{oct}$	– normalized remolding induced pore pressure
$\emptyset$	– rod and casing diameter
$U_{suction}$	– excess pore pressure, suction
$U_{active}$	– active pore pressure from PLAXIS
$U_{excess}$	– excess pore pressure from PLAXIS
$\sigma_r$	– radial total stress
$p'$	– effective mean stress
q	– deviator stress
$S_u/\sigma'_v$	– normalized undrained shear strength
M	– parameter in the soft soil model
$\tau_{max}$	– maximal shear strength from PLAXIS
$\tau_{mob}$	– mobilized shear strength from PLAXIS
$\tau_{rel}$	– relative mobilized shear strength from PLAXIS
$F_{max}$	– maximal recorded resistance from model test
$F_0$	– reference resistance at t = 0 from model test
$S_{r,t0}$	– remolded undrained shear strength from fall cone test at time t0
$S_{r,t1}$	– undrained shear strength from fall cone test at time t1

## D Abbreviations

- API – American Petroleum Institute  
CRS – the constant rate of strain  
DSS – direct simple shear  
FEM – finite element method  
NTNU – Norwegian University of Science and Technology  
OCR – overconsolidation ratio  
POP – pre overburden pressure  
TxCuD – undrained triaxial compression test  
TxEuD – undrained triaxial extension test



# 1 Introduction

Suction caissons are an important foundation solution in several offshore projects. Skirted foundations represent viable and attractive qualities with respect to capacity and cost efficiency. In later years FEM analysis for design of suction caissons has become an important tool. Consolidation settlement analysis is an essential part of this, however evaluation of consolidation settlement is a complex task. To underline the importance of adequate and correct analysis it should be mentioned that consolidation settlements have been determined to be the critical design criterion in several subsea developments.

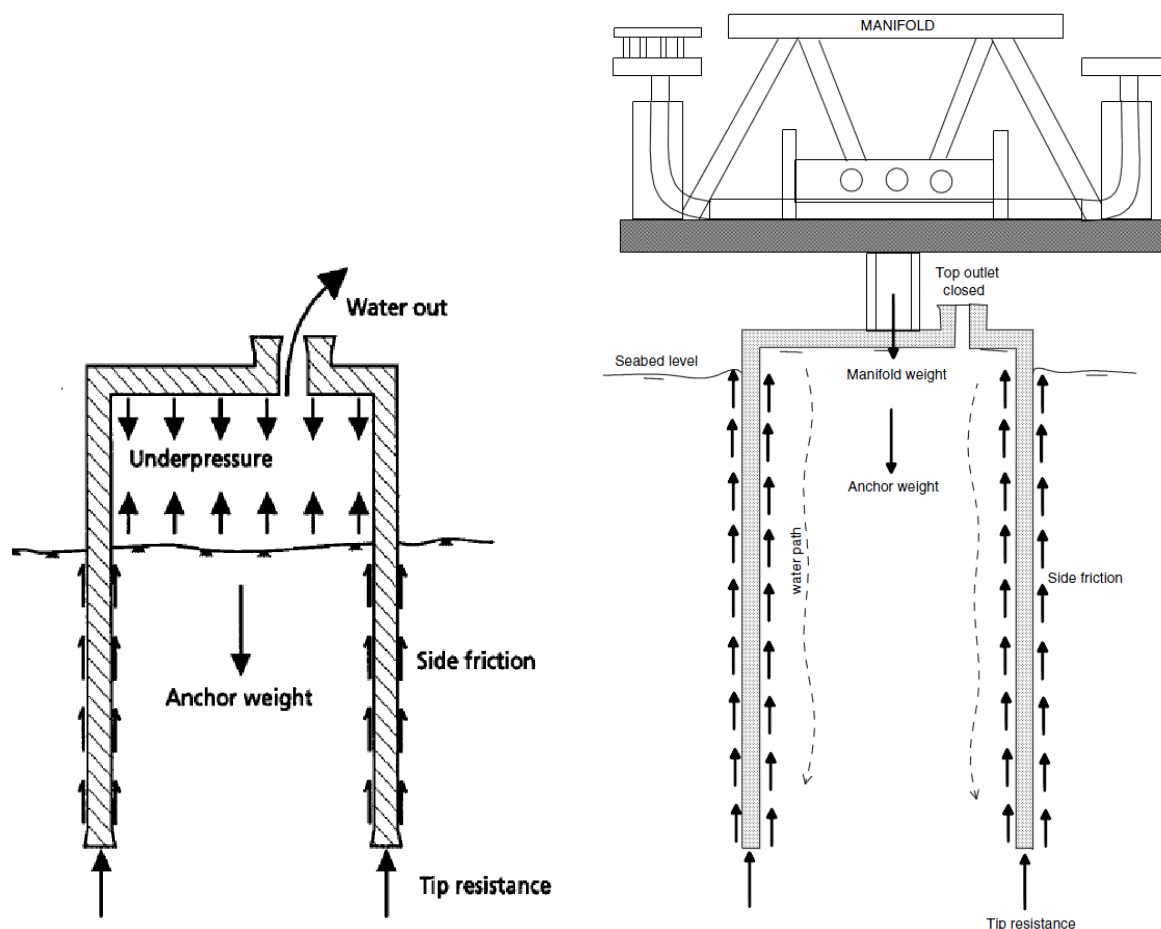
Throughout application of the FEM code PLAXIS and procedures proposed in literature the principles of consolidation settlement analyses will be studied. Emphasize will be put on modeling the increase in undrained shear strength with time along the skirt wall and assessment of final consolidation settlements.

The remainder of the thesis is organized as follows: Chapter 2 gives a short review of important literature and research including suggested calculation procedure for suction caissons. In Chapter 3 the problem to be addressed is thoroughly described and aims for the MSc thesis outlined. Chapter 4 describes the general simulation procedure applied in the FEM analyses and the contents of the model test, field- and laboratory work. Chapter 5 contains primarily two parts, describing and evaluating the results from the FEM analyses and model test respectively. An adjusted FEM analysis is also included in this chapter. Finally a summary and recommendation for future work is given in Chapter 6.



## 2 Literature review

Installation of suction caissons is performed by self-weight penetration and applied underpressure. This process changes the initial stress distribution in the soil plug inside the suction caisson and the surrounding soil. Displacement of the soil plug, remolding of the adjacent soil in the interface zone and generation of excess pore pressure contributes to the change in effective stress. Accounting for the change in shear strength with time and transition from an undrained to a drained design situation is important to avoid limitations in the FEM analysis. (Hernandez-Martinez, Rahim, Strandvik, Jostad, & Andersen, 2009)



**Figure 1** Left hand side: suction caisson with forces during installation (Andersen & Jostad, 2002). Right hand side: caisson with installed manifold and forces acting on the skirted foundation (Hernandez-Martinez, Rahim, Strandvik, Jostad, & Andersen, 2009)

Suction caissons can be subjected to vertical loads, horizontal loads and moments. The loads are often categorized as permanent loads, high frequency loads and low frequency loads. (Andersen & Jostad, 1999) Permanent loads are primarily due to installed subsea structure modulus e.g. manifolds. The frequency loads are often environmental loads like waves, tides and resonance oscillations. Requirements of lifetime foundation stability demand for both short term and long term analysis. Short term capacity analysis with loading and undrained soil response must be verified. In addition interconnected subsea structures and pipelines

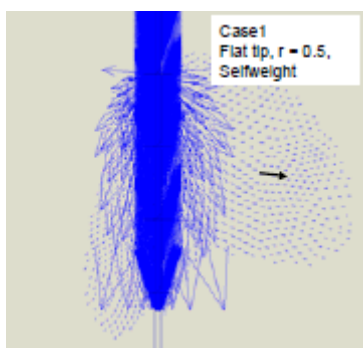
may require long term settlement calculations to guarantee adequate alignment throughout the service time.

The dissipation of excess pore pressure as a result of the installation and loading of the caisson is indicated in Figure 1. After installation the top valve is sealed and the pore water pressure will dissipate slowly. Accordingly the transition from an undrained load situation to a drained load situation changes slowly with time. Additionally the skirt friction will increase with time (set-up phenomenon) due to increased effective stresses, pore pressure dissipation and thixotropy. (Hernandez-Martinez, Rahim, Strandvik, Jostad, & Andersen, 2009)

## 2.1 Impact of installation on the soil outside the suction caisson

Skirt penetration during installation will reduce the shear strength of the clay along the outside of the caisson. The remolded undrained shear strength ( $S_{u,rem}$ ) which is the original undrained shear strength ( $S_u$ ) divided by the sensitivity ( $S_t$ ) is believed to be a good approximation. For comparison the final design undrained shear strength after installation and full regeneration (set-up) of shear strength can be as high as 25-35% higher than  $S_{u,rem}$ . (Andersen & Jostad, 1999)

The soil displacement pattern and hence also the effect on the stress distribution along the skirt is strongly dependent upon penetration procedure. During penetration due to self-weight only, there is significant soil displacement to the outside of the suction caisson (Figure 2). The displacement extends the furthest at the tip of the skirt. Along the upper parts of the skirt wall the mainly influenced zone has a thickness approximately equal to the skirt thickness. (Andersen & Jostad, 2002) Chen & Randolph (2007) performed a series of centrifuge tests which indicated that on an average around 50% of the soil displaced after complete installation (both by self-weight and suction) flows inward into the suction caisson. The same tests also indicated an inward soil flow of approximately 20% during self-weight penetration (modeled by jacking) to a depth equivalent of four diameters.



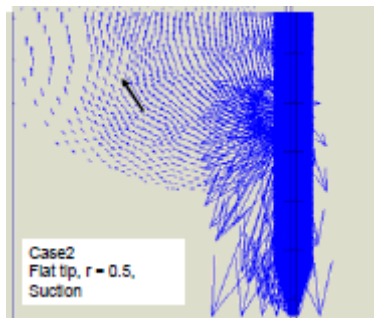
**Figure 2 Incremental soil displacements during self-weight penetration of skirt tip (Andersen, Andresen, H.P., & Clukey, 2004)**

The outward flow of soil results in increased octahedral normal stresses outside the skirt tip. This continuous process will also increase normal stresses along the skirt wall above the



present skirt tip elevation. The stress change initiates an increase in excess pore pressure. With dissipation of excess pore pressure increased effective normal stresses is anticipated. Additionally it gives potential for increasing interface friction (set-up) with time. (Andersen & Jostad, 2002)

When underpressure is applied in order to penetrate the skirted foundation further (after reaching equilibrium between self-weight and skirt friction resistance) the soil distribution changes character. FEM analyses (Figure 3) by Andersen, Andresen, H.P. & Cluckey (2004) show virtually no soil displacement outside the skirt wall as most of the displaced soil moves inside the skirt wall. This is contradictory with the findings of Chen & Randolph (2007). However it should be noted that the diameter ( $d$ ) to wall thickness ( $t$ ) ratio ( $d/t$ ) as well as the design of internal stiffeners differ from the assumptions in the FEM analysis of Andersen et al. (2004). Despite no outwards soil displacement the penetration of the skirt tip could leave some strains outside the skirt wall. In addition, increased shear strength due to high strain rates as a result of the thin shear zone could contribute to the thickness of the remolded zone. Other centrifuge tests, e.g. the centrifugal studies of Renzi, Maggioni, Smits & Manes (1991), indicate that an assumption of a remolded zone with a thickness of one skirt width is reasonable. (Andersen & Jostad, 2002)



**Figure 3 Incremental soil displacements during penetration by self-weight and suction of skirt tip (Andersen, Andresen, H.P., & Clukey, 2004)**

## 2.2 Impact of installation on the soil inside the suction caisson

Soil displacement pattern and the effect on shear strength inside the suction caisson are strongly influenced by geometry and design. Inside stiffeners will affect both the remolded zone and the clay plug inside the caisson. (Andersen & Jostad, 2004) In this MSc thesis a simple design without inside stiffeners will be emphasized. Hence the effect of inside stiffeners and geometry change will not be further discussed in the literature review.

The clay sample inside a soil sampling tube is a good analogue to the clay plug inside a suction caisson after installation. From Figure 4 it is evident that a soil sample may experience extreme shear strains along the soil sampling tube wall. Additionally the clay plug within the thin shear zones seems to deform quite uniformly throughout the sample. This assumption is supported by experience from model test results (Renzi, Maggioni, Smits, & Manes, 1991) and the strain path method. (Andersen & Jostad, 2004)

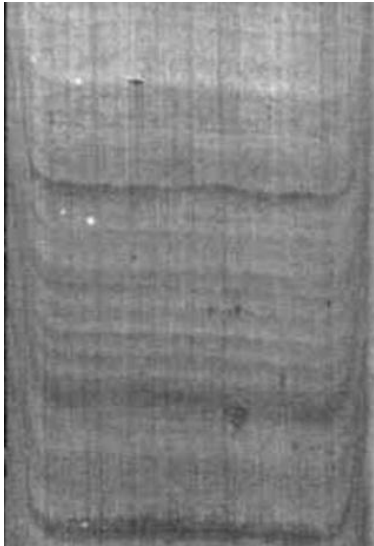


Figure 4 Longitudinal section of a clay sample inside a soils sampling tube (Andersen & Jostad, 2004)

The thickness of the remolded zone along the skirt wall have been studied and described comprehensively, e.g anchor model test (Renzi, Maggioni, Smits, & Manes, 1991), pile model test (Karlsrud & Nadim, Axial Capacity of Offshore Piles in Clay, 1990) and theoretical analyses of soil sampling (Baligh, Azzouz, & Chin, 1987). The basic concept of a remolded zone with a thickness approximately equal to the thickness of the skirt wall seems incorporated in most studies.

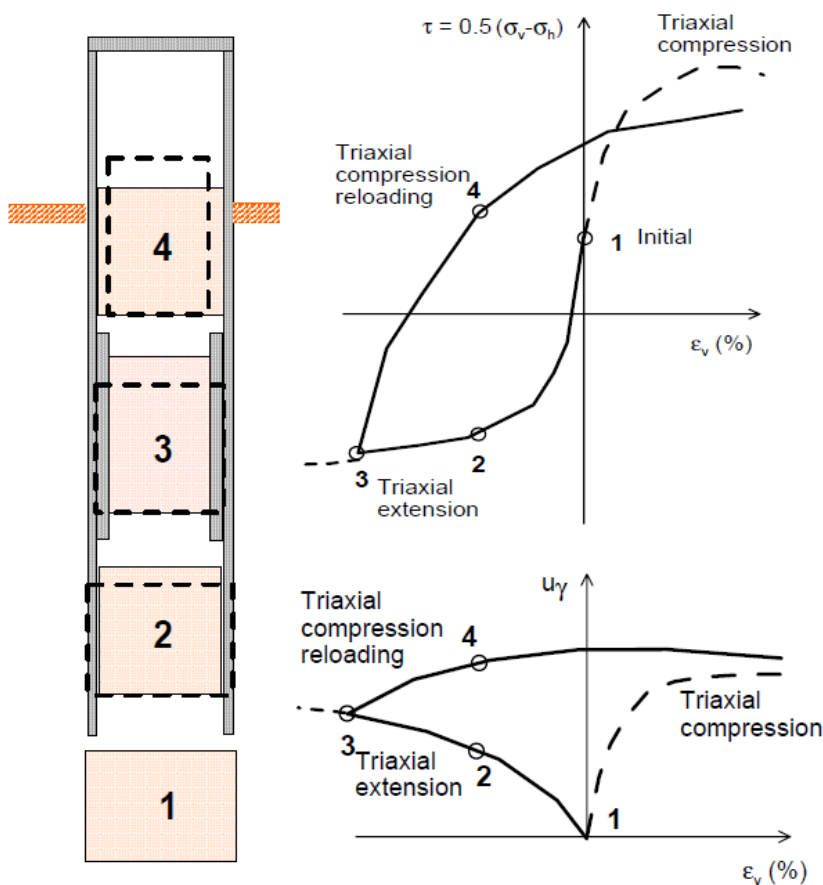


Figure 5 Soil displacement during installation of suction caisson with applied underpressure (Andersen & Jostad, 2004)

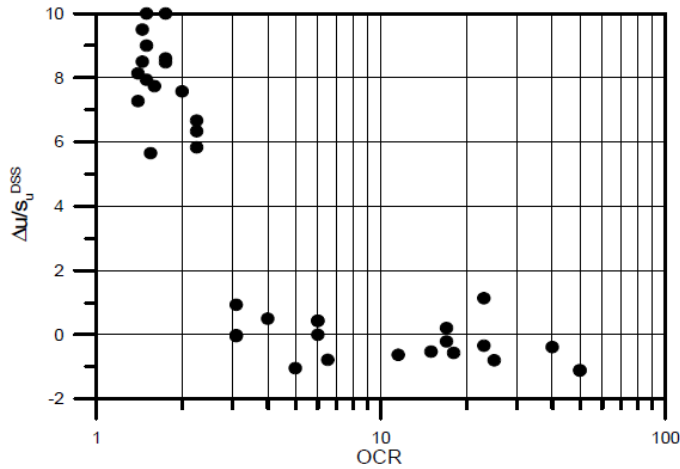
As described in Chapter 2.1 the soil displacement depends on the driving force for the penetration.

Figure 5 indicate the soil displacement path during installation with applied underpressure (suction). For a simple suction caisson without inside stiffeners point 1 and point 2 is relevant. Point 1 is representing the in situ conditions prior to the penetration, while point 2 indicates the situation after caisson penetration of the soil element. Calculation wise it is assumed that the soil element is not subjected to any stress changes before it enters the caisson. This is a reasonable assumption since the caisson is penetrated by suction and there is no additional external load. Subsequently it is assumed that an intact clay plug deforms uniformly. This generates shear strains in the clay plug while deformed inside the suction caisson. Since there is no volumetric change in an undrained load situation the imposed horizontal displacement generates equivalent vertical displacement. (Andersen & Jostad, 2004)

After completed penetration to required depth the underpressure will be turned off. Consequently the total skirt friction will be reduced to equilibrium with the submerged weight of the suction caisson. Since this friction is relatively small compared to the weight of the clay plug, the total stress relative to the seabed after completed skirt penetrations is assumed to be the equivalent effective stress. (Andersen & Jostad, 2004)

Horizontal stress equilibrium is assumed between the clay plug and the remolded zone inside the skirt wall. With no external load this means that the horizontal total stress is the same within the suction caisson. Due to the large shear strains and the remolding of the soil an isotropic stress condition is assumed for the remolded zone. Effectively the vertical total stress is assumed equal to the horizontal total stress inside the remolded zone after completed skirt penetration. The pore pressure in the remolded zone depends on the soil properties. For soft clays the pore pressure is anticipated to be equal to the octahedral total stress after installation. This implies that the initial effective stresses are zero. This assumption is supported by direct simple shear (DSS) testing and field measurement on piles during installation in normally consolidated clays. For overconsolidated clays the tendency of dilatation will affect the generation of excess pore pressure. Generally smaller excess pore pressures are anticipated, and sometimes even buildup of negative pore pressures can occur for large overconsolidation ratios (OCR). Figure 6 indicate a possible tendency that can be used to consider the change in pore pressure in the remolded zones. Despite of the limitation in data there is a clear tendency of high excess pore pressure for low OCR, and low as well as negative excess pore pressure for high OCR. These measurements are further supported by experience from piles and laboratory tests (DSS). However it should be noted that the pore pressures from the CPTU and piles are measured outside the wall. Therefore the generation of excess pore pressure inside the skirt wall might differ, but the data clearly indicate the influence of OCR. (Andersen & Jostad, 2004)

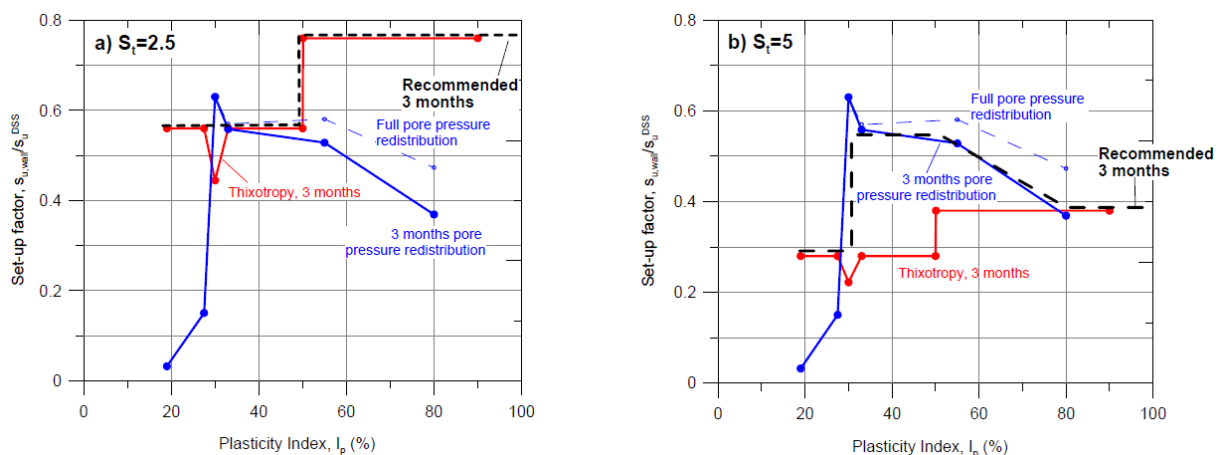
Calculation of strains, excess pore pressure and stresses in both the clay plug and remolded zones are further described in Chapter 2.4.



**Figure 6 Measured pore pressure normalized by undrained shear strength versus overconsolidation ratios (OCR) along the shaft of a CPTU test device (Andersen & Jostad, 2004)**

### 2.3 Set-up effect on steel skirts in soft clay

The increase in shear strength with time described earlier in Chapter 2 is often referred to as “set-up”. The phenomenon describes increase in shear strength due to a combination of dissipation of excess pore pressure, increased horizontal effective stress and thixotropy. Thixotropy is gain in shear strength with time despite no volume change. The individual contribution of the three factors is time dependent and closely related to soil properties (indicated in Figure 7).



**Figure 7 Suggested values for shear strength in remolded zone inside skirt wall after 3 months of horizontal pore pressure distribution and thixotropy effect (Andersen & Jostad, 2004)**

Installation method (penetration by self-weight or additional underpressure) will affect the soil displacement pattern as well as the relative importance of the set-up mechanisms. Generally the soil displacement during penetration will cause significant increase in normal stress in the soil. During penetration by self-weight this will be applicable for both sides of

the skirt wall. For the penetration with applied underpressure it will primarily be valid for the remolded zone inside the suction caisson. The increased normal stresses give potential for high effective normal stresses after dissipation of the excess pore pressure. Nevertheless the soil displacement outside of the suction caisson also generates additional excess pore pressure further away from the wall. This will increase the time of dissipation and regeneration of shear strength. Set-up for suction caisson during self-weight penetration is comparable with set-up for piles. With applied underpressure it is very different as the interface friction may be smaller than the initial shear strength (because of the lack of increase in normal stress). (Andersen & Jostad, 1999)

Det Norske Veritas (DNV, 2005) has proposed to use the set-up factors summarized in Table 1 and Table 2 unless more site specific data is available. The set-up factor values are lower bound estimates for skirts penetrated by applied underpressure. For overconsolidated soils a correction factor ( $\alpha^{OC} / \alpha^{NC}$ ) for the set-up factor along the outside skirt wall is given in Figure 8.

Set-up factor $\alpha = S_{u,rem}/S_u^D$ after 2 months			
$I_p$	<25%	25-50%	>50%
$S_t > 3$	0.58	0.65	0.65
$S_t < 3$	0.58	0.65	$1.95/S_t \leq 1.0$

Table 1 Outside set-up factor ( $\alpha$ ) for suction caissons penetrated by underpressure (DNV, 2005)

Set-up factor $\alpha = S_{u,rem}/S_u^D$		
$I_p$ [%]	10 days	3 months
< 30	$1.15/S_t$	$1.4/S_t$
30-50	$1.15/S_t$ $0.41-0.07(I_p-50))/S_t$	$1.4/S_t$ 0.55
50-80	$(1.15+0.025(I_p-50))/S_t$ $0.34-0.16(I_p-50)/30$	$1.9/S_t$ $0.55-0.17(I_p-50)/30$
> 80	$1.9/S_t$	$1.9/S_t$

Table 2 Inside set-up factor ( $\alpha$ ) for suction caissons penetrated by underpressure (DNV, 2005)

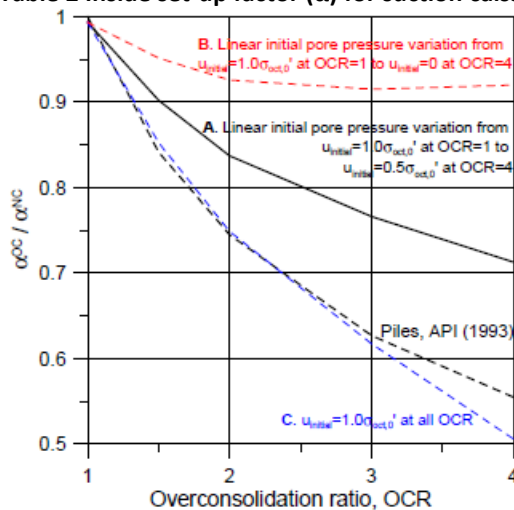


Figure 8 Correction of set-up factor ( $\alpha$ ) as a function of overconsolidation ratio (DNV, 2005)

Investigating and understanding the set-up effect for suction caissons is important since the design holding capacity is strongly influenced. According to Andersen & Jostad (1999) a suction caisson with a  $d/t$  ratio of 5 installed in typical subsea clay with a sensitivity of 4 may have a potential for a 25-35% increase in capacity after full regeneration of the shear strength. Additionally it is important to understand these mechanisms in relation to consolidation settlement calculations. The modeling of the transition from an undrained to a drained design situation in the remolded zones will influence the final consolidation settlements. (Hernandez-Martinez, Rahim, Strandvik, Jostad, & Andersen, 2009)

For his Dr. of Philosophy Thesis, Karlsrud (2012) reported on a comprehensive analyses and interpretation of pile load test results work. Several interesting aspects applicable for suction caisson consolidation settlement problems were discussed. Among them semi-empirical methods for determining capacity build up (re-consolidation/set-up) with time following pile installation as a result of consolidation were proposed. Neglecting surface and tip effects three main factors were determined to influence the radial consolidation process:

1. The extent of the radial excess pore pressure field
2. The shape or form of the excess pore pressure field
3. The coefficient of radial consolidation (stress dependent)

Despite some scatter in the measured and calculated consolidation times, Karlsrud concluded on some very interesting observations:

1. There seemed to be no clear differences in scatter between open- and closed-ended piles
2. The effect of pile diameter was apparently insignificant in relation with the scatter
3. The scatter seemed to be induced by difficulties in determining correct permeability values

In other words the computational model seem applicable both for open- and closed-ended piles, and might be comparable with suction caissons (even though  $d/t$ -ratio often is somehow larger). Additionally permeability is pointed out to be a key factor for estimating correct consolidation times, hence also correct consolidation settlements in the case of suction caissons. (Karlsrud, 2012)

Figure 9 show final radial effective stress ratio ( $K_c = \sigma'_{rc} / \sigma'_{v0}$ ) plotted versus OCR for the interpreted data in the thesis. The trend of increasing  $K_c$  with OCR is distinctive, and the effect of soil properties (plasticity index,  $I_p$ ) is apparently quite significant. The empirical  $K_c$  data presented in the figure may for the time being give the best guideline for assessing final radial effective stress after completed set-up. However ultimate shaft friction might deviate from the expected values when considering development of  $K_c$ .

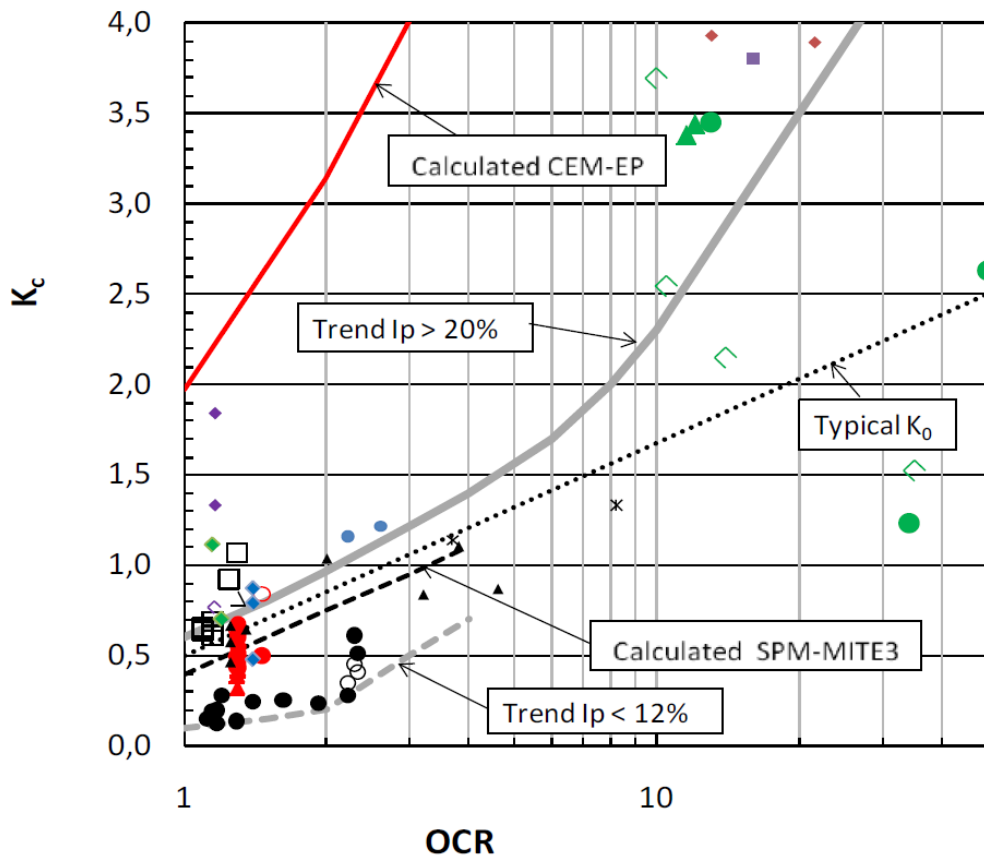


Figure 9 Final radial effective stress ratio  $K_c$  ( $K_c = \sigma'_{rc} / \sigma'_{v0}$ ) versus OCR for piles (Karlsrud, 2012)

Karlsrud (2012) has proposed two different models for prediction of final shaft friction ( $\alpha$ -model and  $\beta$ -model). Both are based on the ideas behind the method originally proposed by the American Petroleum Institute (API). Additionally they are normalized by either an in-situ undisturbed undrained shear strength or vertical effective stress respectively, and also adjusted by soil properties such as  $I_p$  and OCR. The main tendency for all the data is that the ultimate shaft friction will increase with increasing horizontal effective stress. However the scatter in data made it impossible to conclude on a design approach based on correlations between horizontal effective stresses and shaft friction. (Karlsrud, 2012)

For low to moderately overconsolidated clays it is also likely that the increase in horizontal effective stress as a result of consolidation is determining the increase in shaft friction with time. The thixotropy effect will affect the shaft friction continuously and simultaneously with reconsolidation, but is quite hard to isolate and individually determine the relative contributions. Karlsrud (2012) therefore suggests that the increase in ultimate shaft friction for piles is related to the degree of consolidation (Figure 10). Consequently it is worth noticing that the consolidation time is proportional to the square of the pile diameter (important for suction caissons with generally large diameters compared to normal piles). For a pile with a diameter of 2 m and a wall thickness of 50 mm installed in lightly overconsolidated plastic clay the difference in consolidation time ( $t_{90}$ ) for a closed-ended pile compared to an open-ended pile is approximately a factor of 10. This also underlines the importance of considering plugging during design of the suction caisson. (Karlsrud, 2012)

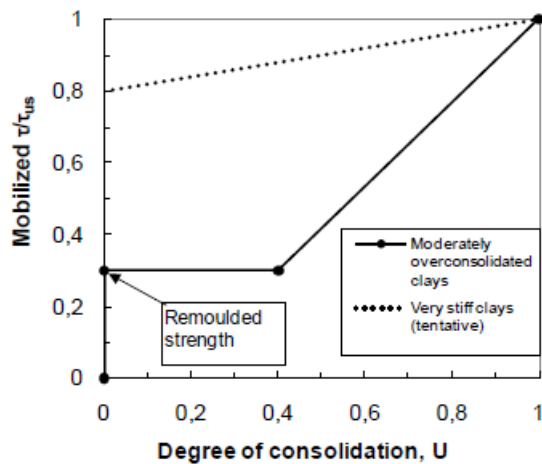


Figure 10 Suggested increase in ultimate shaft friction during re-consolidation ("set-up" effect) (Karlsrud, 2012)

## 2.4 Calculation procedure

The calculation procedure of initial strains, stresses and pore pressures subsequent of suction caisson installation is thoroughly described by Andersen & Jostad (2004).

Penetration analysis and design of ultimate capacity is considered many places in literature, among them the European Standard (EN ISO 19902:2007), Recommended Practice report from DNV (2005) and an article by Andersen & Jostad (1999). This chapter will briefly summarize the calculation procedures and assumptions made for the following FEM analysis in this MSc thesis.

The penetration analysis (also referred to as installation analysis) of a suction caisson is divided in three different assessments; calculation of penetration resistance, necessary underpressure to complete the installation to required depth and maximal allowable underpressure to avoid critical soil heave or cavitation inside the suction caisson. The total penetration resistance ( $Q_{tot}$ ) for skirts without stiffeners is calculated as the sum of the shear force along the skirt wall ( $Q_{side}$ ) and the point end bearing capacity at the skirt tip ( $Q_{tip}$ ):

$$Q_{tot} = Q_{side} + Q_{tip} = A_{wall} \cdot \alpha \cdot S_{u,D}^{av} + (N_c \cdot S_{u,tip}^{av} + \gamma' \cdot Z) \cdot A_{tip}$$

where

$A_{wall}$  = skirt wall area (sum of inside and outside contribution)

$A_{tip}$  = skirt tip area

$\alpha$  = shear strength factor (normally assumed equal to the inverse of the sensitivity)

$S_{u,D}^{av}$  = average DSS shear strength over penetration depth

$S_{u,tip}^{av}$  = average undrained shear strength at skirt tip level (average of triaxial compression, triaxial extension and DSS shear strengths)

$\gamma'$  = effective unit weight of soil

$N_c$  = bearing capacity factor, plane strain condition

$Z$  = skirt penetration depth



At the end of self-weight penetration (equilibrium between suction caisson weight and penetration resistance) the necessary underpressure for further required penetration is given by:

$$\Delta U_n = \frac{Q_{tot} - W'}{A_{in}} \quad (2.2)$$

where

$W'$  = submerged weight of suction caisson during installation

$A_{in}$  = plan view inside area where underpressure is applied

In order to avoid to large soil heave within the suction caisson due to bottom heave allowable underpressure can be calculated from:

$$\Delta U_a = N_c \cdot S_{u,tip}^{LB} + \alpha \cdot S_{u,D}^{av} \cdot \frac{A_{inside}}{A_{in}} \quad (2.3)$$

where

$A_{inside}$  = inside skirt wall area

$S_{u,tip}^{LB}$  = 2/3 of the average of compression, extension and DSS shear strengths at skirt tip level

Additionally it should be checked that the allowable underpressure does not exceed the cavitation pressure at shallow waters. (DNV, 2005)

The installation procedure is relevant to the settlement calculation since it strongly affects the shear strength and displacement pattern of the soil. Andersen & Jostad (2002) suggest that the effect of self-weight penetration linearly reduces to zero from the depth of self-weight equilibrium to a depth of one diameter below this point. In the transition zone between self-weight penetration and penetration by underpressure the solution for self-weight penetration should be used to the depth where it gives the most favorable results.

The formulas and calculation procedure below is based on the discussion in Chapter 2.2 and the findings in Andersen & Jostad (2004). Given that all the displaced soil moves into the caisson during penetration with applied underpressure, and that the clay plug deforms uniformly, the strains in the inner clay plug can be derived from:

$$\varepsilon_r = \frac{t}{r} \quad \varepsilon_v = -2 \cdot \varepsilon_r \quad \gamma = (\varepsilon_v - \varepsilon_r) = 1,5 \cdot \varepsilon_v = -3 \cdot \varepsilon_r \quad (2.4)$$

where

$t$  = skirt wall thickness

$R$  = radius of skirt compartment (inner radius suction caisson)

$\varepsilon_v$  = vertical strain

$\varepsilon_r$  = radial (horizontal) strain

During skirt penetration the average vertical total stress at depth  $z$  in the clay plug is:

$$\sigma_v = \gamma' \cdot z + 2 \cdot \frac{z}{R} \cdot \frac{S_u^{DSS}}{S_t} - \Delta U_{top} \quad (2.5)$$

where

$\gamma'$  = effective unit weight of soil

$z$  = depth in clay plug

$S_u^{DSS}$  = average undrained direct simple shear strength over the penetration depth

$S_t$  = sensitivity of the clay

$\Delta U_{top}$  = applied underpressure (relative to hydrostatic) at the top of the clay plug

After installation of the suction caisson the applied underpressure is turned off. It is a common assumption that the top of the suction caisson then is totally sealed, and that the underpressure at the top of the clay plug will be zero. Accordingly the mobilized friction along the skirt wall will be reduced to equilibrium with the submerged weight of the suction caisson. Since the friction usually is very small compared to the weight of the clay plug, the vertical total stress relative to seabed after installation is assumed to be:

$$\sigma_v = \gamma' \cdot z + u \quad (2.6)$$

The resulting horizontal total stress in the clay plug is then calculated from:

$$\sigma_h = \sigma_v - 2 \cdot \tau \quad (2.7)$$

The shear stress is determined from a triaxial extension test stress-strain curve. Figure 5 in Chapter 2.2 illustrates how the shear stress is determined at the vertical strain given by the actual caisson geometry (equation (2.4)).

Another important aspect during installation of the suction caisson is the generation of excess pore pressures. For the inner clay plug the excess pore pressure ( $\Delta u$ ) is given by:

$$\Delta u = \Delta \sigma_{oct} + \Delta u_\gamma \quad (2.8)$$

where

$\Delta \sigma_{oct}$  = change in octahedral total stress in the clay plug

$\Delta u_\gamma$  = generated pore pressure due to shear strains

The change in octahedral total stress in the clay plug can be expressed as:

$$\Delta \sigma_{oct} = \frac{1}{3} (\Delta \sigma_v + 2 \cdot \Delta \sigma_h) \quad (2.9)$$

where

$$\Delta \sigma_v = \sigma_v - \sigma_{v,c'} \quad (2.10)$$

$$\Delta\sigma_h = \sigma_h - K_0 \cdot \sigma_{v,c}' \quad (2.11)$$

and

$\sigma_v$  = calculated according to equation (2.5) or (2.6)

$\sigma_h$  = calculated according to equation (2.7)

$K'_0$  = lateral earth pressure coefficient

$\sigma_{vc}'$  = initial vertical in situ effective stress ( $\gamma' \cdot z$ )

Shear strain induced pore pressure ( $\Delta u_\gamma$ ) is determined from a triaxial extension test pore pressure – strain curve (Figure 5 in Chapter 2.2). Appurtenant strain is calculated according to equation (2.4). The shear induced pore pressure measurements in Figure 5 are adjusted according to pore pressure changes due to changes in octahedral stress.

Horizontal and vertical stress equilibrium and changes in pore pressure in the remolded zones are discussed in Chapter 2.2. The last contribution to changes in pore pressure is the remolding of the interface zones next to the skirt walls. Further soil testing (cyclic and static DSS test) or correlation with CPTU test can be used to assess the amount of excess pore pressure generated due to remolding. (Andersen & Jostad, 2004)



### 3 Problem

Evaluating consolidation settlement for suction caissons is a complex task. Important soil volume and parameters are directly affected by the installation process. Soil strength and stiffness are changed differently during penetration by self-weight and penetration by applied underpressure. For several subsea developments final consolidation settlements have been the critical design criterion.

The main problem to be addressed in this MSc thesis is; how do the installation and reconsolidation process of suction caissons affect undrained shear strength along the skirt wall and consolidation settlements? Focus should be on understanding the principles of consolidation analyses of suction caissons. In particular FEM analyses will be used to evaluate the modeled shear strength increase with time along the skirt walls and final consolidation settlements.

The aims for this MSc thesis are better understanding of soil behavior after installation of suction caisson, adequate prediction of final consolidation settlements and suggesting a modeling procedure to account for the increased shear strength with time.



## 4 Approach

An extensive literature review formed the basis for this MSc thesis. From the amount of relevant and substantiate literature it was evident that defining a set of premises from the beginning was crucial. Studying consecutive consolidation after installation of suction caissons with FEM analyses on a general basis was at first overwhelming. Consequently the calculations, FEM analyses, discussions and general work presented in this master thesis are based on the following main premises:

- Static vertical load (monotonic load situation)
- Simple caisson geometry without stiffeners
- Simplified installation procedure of the suction caisson (only penetration with applied underpressure)
- Uniform and homogenous soil profile (soft clay)

Introductory FEM analyses of a suction caisson applying initial stress situation according to the discussions in Chapter 2 and performing consolidation analysis provided basic conceptual understanding of the problem. However this was quite time consuming due to numerical challenges in the FEM model. General experiences with generating a functional FEM model are further described at the end of Chapter 4.1.

During the early stages of combined FEM analyses and search for literature on specific topics it was discovered a need for further understanding of the consolidation process and set-up of the remolded zones next to the skirt walls. Therefore it was decided to establish a simple model test in order to study the effect of reconsolidation (Chapter 4.2). Ideally it would contribute to making better assumptions for some of the less certain parameters in the FEM model. In the end the goal was to correlate some of the findings in the model test with some of the suggested assumptions in the FEM model.

### 4.1 FEM model of suction caisson

FEM code PLAXIS 2D version 2010.01 (PLAXIS, 2012) was used for the numerical consolidation analysis. The Soft Soil material model using stress dependent stiffness and failure criterion according to Mohr-Coulomb was preferred. Two dimensional axis symmetry analyses consisting of 859 15-noded soil elements were utilized in the FEM model. Figure 11 indicates the connectivity plot and model boundaries, eight times (8d) and twenty-four times (24d) the suction caisson diameter in width and depth respectively. Several square clusters surrounding the suction caisson tip was added to improve soil element geometry. Plate elements were used to model the suction caisson top lid and skirt wall. The material properties were determined by choosing a structural stiffness considerable higher than the soil stiffness, and being rigid enough to avoid large deflections of the steel structure (Table

3). Interface elements were added to make the skirt wall impermeable. However they were not switched on in the “staged construction interface” in order to avoid too slender elements in the relatively thin interface zones. The modeled interface zones next to the skirt wall had a thickness of 0.04 m. The load was applied on the suction caisson using a distributed load across the top lid. The total load was assumed to be 2500 kN.

Material parameters suction caisson	
Design load, L [kN]	2500
Caisson diameter, D [m]	5,0
Skirt wall thickness, t [m]	0,03
Axial modulus, EA [kN/m]	3,19E+12
Rigidity modulus, EI [kN/m <sup>2</sup> /m]	2,58E+08
Distributed weight plate elements, w [kN/m/m]	0
Distributed load, A-A [kN/m <sup>2</sup> ]	127,3

Table 3 Material parameters suction caisson (plate elements)

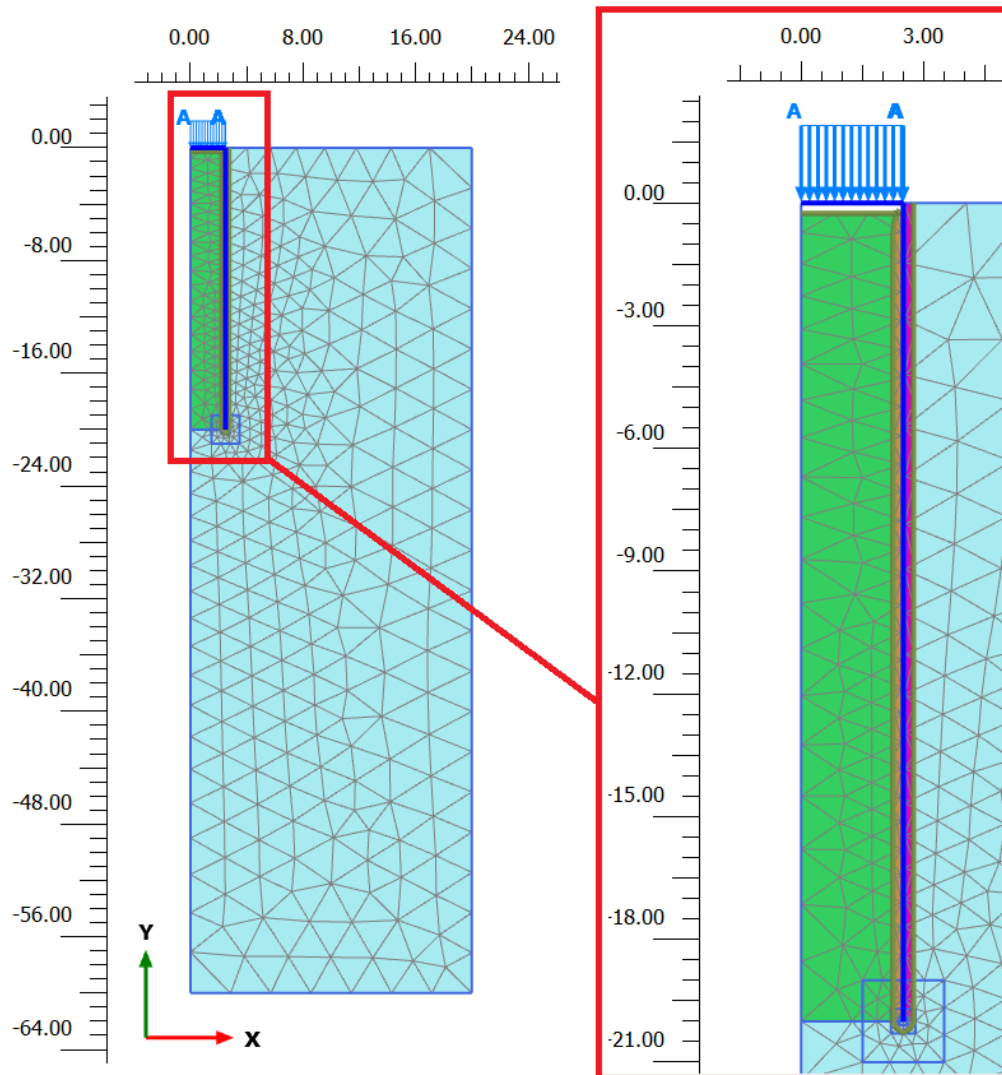


Figure 11 Connectivity plot and dimensions complete FEM model and detailed cut of the suction caisson (note: the interface zones are automatically scaled up by PLAXIS and displayed too large in this figure)



The soil consists of a homogeneous layer of soft clay. The clay plug and interface zones close to the skirt wall have updated soil properties to account for initial conditions and numerical convergence problems. Typical soil parameters for deep water soft clay from the west-coast of Africa was used (Appendix A). The built-in soil test functionality in PLAXIS was utilized to adjust the input parameters to correlate better with the available soil investigation data. The oedometer curves from the constant rate of strain (CRS) consolidation test were prioritized in order to obtain best possible soil deformation parameters (Figure 12). The stiffness from CRS oedometer test from depth = 6.7 m below seabed was used to determine a representative stiffness. Secondly the soil parameters were adjusted by correlation between the shear strength obtained by an undrained triaxial test (TxCuD) according to the suggested undrained shear strength profile (Figure 13). Total overview of the soil test correlation is given in Appendix B. Evaluation of actual modeled undrained shear strength based on generated effective stress state in PLAXIS is discussed in Chapter 5.1.

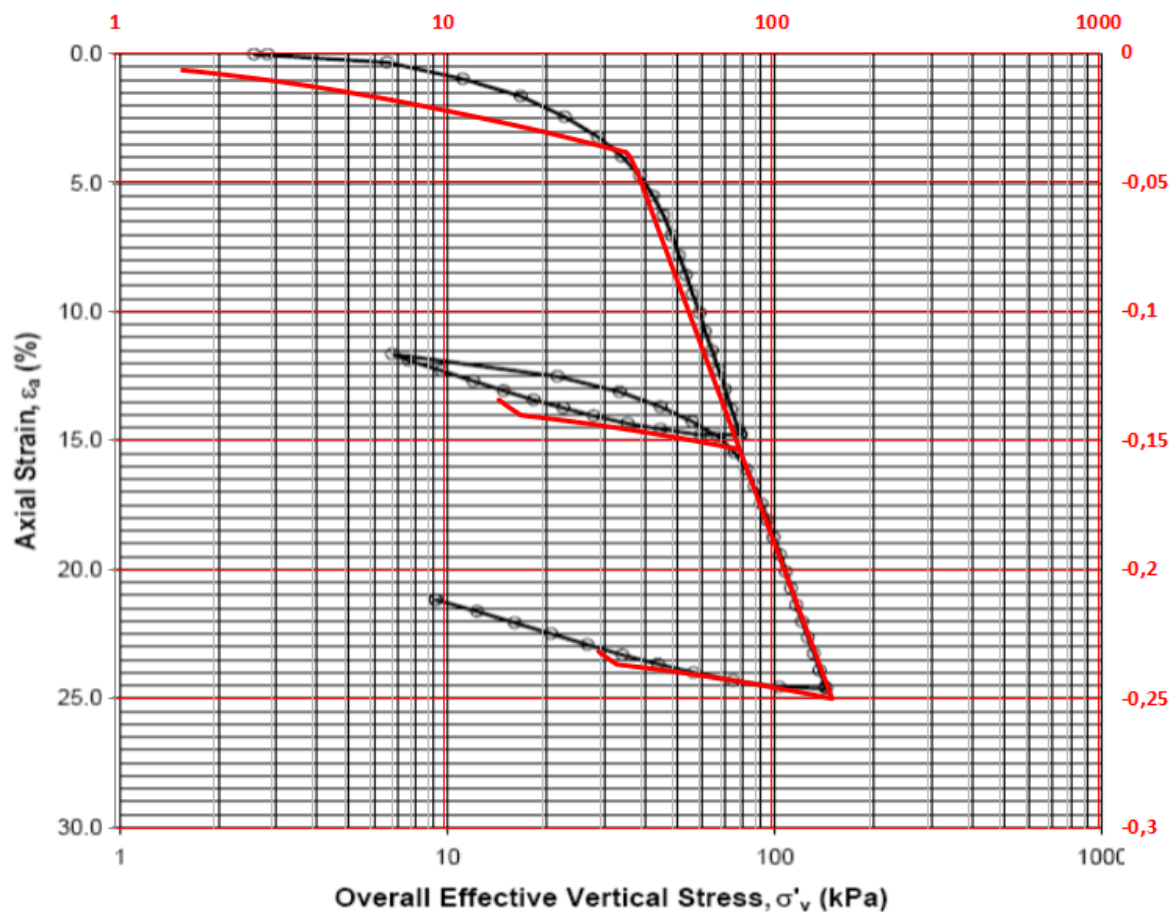


Figure 12 Constant rate of strain consolidation test correlation from PLAXIS soil test

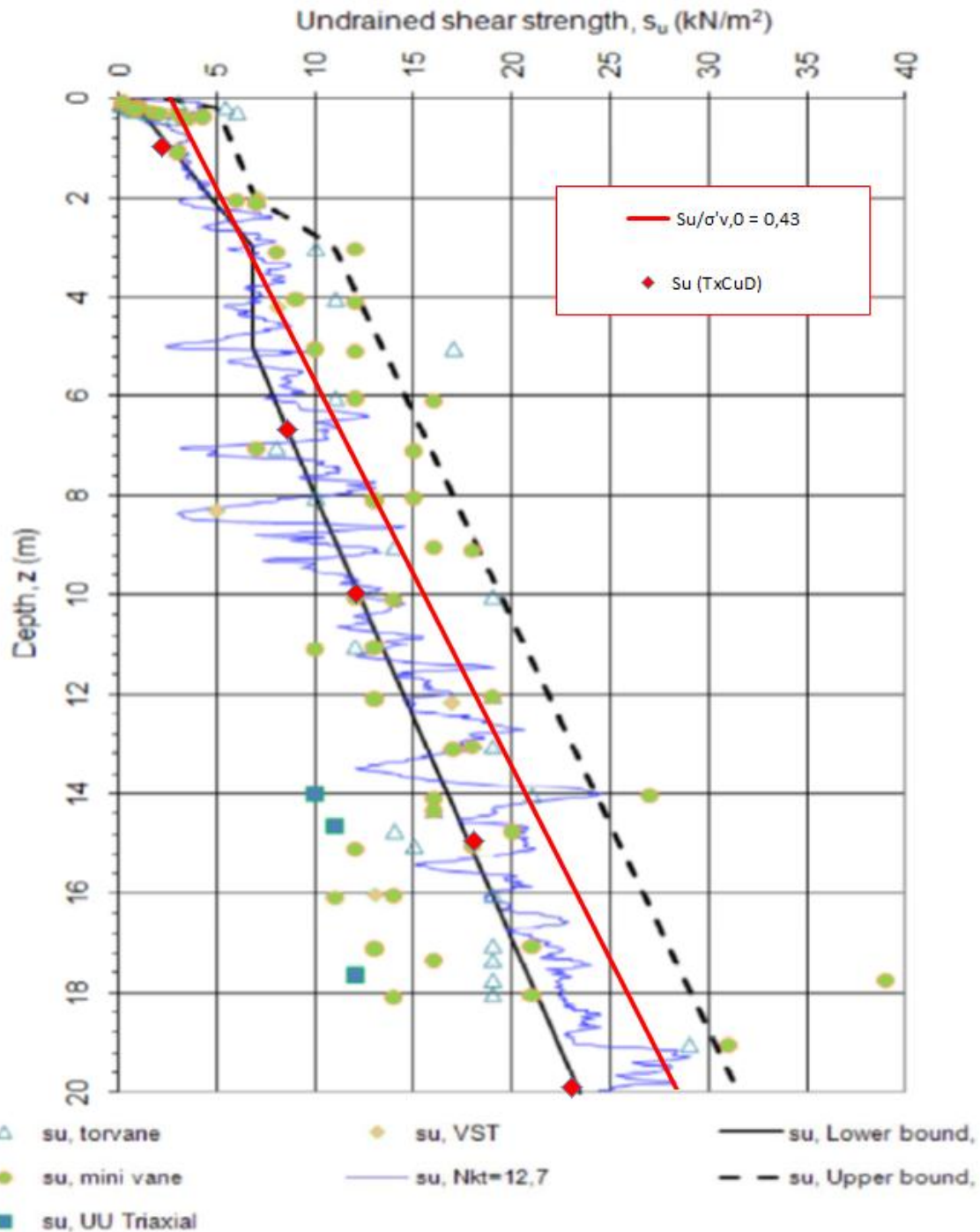


Figure 13 Undrained shear strength values from TxCuD in soil test plotted versus suggested undrained shear strength profile

From the soil investigation data (Appendix A) and correlation with original test data and soil test in PLAXIS (Figure 12 and Figure 13) the general clay parameters utilized in the soft soil material model are given in Table 4. The unloading-reloading Poisson ration ( $\nu_{ur}$ ) is often assumed to be between 0.10-0.20 for soft lightly overconsolidated clays, and a  $\nu_{ur} = 0.15$  was used for all of the FEM analyses. The lateral earth pressure coefficient for normally consolidated clay is calculated from Jaky's formula ( $K_0^{nc} = 1 - \sin(\phi)$ ) (Jaky, 1948).

Clay parameters soft soil material model	Surrounding clay & clay plug	Interface zones
Effective unit weight soil, $\gamma'$ [kN/m <sup>3</sup> ]	3	3
Virgin compression ratio, $\lambda^*$ , $\lambda^*$ [-]	0,148	0,136
Recompression ratio, $\kappa^*$ , $\kappa^*$ [-]	0,014	0,019
Cohesion, $C'_{ref}$ [kPa]	1	2
Friction angle, $\phi'$ [°]	39,5	8
Dilation angle, $\psi$ [°]	0	0
Poisson ratio unloading-reloading, $\nu'_{ur}$ [-]	0,15	0,15
Lateral earth pressure coefficient (NC), $K_0^{nc}$ [-]	0,36	0,86
Lateral earth pressure coefficient (in situ), $K'_0$ [-]	0,45	0,45
Horizontal permeability, $k_x$ [m/day]	2,01E-04	2,01E-04
Vertical permeability, $k_y$ [m/day]	1,54E-04	1,54E-04

**Table 4 Clay input parameters for the soft soil material model**

According to the deduction in Chapter 2 the installation of the suction caisson creates three main zones; the clay plug, the interface zone inside the skirt wall and the interface zone outside the skirt wall. The effect of the installation process is embedded in the initial stress generation in the FEM model. For the inner clay plug the excess pore pressure generated is calculated by formula (2.8). In order to account for the remolding of the inner interface zone additional excess pore pressure is added. The remolding induced pore pressure is estimated from static DSS test to high strains and the relation between undrained shear strength and OCR (Figure 6). Due to the high water content and plasticity the average value from the static DSS test was assessed more representative compared to the relation with undrained shear strength. For less plastic clays with higher effective unit weight and/or lower normalized undrained shear strength profile ( $S_u/\sigma'_v < 0,43$ ) the CPTU measurements may be more emphasized. During penetration with applied underpressure generation of excess pore pressure in the outer interface zone is assumed to be only due to remolding of the clay.

In general, soil properties in the FEM model can be adjusted to incorporate the effect of initial stress and pore pressure changes after complete installation of the suction caisson. For the soft soil model incorporated in PLAXIS (PLAXIS, 2012) the following adjustments were done:

$$K'_{0,up,plug} = \frac{\sigma_{h,up} - u_{up}}{\sigma_{v,up} - u_{up}} = \frac{\sigma_{v,0} - 2 \cdot \tau - u_{up}}{\sigma_{v,0} - u_{up}} \quad (4.1)$$

$$K'_{0,up,rem} = K'_{0,up,plug} + \frac{u_{up,plug} - u_{up,rem}}{\sigma'_{v,0}} \quad (4.2)$$

$$OCR_{up} = \frac{OCR_0}{(1 - \frac{\Delta u}{\sigma'_{v,0}})} \quad (4.3)$$

Complete derivation of formula (4.1), (4.2) and (4.3) is given in Appendix E. The  $K'_0$  is updated to account for the change in horizontal effective stress due to the increase in pore pressure. Since the soft soil model is dependent on the OCR, it is updated to account for the increase in pore pressure in the initial phase stress generation. In the remolded zones the stress history is assumed to be “reset” due to the remolding of the clay, hence  $OCR=1$ . Based on the idea of no outward soil displacement during ideal conditions  $K'_0$  is not updated in the outer interface zone.

Input data used to calculate the adjusted initial stress generation is given in Table 5. An average value for OCR and  $K'_0$  was determined directly from the available soil investigation data. The shear stress at maximum vertical strain and shear strain induced pore pressure was derived from the triaxial extension test at depth = 21.6 m. These values were assumed to be most representative since it presented data at the necessary strain level and experienced localized necking at a later stage compared to the shallower test specimens. Correction of shear induced pore pressure due to the octahedral stress changes in the triaxial test is derived in Appendix A.

Input for updated soil parameter calculations	
OCR [-]	1,7
$K'_0$ [-]	0,45
Shear stress at maximum vertical strain, $\tau/\sigma'_{v,0}$ [kPa]	-0,10
Shear strain induced pore pressure, $U_\gamma/\sigma'_{v,0}$ [kPa]	-0,05
Remolding induced pore pressure, $\Delta U/\sigma'_v$ [kPa]	0,58

**Table 5** Input data for adjusted initial stress generation calculation

Table 6 present the updated input parameters for the clay plug and the two interface zones.

Parameter	Clay plug	Inner interface zone	Outer interface zone
Radial strain, $\epsilon_r$ [%]	1,20	1,20	-
Vertical strain, $\epsilon_v$ [%]	-2,40	-2,40	-
Octahedral total stress change, $\Delta\sigma_{oct}/\sigma'_{v,0}$ [kPa]	0,50	0,50	-
Shear strain induced pore pressure change, $\Delta U_\gamma/\sigma'_{v,0}$ [kPa]	-0,05	-0,05	-
Remolding induced pore pressure, $\Delta U/\sigma'_v$ [kPa]	-	0,58	0,58
Excess pore pressure, $\Delta U/\sigma'_{v,0}$ [kPa]	0,45	1,03	0,58
Updated $K'_0$ , $K'_{0,up}$ [-]	1,36	0,78	-
Updated OCR, $OCR_{up}$ [-]	3,10	1,00	1,00

**Table 6** Updated parameters for the different zones

The generation of pore pressure in the initial phase was done by specifying user defined pore pressure distributions in the clusters representing the three updated zones (Appendix

B). General phreatic level defined the pore pressure distribution in the rest of the model. These settings were reset in the simulation stages following the “equilibrium phase”, and general phreatic level defined pore water pressure distribution in the complete model. This ensure that the numerical model consolidate to an original pore pressure distribution prior to suction caisson installation. An overview of the general simulation procedure is given in Table 7.

#	Identification	Calculation type (PLAXIS)	Comment
1	Initial phase	$K'_0$ -procedure	User defined pore pressure (p.p.)
2	Equilibrium phase	Plastic, staged construction	User defined pore pressure (p.p.)
3	Add load	Plastic, staged construction	General phreatic level p.p.
4	Consolidation	Consolidation, staged construction	Sufficient time interval (20 years)

**Table 7 Simulation procedure in FEM (PLAXIS)**

Some important aspects when analyzing final consolidation settlement on a real suction caisson case have been simplified in this MSc thesis. Martinez et. al (2009) emphasized the importance of modeling correct soil behavior with respect to interface zone thickness, remolded undrained shear strength and remolded stiffness parameters. This is further discussed and exemplified in Chapter 5.1 (Figure 20). Based on the absence of soil data and aims for the MSc thesis remolded stiffness in the interface zones have been neglected (intact stiffness applied). Additionally the thickness of the remolded zone was assumed to be 0.04 m without further assessment. The lower bound estimates for undrained shear strength (completely remolded) were used in the remolded zones. Permeability is often considered to be significantly different in remolded material compared to the in-situ condition. However this is not accounted for in the FEM analyses. According to the discussions in Chapter 2 installation procedure strongly affects the soil displacement. Additionally the suggested calculation procedure for penetration analysis is given (see Appendix C for detailed calculation sheet). However a simplified installation procedure with applied underpressure during all stages of the penetration is assumed. This translates to the aim of understanding the effect of this installation procedure quite unique to suction caissons. Self-weight penetration is relatively well documented through work done on piles, as well as the process is more intuitive with respect to soil displacement and stress changes. For comparison one FEM analysis considering a complete penetration procedure (both self-weight and applied underpressure) has been performed (Case 3, Figure 20).

During initial construction and trial of the FEM model the author experienced some unexpected difficulties. In the early stages there seemed to be difficult to run analysis with the relatively slender elements generated in the interface zones (as a consequence to the small thickness). Alternative methods for modeling the interface zones were considered, unfortunately without sufficient success. This process was quite time consuming and distracting, and in the end the numerical problem was solved by applying a small cohesion to

the material input parameters. The FEM model's very high sensitivity to such an adjustment was somewhat surprising.

During the later stages of the MSc thesis better conceptual understanding of the problem and model procedure revealed some faulty assumptions and small errors with quite large impact on the estimated settlements. Somewhat comprehensive understanding and assessment of the material model's behavior and features was needed to ensure best possible results. The application of cohesion ( $c'$ ) in the soft soil model is discussed in Chapter 5.1, and the importance of understanding the input and output of the FEM model is highlighted.

Other practical aspects are the user interface and appurtenant zoom functionality in the PLAXIS software. With model dimensions approximately 500 times larger than the thickness of the interface zones (with respect to width) changing and operating the interface zones were quite impractical. In order to be able to select the interface zone clusters both in the input and calculation ("define") interface the clusters had to be temporarily expanded. After the adjustments to soil parameters, cluster material or pore pressure generation input had been completed, the cluster size was reset to correct dimensions before running the FEM analysis. This made small adjustments to the FEM model quite time consuming.

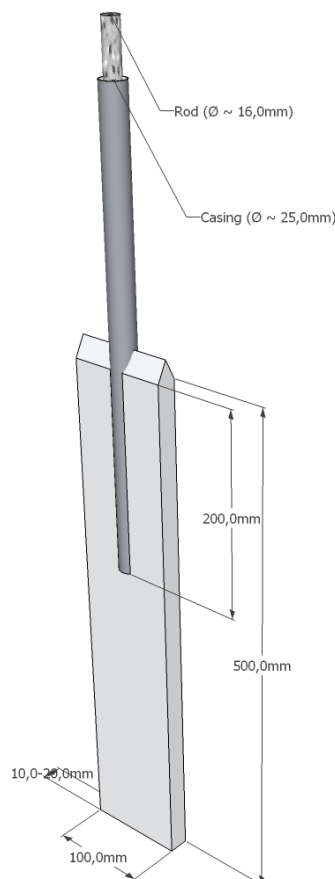
## 4.2 Model test

The need for in-situ measurements of stress and strain during installation and subsequent consolidation of a suction caisson has been stressed by several articles referred to in the literature review (Chapter 2). Several possibilities were conducted during the early stages of the MSc thesis. Both the use of actual downscaled geometry in the laboratory as well as large scale in-situ plate test were considered. However it was in the end decided to keep the model test as minimalistic and simple as possible due to time and cost assessments. Therefore a simple set-up on plate in soft clay model test was designed. The general idea was to underline some of the assumptions that form the basis for the FEM analysis. In short the main aims for the model test were to investigate the following hypothesis (assumptions):

1. Plate (skirt) thickness and amount of displaced soil will have significant impact on the reconsolidation time as well as final set-up factor.
2. Set-up effect on the remolded zone is closely related to thixotropy at an early stage.
3. Effects related to consolidation will dominate the influence on set-up after necessary elapsed time.

Figure 14 indicates the design of the model test equipment. The 20 individual plate systems were designed with a common plate height of 500 mm and a plate width of 100 mm. For investigation purposes two different plate thicknesses were used (10 mm and 20 mm). The rod and casing was used for installation purposes. Installation with a casing ensures enough capacity with respect to bending moment. This is important to make sure the plates are

installed in a satisfactory vertical position and to avoid decisive deflections. Additionally the casing avoids significant influence of rod resistance by pre-pulling the casing before lifting and measuring resistance of the rod and plate. Any influence of soil-rod interaction is then assumed to be insignificant compared to the plate side friction resistance. Initially the design included tapered upper end of the plate to minimize the influence of point end bearing capacity, however this was not included in the final design. The steel plates were made from crude hot rolled steel (S235 JR) and had no initial treatment, neither significant corrosion compared to anticipated corrosion on suction caissons prior to installation. Initial design of the model test equipment is given in Appendix G.



**Figure 14 Model test equipment design**

After conducting a soil investigation at the desired test area at Tiller (Trondheim) the appropriate installation depth of 3.5 m was decided, implying a rod and casing length of approximately 3 m. All of the plate arrays were installed simultaneously, at least in perspective to consolidation time in the soft clay. Figure 16 indicates the installation pattern and numbering of the individual plate systems. At given intervals one plate of each thickness was tested (pulled upwards) while measuring the resistance. The old geotechnical soil investigation rig at the Geotechnical Division was utilized. Since there was no automatic adjustment of upward vertical movement rate an approximately constant speed was manually controlled. Further comments are made to the interpretation of the test results. A portable load cell device and preconfigured software ensured correct reading of resistance. The data is presented in time-force (t-f) plots. Based on the progression and apparent

reconsolidation process the time intervals were assessed throughout the test period. The results are further discussed together with all available data from the model test in Chapter 5.3.



Figure 15 Model test equipment pre-assembled (left hand side), ready for installation (in the middle) and ready for testing (right hand side)

**Installation pattern**

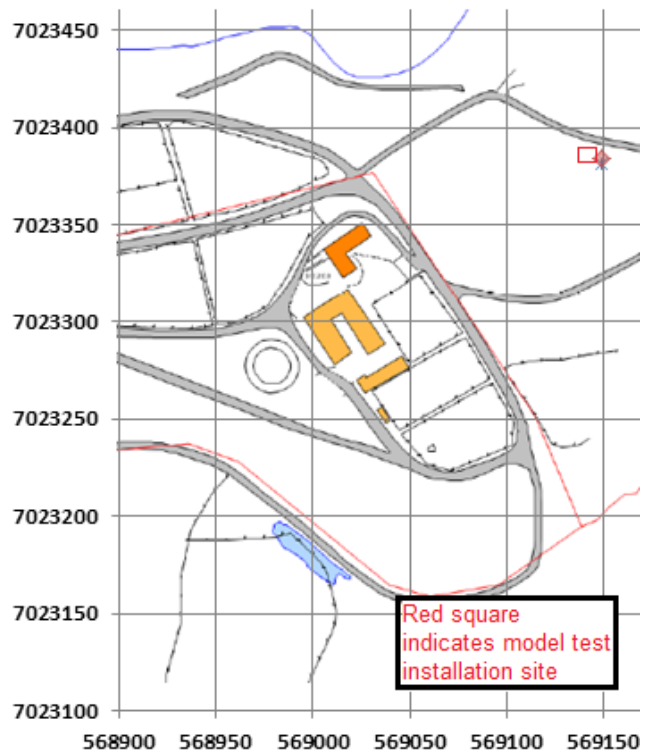
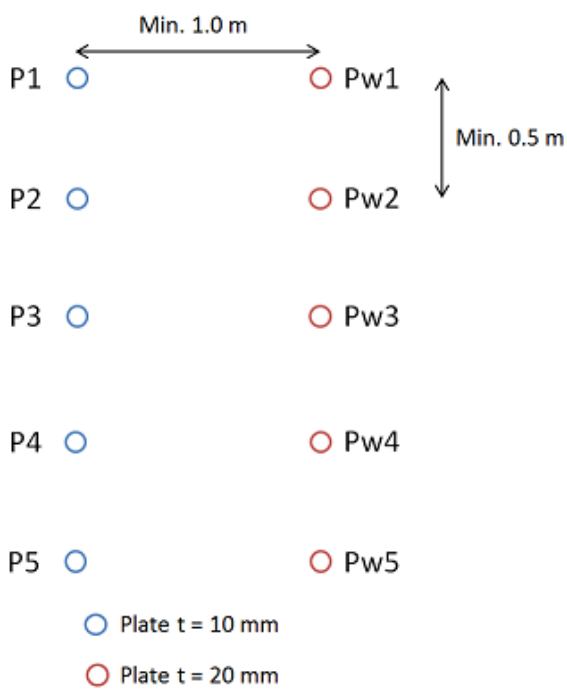


Figure 16 Model test installation pattern and detailed map indicating model test installation site



The simple model test with has some notable limitations that are important to consider when evaluating the test results. An important aspect dealing with reconsolidation is time. Due to several delays in the process of creating the model test equipment the maximal time from installation to testing was invidiously short. However the model test results give an indication of the reconsolidation with time during the early stages of consolidation. Since the resistance is measured at the top of the rod influence of possible installation flaws, rod resistance and point end bearing capacity at the top of the plate have to be evaluated. Adjusting the data for measured simple rod resistance and possibly assumed bearing capacity could isolate the increase of side friction with time. Plain strain conditions are assumed when designing and calibrating the test results, assuming insignificant three dimensional effects. This is believed to give decent results, but abnormalities in the eventual test results could originate from such effects. Impact and evaluation of these aspects in relation to the model test results is discussed in Chapter 5.3.

Originally back calculation of the model test results utilizing FEM analysis was planned. This could couple the assumptions in the FEM analysis with model test results. Further correlation and adjustments could increase understanding and viability of the assumptions. Due to the model test delays and consequently relatively short model testing time period it was aborted. Primarily the short time aspect is thought to make the results too rough for correlation with FEM analysis and hence the results to uncertain. However the extensive documentation of soil properties through the soil investigation including CPTU and oedometer tests origin from this idea. Adding additional advanced soil tests (TxEuD and CRS on remolded soil) would make these data a good basis for correlative FEM analysis.

#### 4.2.1 Soil investigation

The model test site at Tiller in Trondheim (Figure 17) has been used by the Geotechnical Division at NTNU for several years. Sandven (1990) conducted a series of CPTU tests in the same area, and the Geotechnical Division has an extensive soil investigation booklet with index-, oedometer- and triaxial test results. In general the soil profile consists of relatively homogenous layers of dry crust, relatively stiff silts, soft moderately overconsolidated clays and quick clay. The quick clay appears at a depth of approximately 7 m, while the layer of moderately overconsolidated soft clay reaches from approximately 3-7 m. The clay layers are quite sensitive ( $S_t > 5-10$ ) and increasing rapidly in the transition zone towards quick clay.

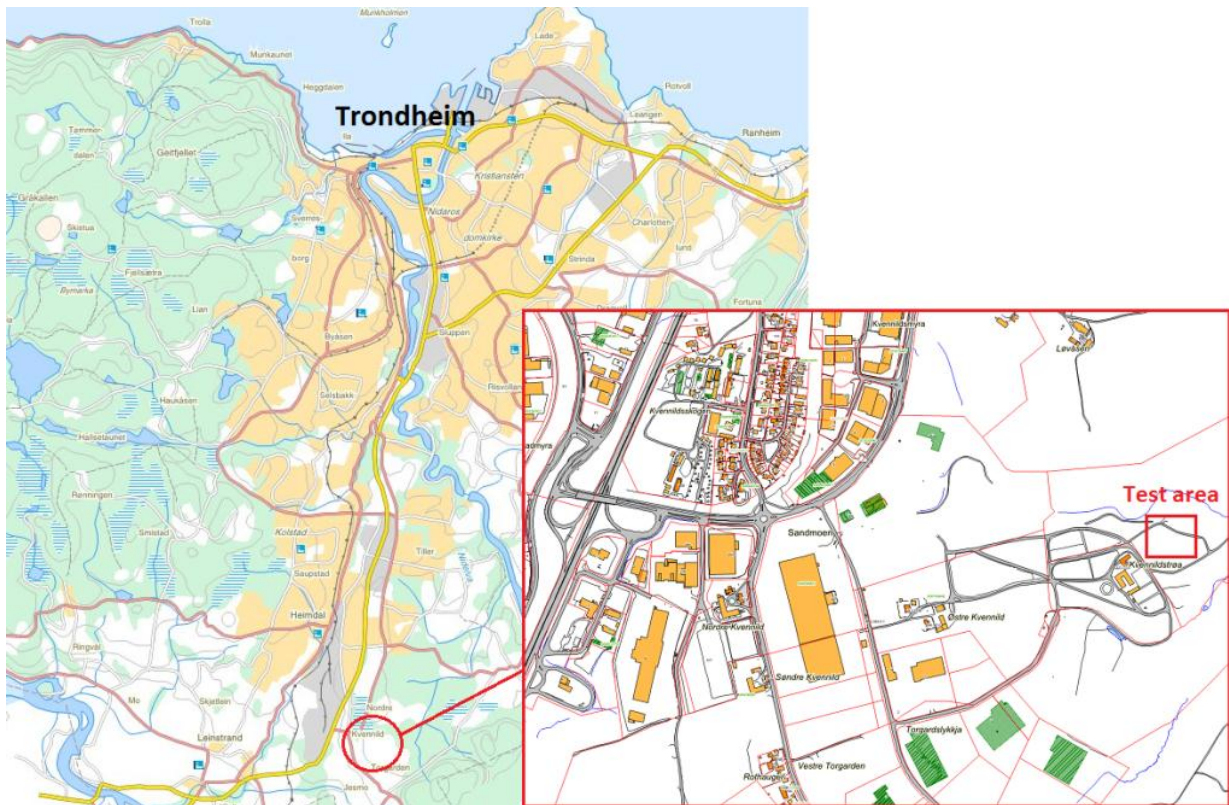


Figure 17 Overview of Trondheim marked with test area at Tiller

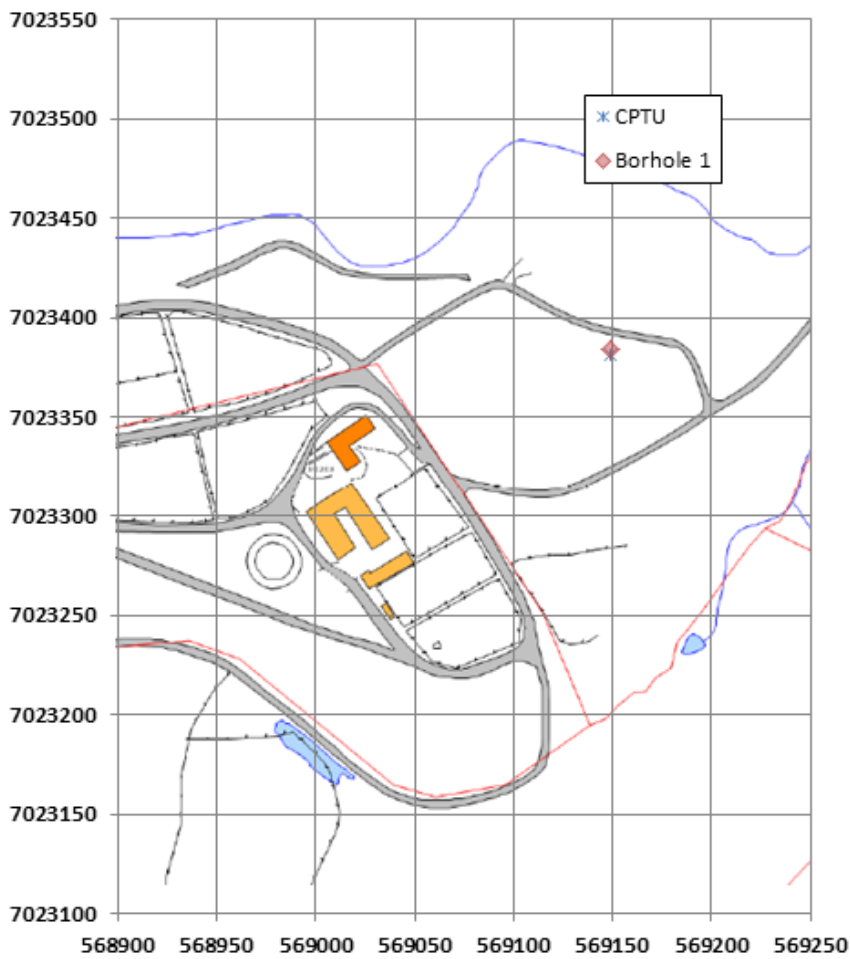


Figure 18 Detailed map with coordinates of soil investigation area

In cooperation with another technology student also working on his MSc thesis which included model testing in the same area, a soil investigation was planned and executed. The most critical parameters for the “set-up” model test was undrained shear strength, sensitivity, water content, plasticity limits and unit weight. With respect to this the basic routine soil investigation contained:

- Unconfined uniaxial tests
- Triaxial tests
- Oedometer tests
- Water content
- Liquidity index
- Plasticity index
- Fall cone tests
- Pycnometer (relative density) tests

Four soil specimens were extracted and index testing performed in 0.8 m intervals from 0.0-3.8 m. Additionally a CPTU test was executed for additional basis of comparison with the undrained shear strength profile suggested by index test result.

Lightly overconsolidated soft clays are often representative for deep water soil profiles. The soft clay at Tiller is slightly too sensitive and overconsolidated for a perfect fit. However it is believed that the effect of reconsolidation also is representative for less sensitive and overconsolidated clays. In general the soil samples from Tiller were of good quality, and seemed to be quite homogenous and undisturbed (with exception of the sample from the dry crust including buildup of frozen peat from the winter). One of the triaxial tests indicated a somewhat disturbed sample. Unfortunately there were also some complications when consolidating this sample (delayed registration of increase in cell pressure) that makes it hard to conclude on the sample quality directly. Despite this indication the rest of the index tests seemed to correlate very well with older test results as well as the other soil samples. All test results from the soil and field investigation is given in Appendix F.

#### 4.2.2 Thixotropy test

As discussed in Chapter 2 thixotropy is gain in shear strength with time despite no volumetric changes. It is an important part of the set-up effect in early stages of reconsolidation. For correlation and comparison purposes it was decided to conduct a simple thixotropy test with the fall cone test.

Another soil sample from Tiller at the depth of installation of the model test (3.0-3.8 m) formed the basis of 10 fall cone test samples. The soil sample was divided into 13 test specimens. Three of the pieces (from the top, middle and bottom) was used to determine average undrained shear strength for the soil sample, and used for plasticity testing. Additionally water content was also measured across the sample to make sure the sample

was representative compared to the other soil test in Chapter 4.2.1. Secondly the 10 pieces used for the fall cone thixotropy test were satisfactory remolded before the remolded undrained shear strength was tested. The test pieces were then stored in standard plastic cups (water and air tight) in a storage refrigerator (Figure 19). A small piece of saturated paper was added between the soil sample and the plastic lid in order to avoid any dissipation of pore water (consolidation). At given time intervals the undrained shear strength was determined by a fall cone test on the stored test specimens.



Figure 19 Remolded sample stored in plastic cup prepared for thixotropy fall cone test

Originally the idea was to use the same time intervals for the thixotropy test as for the model test. Due to the delay of the model test it was however decided to run the thixotropy test separately, with reasonable time intervals. Appendix H includes all the data from the thixotropy test.

## 5 Results and evaluation

The general idea was to compare the output from the FEM analyses with the data available from the model test. Correlation between model test results and FEM analysis of the actual model test would form the basis of discussion for some of the different assumptions made in the “real case” analysis. However delay of the model testing made correlation of test results with FEM analysis of the model test impossible. This idea was abandoned and emphasis was placed on evaluating the available FEM analysis output. If possible the model test results were used to underline different aspects of the FEM model. Chapter 5.1 first presents some introductory FEM analyses. Secondly general aspects of FEM analysis of suction caisson installation and consolidation process, as well as experiences during FEM modeling with respect to different parameters and modeling principles are discussed. Subsequently Chapter 5.3 presents the model test results and general discussion of applicability for assessing different assumptions in the FEM model.

### 5.1 FEM analyses

Initially a series of FEM analyses was carried out to put final consolidation settlement estimates in perspective with different assumptions (Table 8). Figure 20 indicates the results of the FEM analyses. Base case 1 is a reference analysis assuming no initial stress changes or material parameter updates prior to the loading and consolidation of the suction caisson. This situation is not realistic with respect to a normal installation process. However it gives a lower bound value and highlights the effect of adding the design load to a similar preinstalled and completely reconsolidated foundation structure. Estimated settlements of approximately 10 times less than the upper bound estimate (Case 5) underline the effect of installation and initial changes of stresses and soil properties.

Comparing base case two with case four and five indicate how the remolded interface zones influence consolidation settlement. The effect of only updating initial soil parameters and stress properties in the clay plug (inner interface zone embedded as the clay plug) is hardly noticeable when comparing base case one and two. However adding interface zones (Case 4 and 5) have a significant effect on the final consolidation settlements. Although the installation procedure in general was simplified (assumed applied underpressure during the complete installation) a more advanced FEM analyses incorporating both self-weight and suction penetration was performed (Case 3). In short the simplified installation procedure is somewhat conservative. Self-weight penetration would generate different excess pore pressure distribution due to installation and allow for buildup of higher horizontal stresses along parts of the skirt wall, consequently reducing final consolidation settlement.

Initial vertical displacement during undrained loading between simulation case four assuming intact undrained shear strength in the interface zones ( $S_u^{DSS}$ ) and case five utilizing

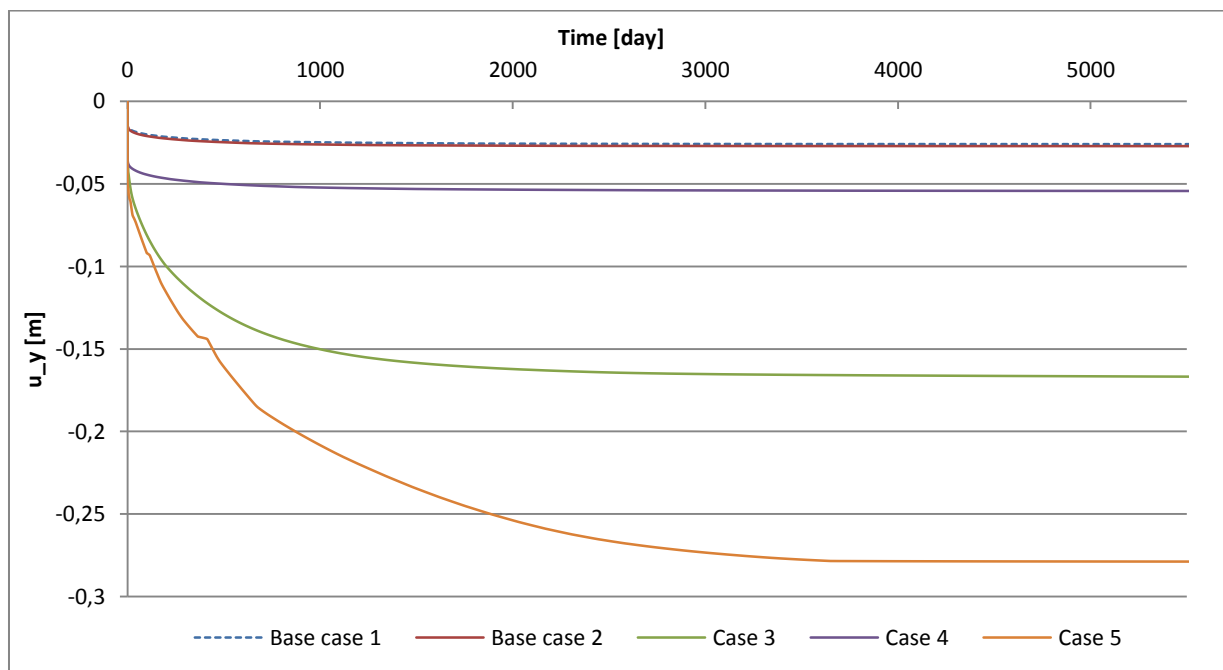
remolded undrained shear strength ( $S_{u,rem}$ ) reveal an expected pattern. Case four experiences lower initial vertical displacement than case five due to higher undrained shear strength in the remolded zones, hence also mobilization of more surrounding soil. Development of final consolidation settlement also compares very well with initial expectations with case five being the most conservative.

Case 5 was used for all further analyses, interpretation and evaluation of different aspects regarding the FEM analysis.

Simulation case	Aberration from soil parameter updates described in Table 5 and Table 6		
	Clay plug	Inner interface zone	Outer interface zone
Base case 1	No updates applied	No updates applied	No updates applied
Base case 2	-	Updated according to the clay plug	No updates applied
Case 3	Combined penetration analysis (self-weight and underpressure)*	Combined penetration analysis (self-weight and underpressure) *	Combined penetration analysis (self-weight and underpressure) *
Case 4	-	$\phi' = 39.5^\circ$	$\phi' = 39.5^\circ$
Case 5	-	-	-

**Table 8 Aberration from original updates for the initial simulation cases**

\* Complete input data for the FEM analysis is described in Appendix D



**Figure 20 Settlement of suction caisson center point for the initial FEM analyses**

### 5.1.1 Initial stress generation

In accordance with the deduction in Chapter 2 and the described procedure in Chapter 4.1 evaluation of the output from the initial stress generation is important. During penetration with applied underpressure all displaced soil is assumed to move inside the suction caisson

leaving the surrounding soil intact (except for the thin remolded zone). The initial stress generation in the FEM code is based on the assumed stress state just after completed installation. Secondly the design load is applied generating excess pore pressure and stress changes with time during consolidation. During phase 2 (Table 7) equilibrium with respect to the effective stress generation in the initial phase ( $K'_0$ -procedure) and applied pore pressures is achieved. This stress state must be verified to ensure that the FEM model is adequately correct.

Figure 21 display the initial stress conditions after phase 2 in the FEM analysis. The generated pore pressures are consistent with the applied pore pressure for the clay plug and inner interface zone. Comparing the pore pressure distribution for the outer interface zone with the distribution in the clay plug it is obviously smaller than the specified pore pressure. Additionally it is too low since the pore pressure for the inner interface zone should equal the sum of the two contributions. This is explained in Figure 22 were pretty large excess pore pressures (suction) is generated in the outer interface zone, as well as a small contribution in the clay plug. For the inner interface zone a slight excess pore pressure (overpressure) is generated. The excess pore pressures are a result of a non-equilibrium state during application of initial pore pressure and stresses.

The vertical total stress inside the clay plug is approximately equal to the vertical total stress prior to installation. In the interface zones the results show a slight increase (inner interface zone) and decrease (outer interface zone) in total vertical stress. Total horizontal stress is in equilibrium between the clay plug and inner interface zone. However it is higher compared to the surrounding soil, generating radial stress on the skirt wall. Additionally the horizontal stress in the outer interface zone is equal the in-situ value (reference value at  $x = 20$  m) with exception of some abnormalities at the skirt tip. The soil tends to swell both inside the suction caisson as well as outside the skirt wall. For the soil inside the suction caisson the magnitude of swell and generated excess pore pressures are negligible. In the outer remolded interface zone the remolding process is comparable with filling an imaginary predrilled hole in the ground with a heavy liquid ( $\gamma = 13 \text{ kN/m}^3$ ). This would generate an isotropic stress condition implying an increased total lateral earth pressure coefficient (approximately  $K_0 = 1.0$ ) and higher total horizontal stress. This generates significant suction in the lower part of the outer interface zone ( $U_{\text{suction}} \approx 24 \text{ kPa}$ , Figure 22). However it is quite small to the generated excess pore pressures during undrained loading and the influence on the final results is believed to be minor.

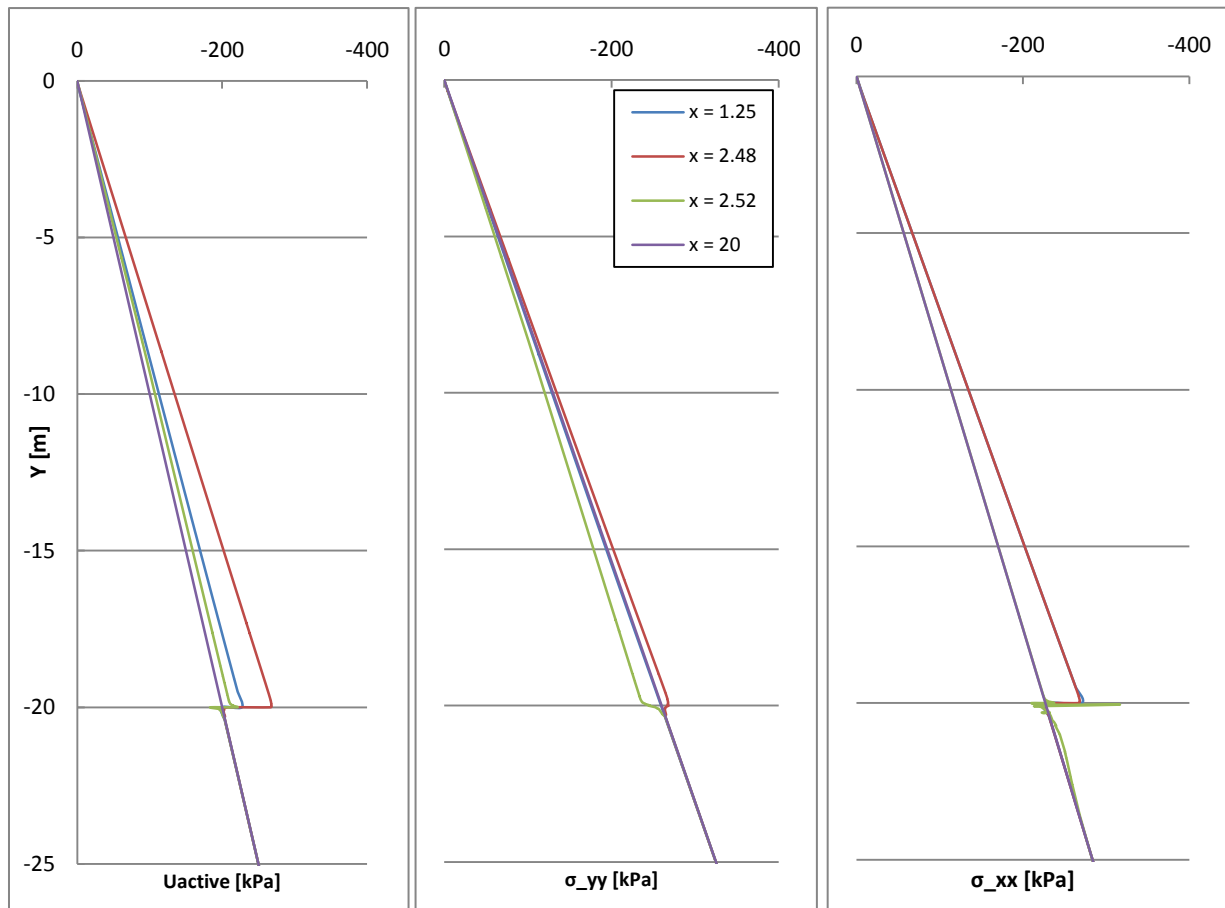


Figure 21 Pore pressure ( $U_{active}$ ), vertical ( $\sigma_v$ ) and radial total stresses ( $\sigma_r$ ) after initial stress generation

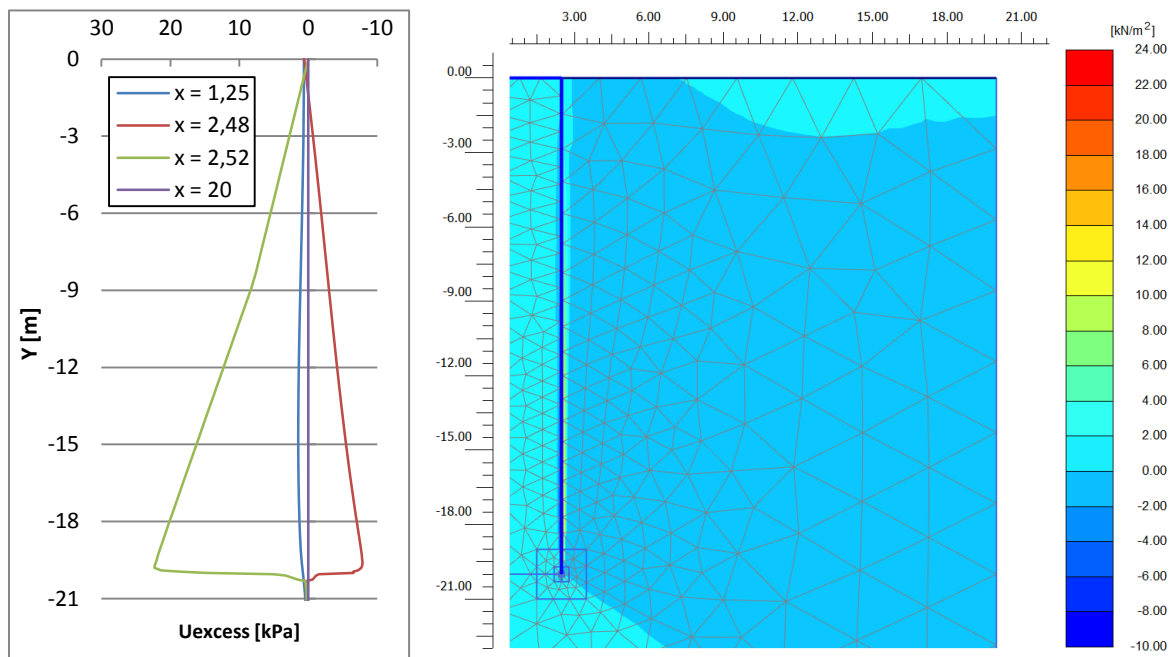
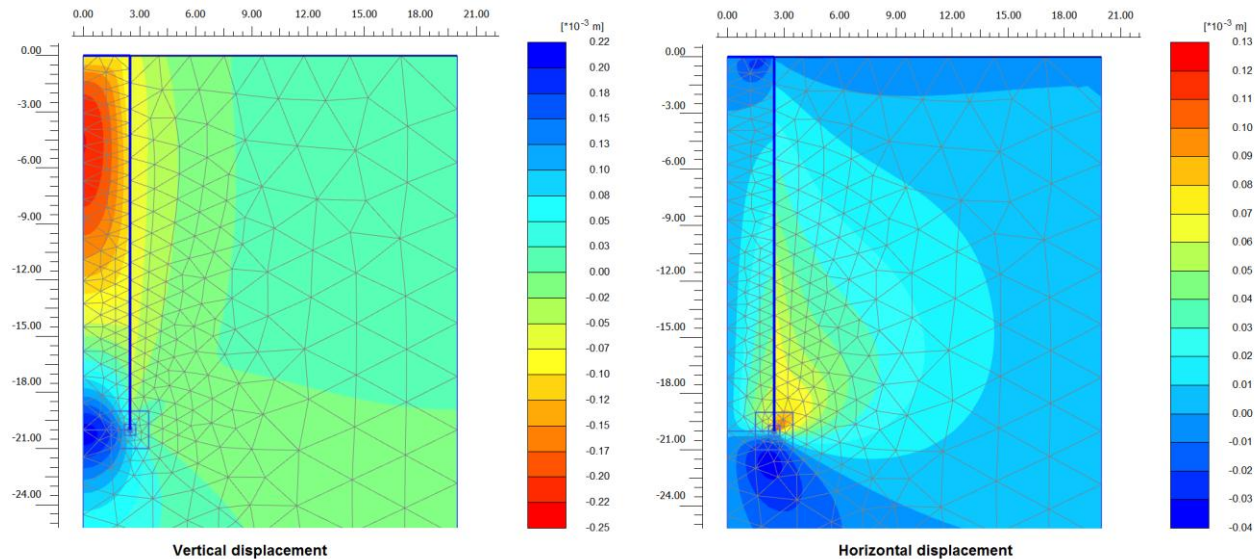


Figure 22 Excess pore pressures from initial stress generation

Figure 23 indicate vertical and horizontal displacement during initial stress generation. In conformity with the deviation in initial stress generation and generation of excess pore pressure the displacements are related to inaccuracies in the FEM model. All assumptions of displacement and stress changes due to installation of the suction caisson are accounted for



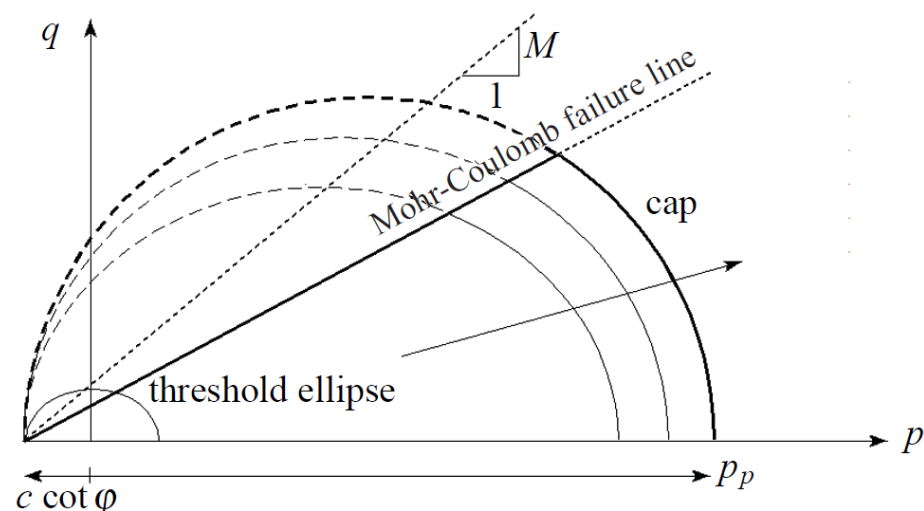
and supposed to be embedded into the initial stress generation. The horizontal displacements indicate swelling of the soil outside the skirt wall. Below the skirt tip a counter movement due to the undrained behavior comes into being. Comparable displacement paths apply for the vertical displacements as well. However the displacements in the equilibrium phase are very small (less than 0.3 mm), hence the impact on the final results are most likely small.



**Figure 23 Vertical and horizontal displacement during initial stress generation**

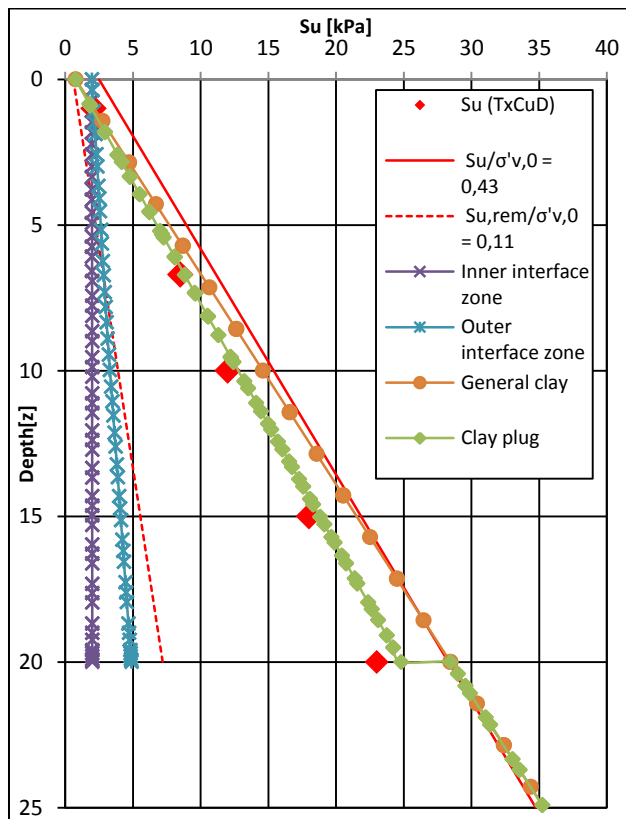
Despite of the initial correlation between the modeled soil behaviors in Soil Test and available soil investigation data (TxCuD plot versus undrained shear strength profile) actual modeled undrained shear strength should be validated. The soft soil material model utilizes a perfectly-plastic Mohr-Coulomb type yield function to model the failure state. Figure 24 illustrates the Mohr-Coulomb failure criterion in the  $p'$ - $q$  – plot. In general the Mohr-Coulomb criterion in the  $p'$ - $q$  – plot is given by:

$$S_u = \tau_{max} = \cos \varphi \cdot c' + \left(\frac{\sigma'_x + \sigma'_y}{2}\right) \cdot \sin \varphi \tag{5.1}$$



**Figure 24 Yield surface of the Soft Soil model in  $p'$ - $q$ -plane including Mohr-Coulomb failure criterion (PLAXIS Manual)**

From equation (5.1) the undrained shear strength profile has been calculated from the effective stresses given by PLAXIS after phase 2. The result is compared against the design undrained shear strength profile (Figure 25).



**Figure 25 Undrained shear strength calculated from effective stresses during initial stress generation**

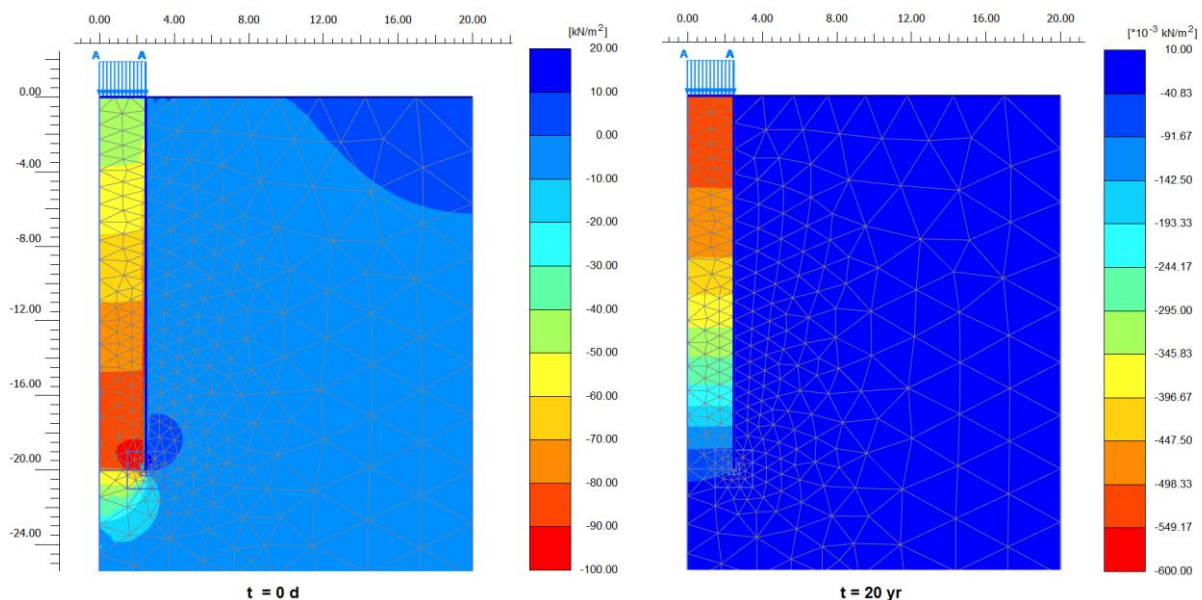
For the clay plug and general clay the modeled undrained shear strength is somewhat lower than the average design undrained shear strength ( $S_{u}/\sigma'_{v} = 0.43$ ). However it fits reasonable well with the lower bound undrained shear strength profile from the soil investigation (Appendix A) indicated with the correlation points (TxCuD) from Soil Test. Generally the undrained shear strength is conservative to a depth of approximately 22 m below seabed. The transition between the clay plug and the undisturbed soil below fits very well, and is mainly influenced by the change in pore pressure distribution hence effective stresses. For the remolded interface zones the initial effective stresses are quite low, or zero in the case of the inner interface zone. This is reflected in the modeled undrained shear strength where the cohesive contribution is dominant. Consequently the increase in undrained shear strength is minor meaning that the average undrained shear strength along the interface zones is conservative. The modeled undrained shear strength profiles were assumed accurate enough for further analyses. The aspect of modeled undrained shear strength is extensively discussed in Chapter 5.1.3.

Another possible issue related to initial low effective stress state and the soft soil model is the interpretation of OCR. The cap in  $q$ - $p'$  plane is determined by the  $M$ -parameter (height of the ellipse) and the pre consolidation stress ( $p_p$ ). Effectively very low effective stresses will

neutralize the effect of OCR since it is a factor times the mean effective stress. In the case of the remolded interface zones ( $OCR = 1.0$ ) it will not directly affect the analysis, but in case of other assumptions regarding OCR particular consideration is needed. Alternatively to OCR it is possible to specify a pre overburden pressure (POP) independent of the effective stress state. Unfortunately the soft soil material model do not allow for manual input of  $K'_0$  if POP is used to describe the previous stress history.

### 5.1.2 Undrained loading and consolidation

During undrained loading of the installed suction caisson excess pore pressure is generated. The buildup of excess pore pressure is largest at the bottom of the clay plug (inside the suction caisson). Generally the excess pore pressure is larger along the inner interface zone. Below the clay plug excess pore pressure generation is reduced accordingly to the shape of a point end bearing capacity failure pattern. Figure 26 displays how the excess pore pressures are reduced within the clay plug and interface zone through global dissipation, hence the excess pore pressure just below the suction caisson lid is reduced the slowest.



**Figure 26 Excess pore pressure ( $U_{\text{excess}}$ ) after undrained loading and at the end of consolidation**

Many of the global aspects related to stresses, strains and displacement are closely related to the modeling of the remolded interface zones. Different assumptions with respect to selected material parameters and increase in horizontal stress and pore pressure during installation of the suction caisson will affect the general analysis results. The pore pressure in the interface zones dissipates through horizontal redistribution within a short period of time. Horizontal cross section at a depth of 10 m at different time intervals during consolidation indicates the difference in horizontal redistribution and global dissipation (Figure 27). Within half a day the difference in active pore pressure in the inner remolded zone is reduced from approximately 20 % of hydrostatic pore pressure to less than 5 %. During the same time interval the difference between the outer interface zone and surrounding soil becomes neglectable. The first period of consolidation (illustrated at  $t=10$  days) redistributes the

excess pore pressure between the inner remolded zone and clay plug (Figure 28). After 100 days of consolidation the active pore pressure is about equalized within the suction caisson. From this point and beyond further consolidation ensure global dissipation towards a uniform hydrostatic pore pressure distribution in the entire FEM model.

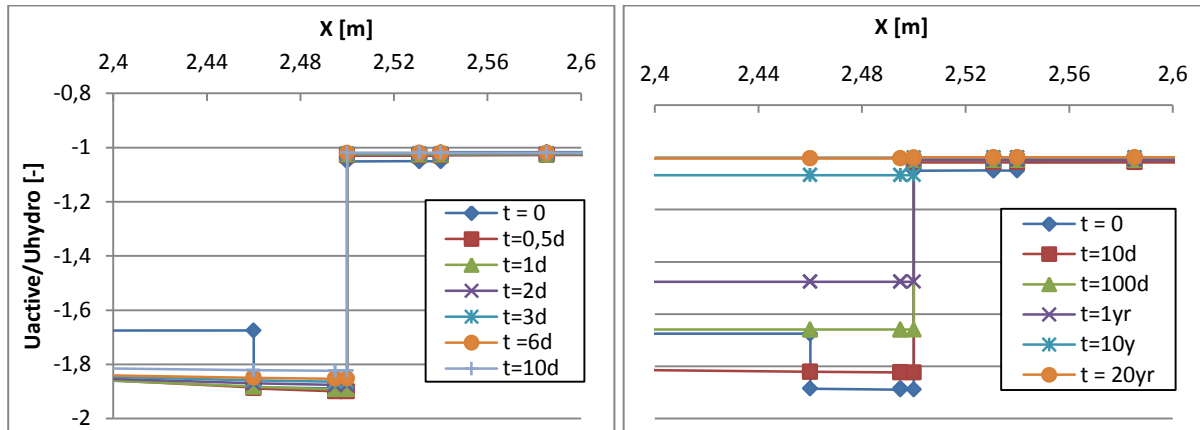


Figure 27 Horizontal cross section of normalized active pore pressure in the interface zones at depth = 10 m and different time intervals

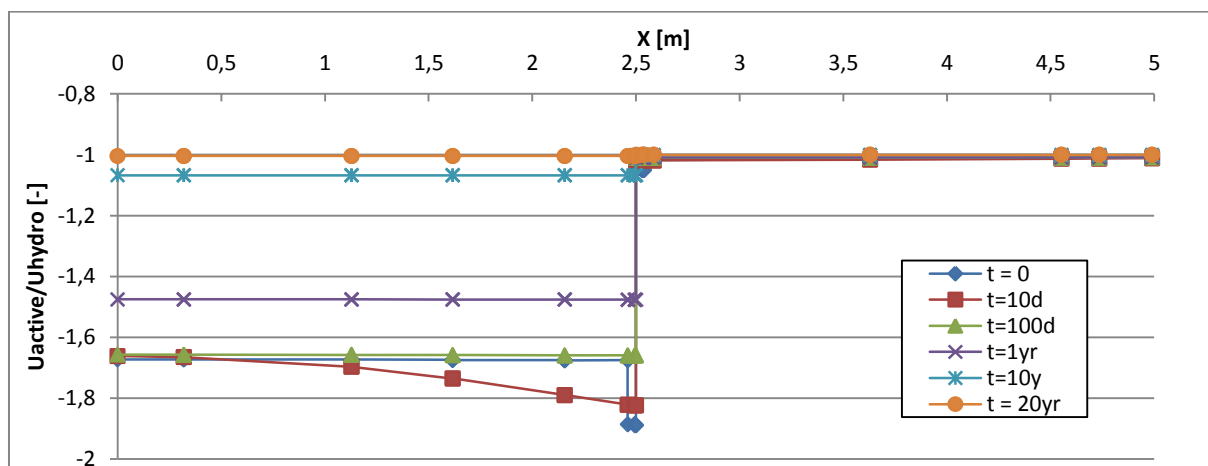
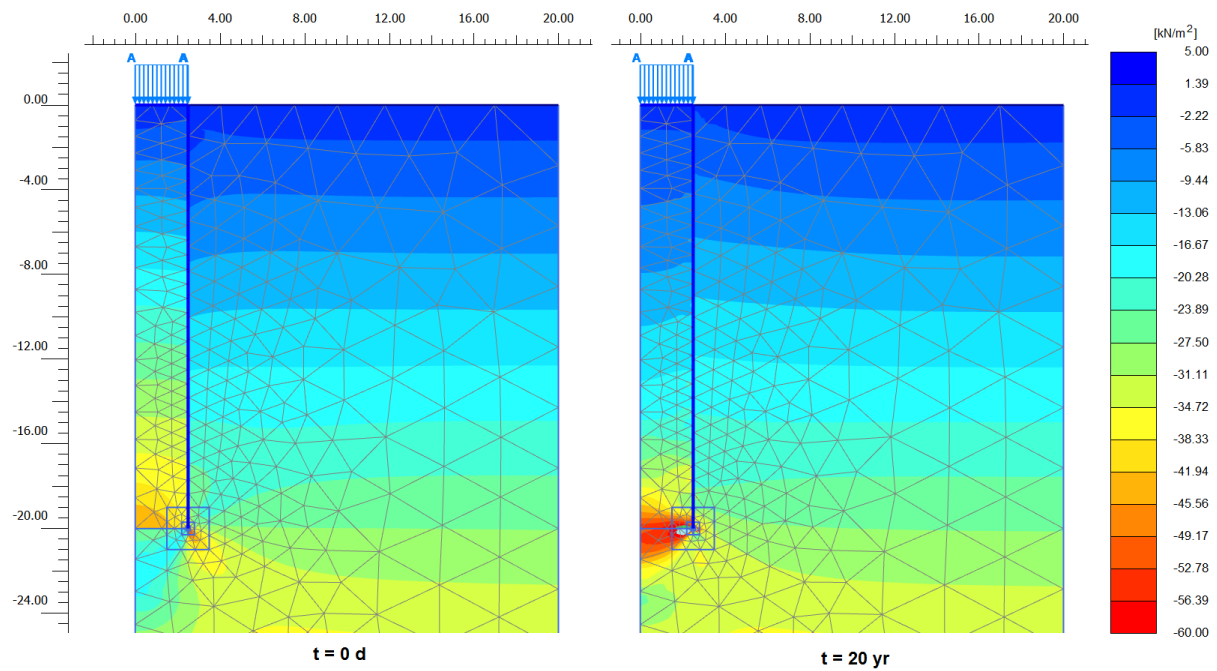


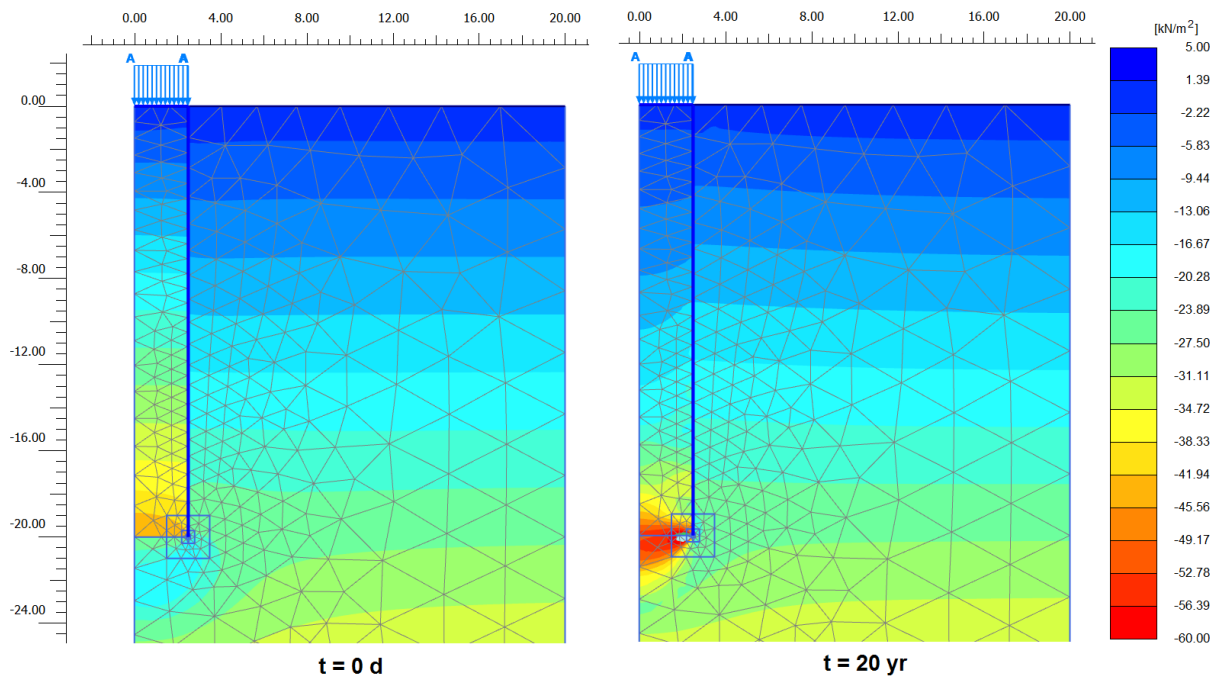
Figure 28 Horizontal cross section of normalized active pore pressure in the clay plug, interface zones and surrounding soil at depth = 10 m and different time intervals

During dissipation of excess pore pressure increasing effective stresses are expected. Both horizontal effective radial and tangential stresses (Figure 29 and Figure 30) show some similar tendencies at the end of loading as well as the end of consolidation. However there are some notable differences along the skirt wall as well as below the skirt tip. After being significantly reduced due to high excess pore pressures in the remolded zone during loading, radial effective stress along the outside of the skirt wall increase with time during consolidation. The initial high radial stress inside the suction caisson due to installation (equivalent with  $TxEuD$ ) is reduced with time, however the final pattern also show higher radial effective stress along the inside of the skirt wall. At the clay plug and skirt tip a final radial stress concentration develops. Below the clay plug the increase in radial effective stress can be explained by load transfer (dissipation of excess pore pressure) from the clay plug to the soil below the suction caisson. The tangential effective stress is however less

affected during loading of the suction caisson outside the skirt wall. Additionally it only shows a modest increase during consolidation. The effect of the skirt tip is also less compared to the influence on radial effective stress.



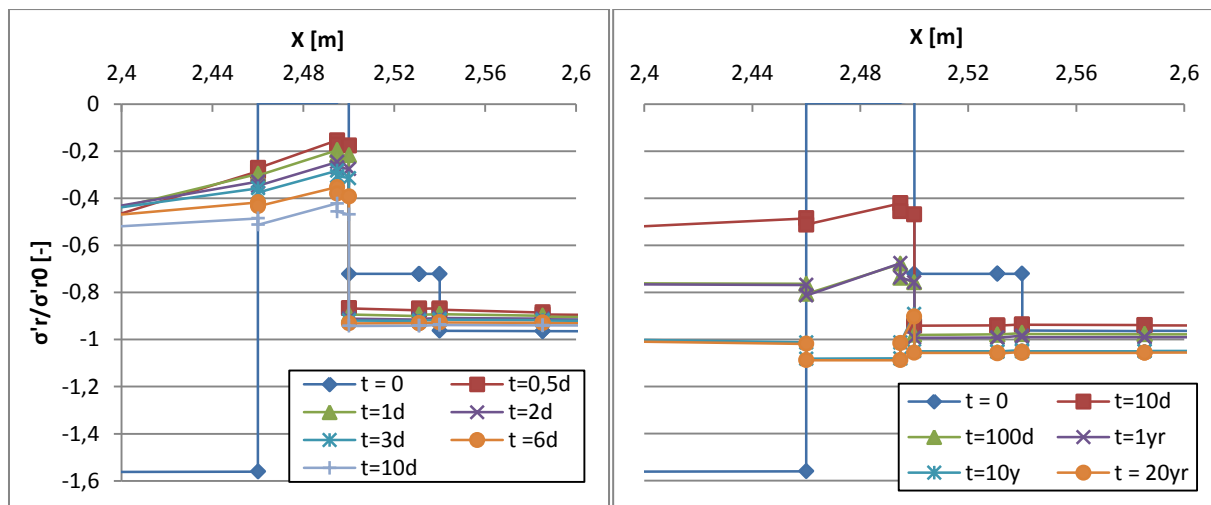
**Figure 29 Radial effective stress ( $\sigma'_r$ ) after undrained loading and at the end of consolidation**



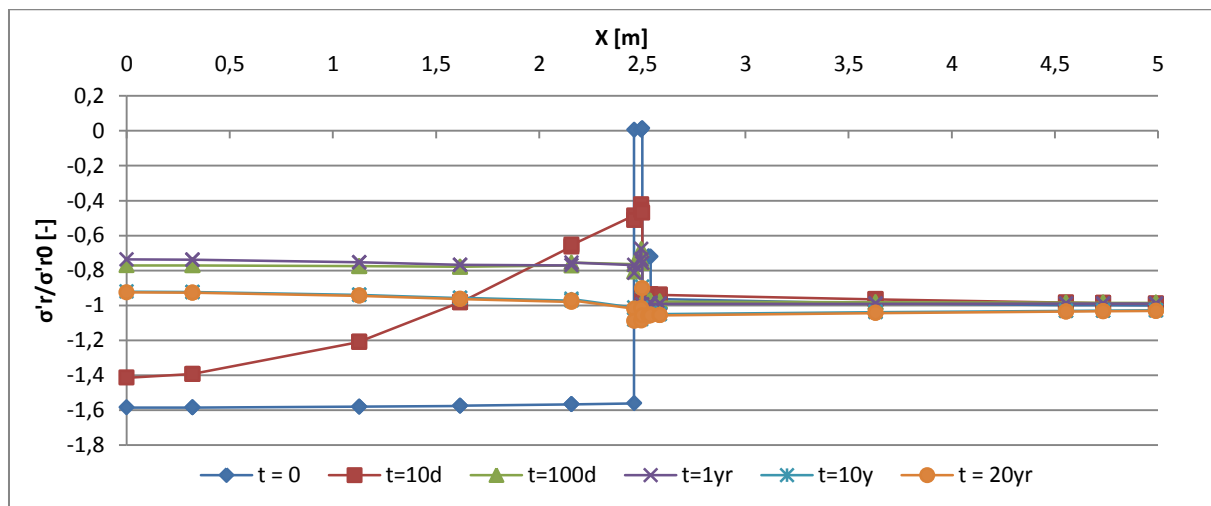
**Figure 30 Tangential effective stress ( $\sigma'_\theta$ ) after undrained loading and at the end of consolidation**

Figure 31 and Figure 32 indicate the change in effective radial stress with time. Compared to the change in active pore pressure the radial stress change is more dominant through the clay plug. Additionally the elapsed time until significant increase in effective stress in the remolded zones is longer. The change in radial effective stress in the outer interface zone is primarily due to dissipation of excess pore pressure ( $K'_0$  is not updated). There is some

increase relative to in-situ horizontal effective stress prior to installation with time after approximately one year, although it is less than maximum 5 %. Inside the suction caisson analogues increase corresponds to approximately 10 %. During consolidation the average radial stress in the clay plug is first reduced below the original in-situ value before gradually increasing after sufficient time interval (somewhere between 1-10 years). The radial effective stress in the inner interface zone is rapidly increasing from zero (due to high excess pore pressure and low effective soil unit weight) to a significant level. Between 0.5-10 days of consolidation the radial stress increases by approximately 18 % to 40 % of final stress level. The extensive change in radial effective stress would be less if the generated excess pore pressure during installation versus soil effective unit weight ratio was lower.



**Figure 31** Horizontal cross section of normalized horizontal radial stress in the interface zones at depth = 10 m and different time intervals



**Figure 32** Horizontal cross section of normalized horizontal radial stress in the clay plug, interface zones and surrounding soil at depth = 10 m and different time intervals

The increase in radial effective stress in the interface zones is also related to radial strains. Figure 33 show that there is some radial strain (swelling) in the clay plug after consolidation. However it is very small compared to the radial strain in the inner interface zone that is considerably compressed (almost 25%, Figure 34). The radial strain at the edge of the skirt

wall corresponds with the influence on effective stresses described earlier. Development of radial strain during consolidation is shown in Figure 35. Initial dissipation of high excess pore pressures and compression of the inner interface zone generates swelling in the clay plug close to the skirt wall. In the time interval between 10 days and 100 days of consolidation the radial strain maximizes closes to the model center line. Effectively this expansion squeezes the remolded and weak interface zone against the skirt wall, generating potential higher effective radial stress.

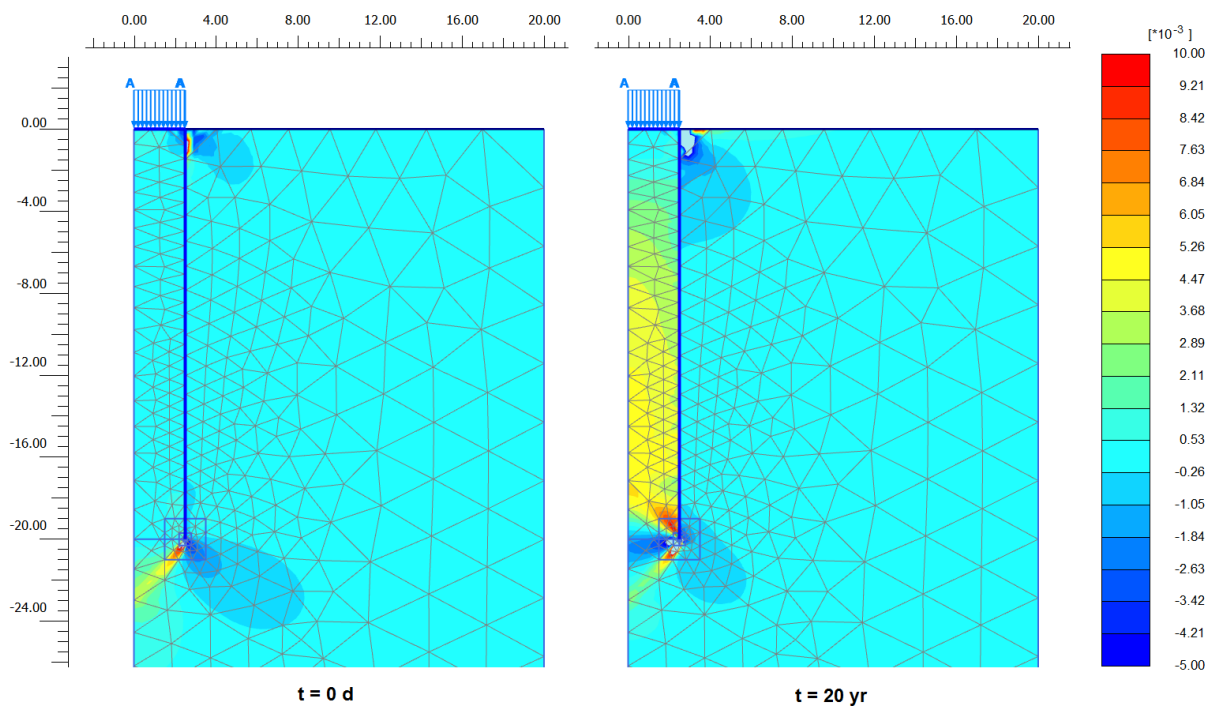


Figure 33 Radial strains after undrained loading and at the end of consolidation

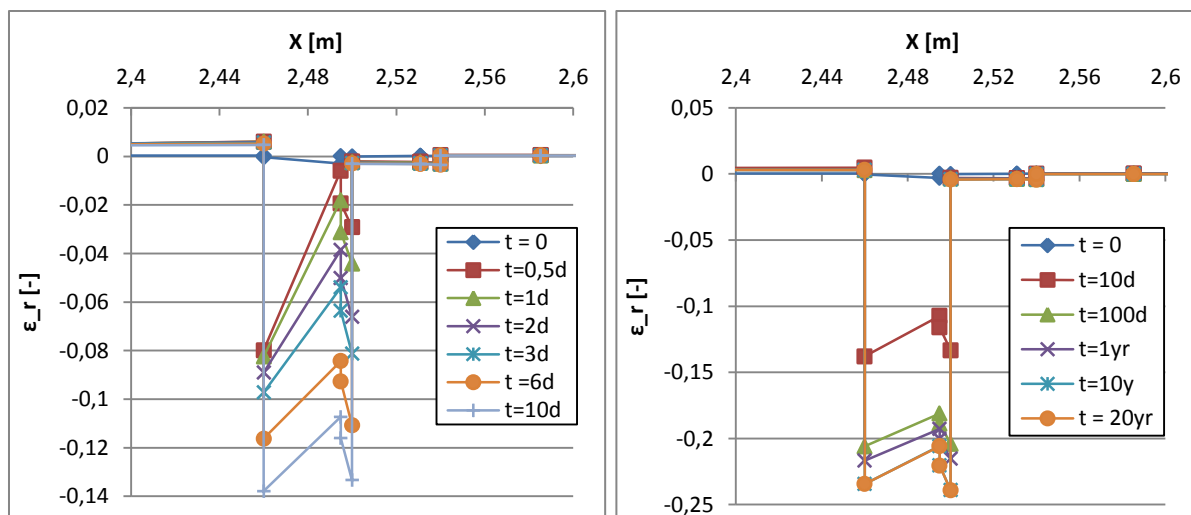
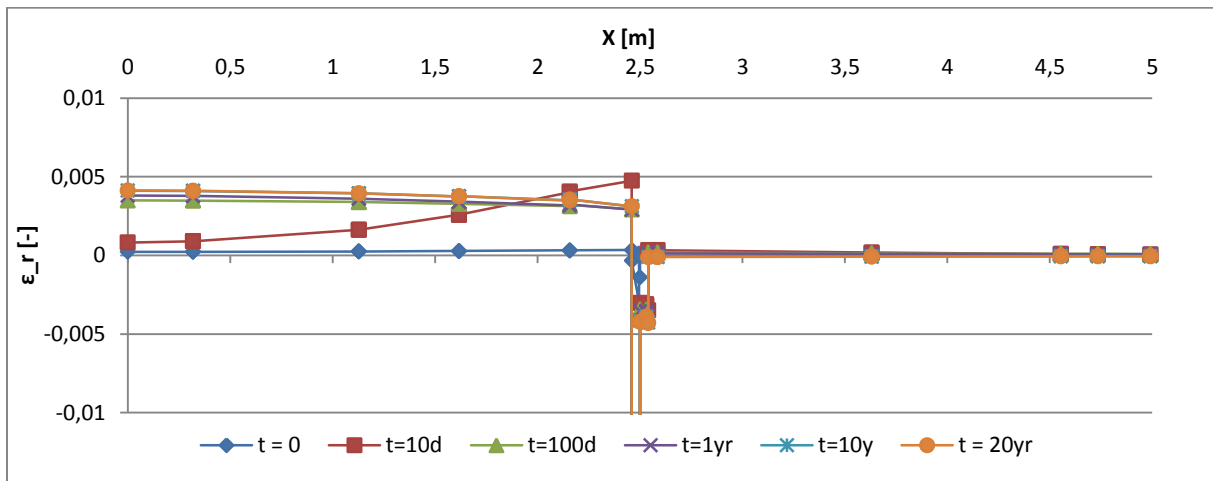
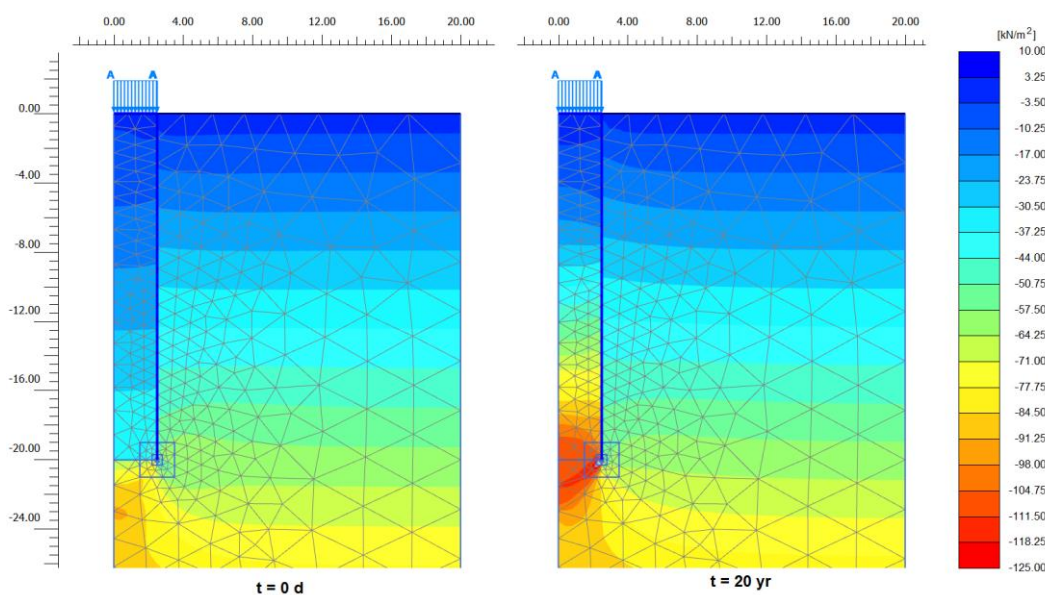


Figure 34 Horizontal cross section of radial strains in the interface zones



**Figure 35** Horizontal cross section of radial strain in the clay plug, interface zones and surrounding soil at depth = 10 m and different time intervals

Figure 36 show how the vertical effective stress increases inside the clay plug during dissipation of excess pore pressure after loading. The clay plug and appurtenant zone below experience the largest increase, while the effect reduces with increasing radial distance to the suction caisson. Evaluation of the effective vertical stress from Figure 37 and Figure 38 underline some interesting tendencies. The effective vertical stress increases above the initial in-situ value in the surrounding soil after consolidation, radially reducing to the original in-situ value. In the outer interface zone the final vertical effective stress is approximately 45 % lower compared to this value. Inside the suction caisson the increase in vertical effective stress is a response to the applied load. However the vertical effective stress is also lower in the inner interface zone (despite evenly distributed load), creating a final accompanying radial increase in vertical effective stress from the model center line. Despite the applied load the final vertical effective stress in the inner interface zone is minimally larger compared with the outer interface zone, and 50 % lower than the in-situ value prior to installation.



**Figure 36** Vertical effective stress ( $\sigma'_v$ ) after undrained loading and at the end of consolidation



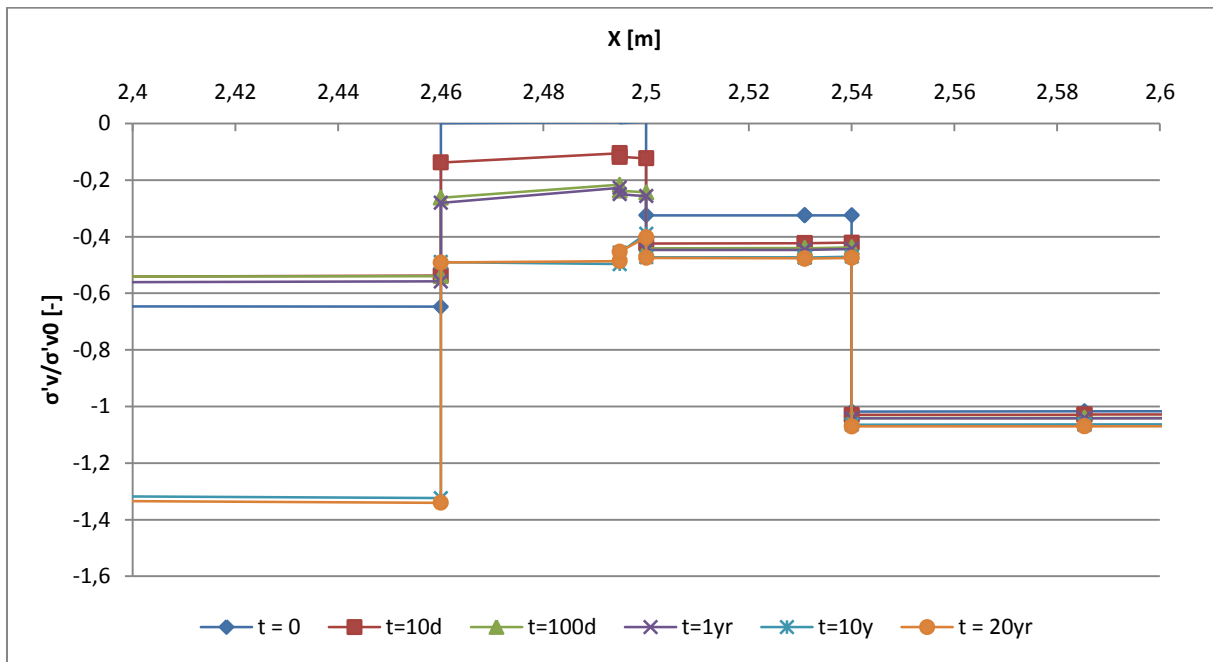


Figure 37 Horizontal cross section of normalized effective vertical stress in the interface zones at depth = 10 m and different time intervals

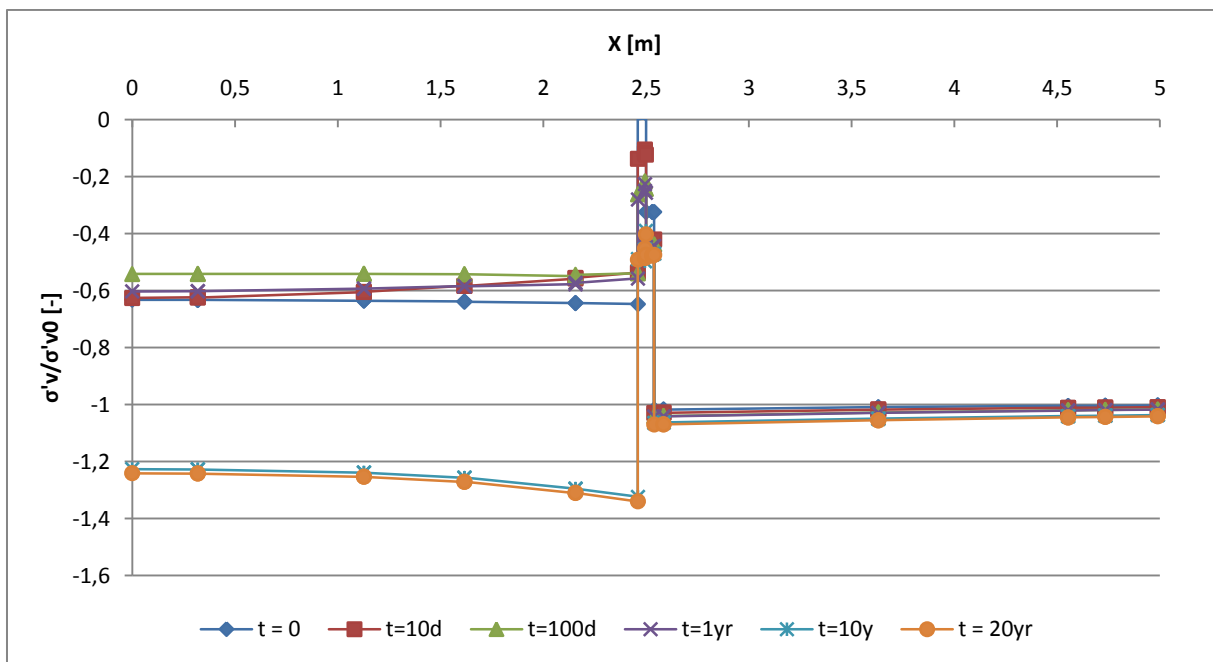
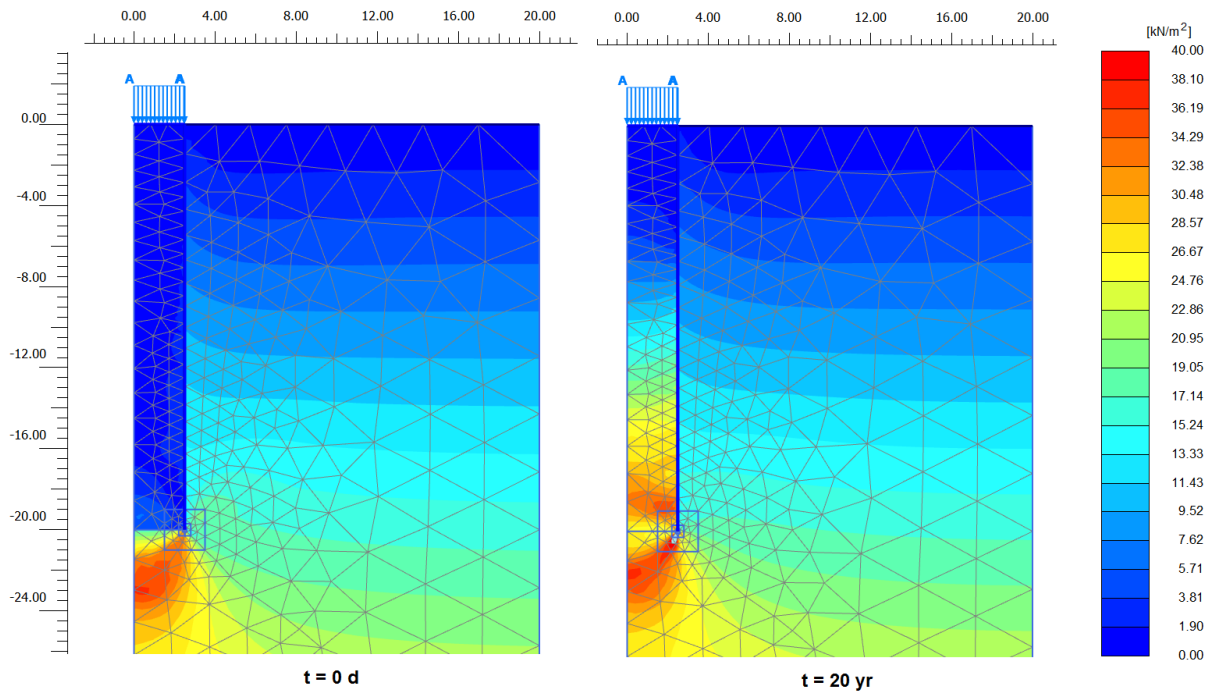
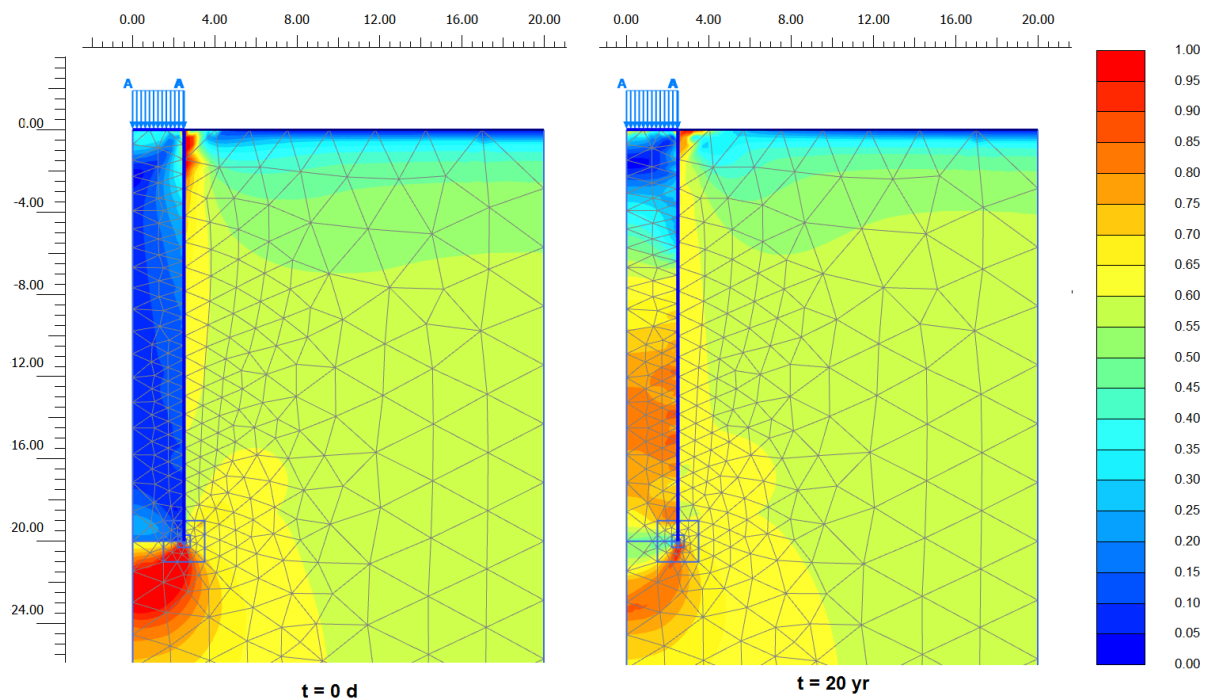


Figure 38 Horizontal cross section of normalized vertical effective stress in the clay plug, interface zones and surrounding soil at depth = 10 m and different time intervals

Due to the high excess pore pressures in the remolded zones (consequently low initial effective stress) the load is primarily carried by pile tip resistance during undrained loading. Dissipation of excess pore pressures and increase in effective stresses give potential for increased shear stress. Accordingly the mobilized friction increases with time and the load is distributed more to skirt wall friction. Figure 39 and Figure 40 clearly show how the mobilized friction is very low in the clay plug after undrained loading and significantly increasing during consolidation. The increase is largest along the inner parts of the skirt wall, while similar effect is primarily seen at the lower parts of the outer skirt wall.



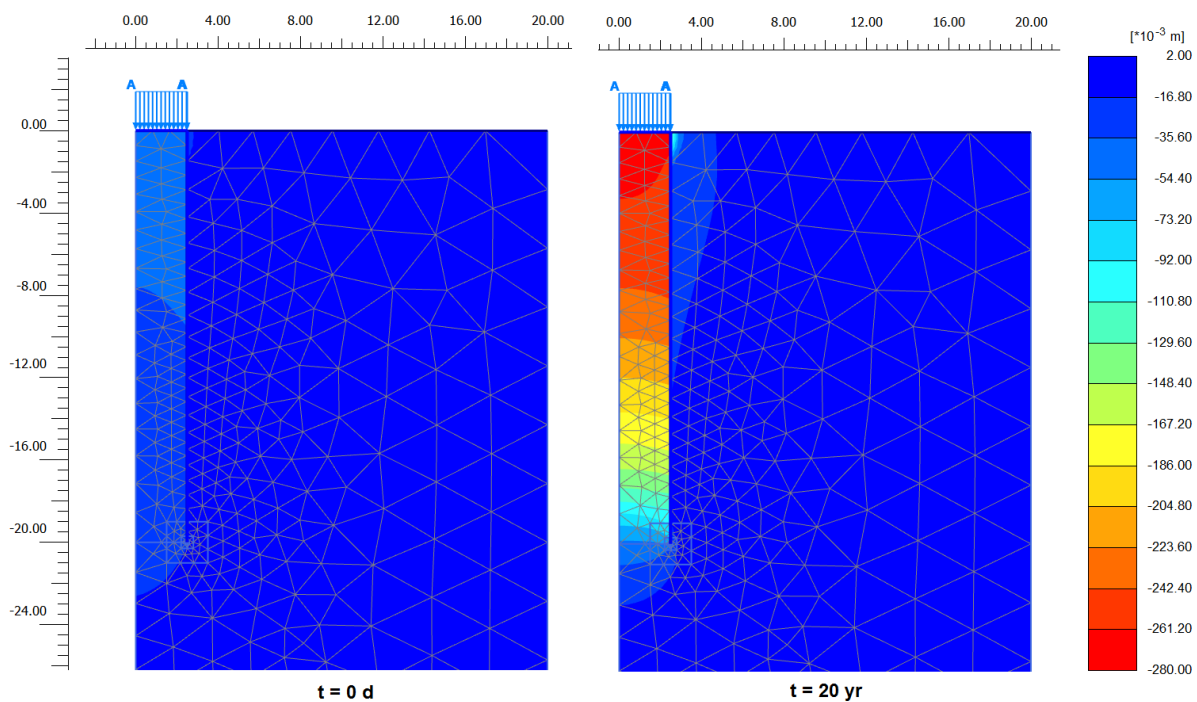
**Figure 39 Mobilized shear stress ( $\tau_{mob}$ ) after undrained loading and at the end of consolidation**



**Figure 40 Relative mobilized shear stress ( $\tau_{mob}/\tau_{max}$ ) after undrained loading and at the end of consolidation**

The vertical displacement of the suction caisson is shown in Figure 41. As indicated in the development of settlement versus time (Figure 20) the maximal initial undrained vertical displacement is approximately 5 cm. During consolidation the clay plug settles the most, affecting the surrounding soil at the seabed to some extent. This radial effect is rapidly reduced with depth, and the low shear strength in the remolded zone enhances the reduction in surrounding settlement. To some extent the suction caisson is modeled as being installed into a predrilled hole with a thin and very weak interface layer in between the skirt

wall and surrounding soil. Increasing the shear strength along the interface zone will reduce this effect and more evenly distribute the settlement across the cross section. Consequently it will reduce the final vertical settlement of the suction caisson center point. Comparing settlement across the upper part of the clay plug indicate a potential drag-down effect on the soil. The clay plug settles more at the center line compared to the soil close to the skirt wall just below the top lid (with uniform settlement). This effect is neutralized at a depth of approximately 5 m of an opposite trend (larger settlement close to the skirt wall).



**Figure 41 Vertical displacement after undrained loading and at the end of consolidation**

The applicability of the FEM model is partially determined by the ability of correctly modeling the consolidation process after initial stress generation based on the assumptions related to the installation of the suction caisson. Some features such as increasing effective radial stress, strains as well as pore pressure dissipation indicate that the FEM model can cope with some realistic “set-up” features during consolidation. However the magnitude of this effect is uncertain and some aspects seem to be highly sensitive to small changes. E.g. the effective stress in the remolded zone is primarily related to the generation of excess pore pressure. This has huge impact on the final settlement calculation as shown in the initial analyses (Figure 20). Since the remolding induced contribution to excess pore pressure utilizes quite conservative values there might be potential for using less conservative and more correct values beneficial for design.

In Chapter 2.3 final effective radial stress ratio ( $K_c$ ) was discussed. In Figure 42 Final effective radial stress ratio ( $K_c$ ) versus depth in the outer interface zone and surrounding soil  $K_c$  versus depth is plotted for two vertical cross sections, inside the outer interface zone and at the edge of the surrounding soil. According to Karlsrud’s (2012) compilation of pile test results suggest that the final effective radial stress ratio for soft soil with  $OCR = 1.7$  and  $I_p > 20\%$

should have a magnitude of 0.8-1.0. For the representative parts of the vertical cross section (excluding the upper 2 m and transition from skirt tip to undisturbed surrounding soil) the  $K_c$  is between 0.4 and 1.0. The average value is approximately 0.5, somewhat larger than the original  $K'_0$  value (0.45). This could indicate that the final effective radial stress is within satisfactory limits. However care should be taken in concluding since the dimensions ( $d/t$  ratio and diameter) is quite different for the suction caisson compared to the average pile discussed by Karlsrud.

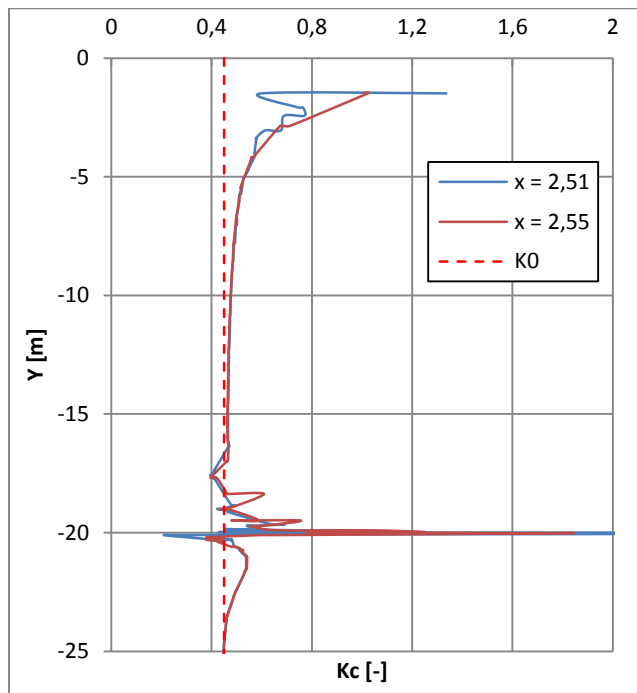


Figure 42 Final effective radial stress ratio ( $K_c$ ) versus depth in the outer interface zone and surrounding soil

### 5.1.3 Undrained shear strength

According to the discussion in Chapter 2.3 significant increase in undrained shear strength is expected during consolidation after undrained loading. It is important that this is covered by the FEM model since development of consolidation settlements is highly influenced and subsequent loading might be dependent on the increased shear strength with respect to design.

At first the undrained shear strength in the outer interface zone was evaluated. The modeled undrained shear strength after phase 2 ( $t = 0$ ) was assumed acceptable compared to the design undrained shear strength profile and used as a reference value. For initial comparison the expected set-up factor for 3 months of consolidation was used. This value is indicated by the line in Figure 43 denoted  $\alpha/S_t \cdot \tau_{max}$ , and is the equivalent of the set-up factor times the original undrained shear strength. The figure show modest increase in undrained shear strength ( $\tau_{max}$ ) with time, however the values are far from the expected increase due to set-up. The relative mobilized shear strength ( $\tau_{rel}$ ) is the ratio of mobilized shear strength by undrained shear strength ( $\tau_{mob}/\tau_{max}$ ). With exception of the first phase ( $t = 0$ ) close to all of the available skirt friction outside the skirt wall is fully mobilized. Interference at the

skirt edges (top and bottom) is mainly due to numerical and model related issues. Nevertheless some irregularities around the skirt tip are expected for an in-situ situation where perfect idealized conditions are not valid.

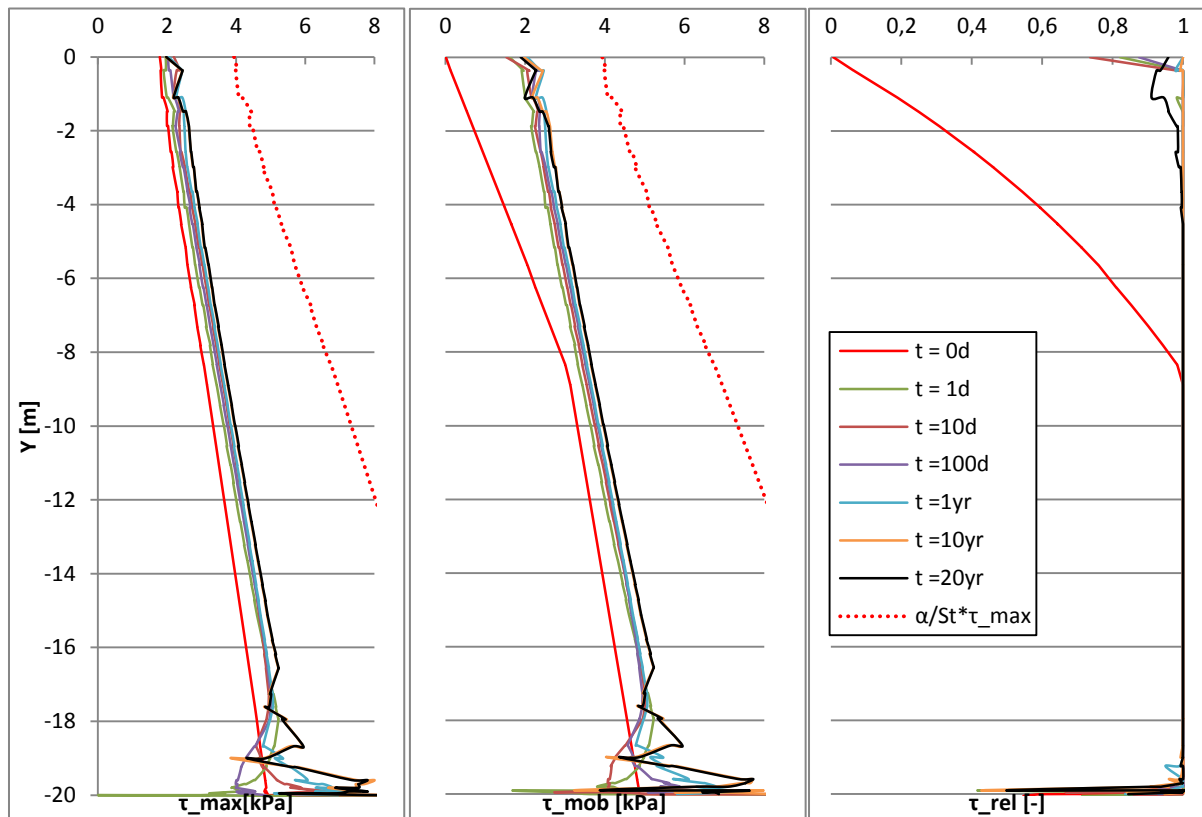


Figure 43 Maximal shear strength, mobilized shear strength and relative mobilized shear strength at different time intervals in the outer interface zone (x = 2.52 m) for Case 5

In order to improve modeling of the undrained shear strength increase with time it was decided to update the friction angle ( $\phi'$ ) for the interface zones during consolidation (Table 9). Set-up factors were calculated from Table 1 and Table 2, and derivation of a simplified formula for updated friction angle is given in Appendix E.

Time [days]	Inner interface zone		Outer interface zone	
	Set-up factor, $\alpha$ [-]	Friction angle, $\phi'$ [°]	Set-up factor, $\alpha$ [-]	Friction angle, $\phi'$ [°]
10	0.475	16.4	0.45	15.5
100	0.475	16.4	0.55	19.0

Table 9 Set-up factor and corresponding updated friction angle for the interface zones

Changing the friction angle in the soft soil material model will automatically update  $K_0^{NC}$  (according to Jaky’s formula) hence also adjusting the M – parameter. Since the M – parameter determines the height of the ellipse this will impact the cap. After updating the friction angle in the remolded zones the output from the staged construction was evaluated. Figure 44 show plastic points for Case 5 after 100 days of consolidation compared against only updating the friction angle in addition to updating both friction angle and  $K_0^{NC}$  (adjusting the M-parameter). In both cases with updated friction angle the shear strength is sufficiently increased for the majority of stress points in the interface zones to be reduced

below the failure line (reduction in MC-points). However the stress state representation seems better when updating  $K_0^{NC}$  in addition to the friction angle as the cap points is less affected. According to Figure 49 development in relative mobilized shear strength with time after further consolidation correspond better with the initial development (after  $t = 0$  days) when updating  $K_0^{NC}$ . Gradually increasing mobilization upwards along the skirt wall from a maximal value at the skirt tip is intuitively more realistic. Based on this both updating the friction angle and  $K_0^{NC}$  was determined as the best option. This will increase the shear strength and maintain the stress state at the cap.

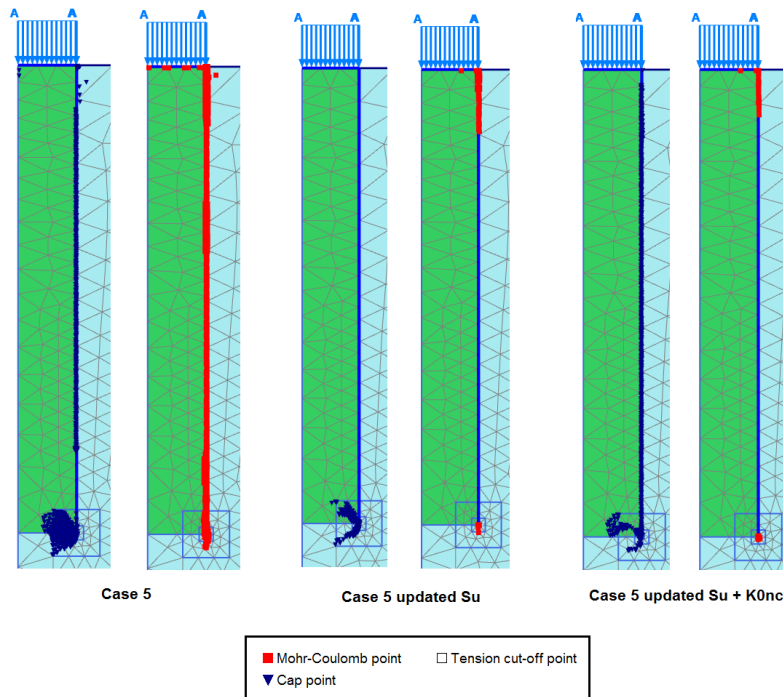


Figure 44 Plastic points after updating friction angle in the remolded zones ( $t = 100$  days)

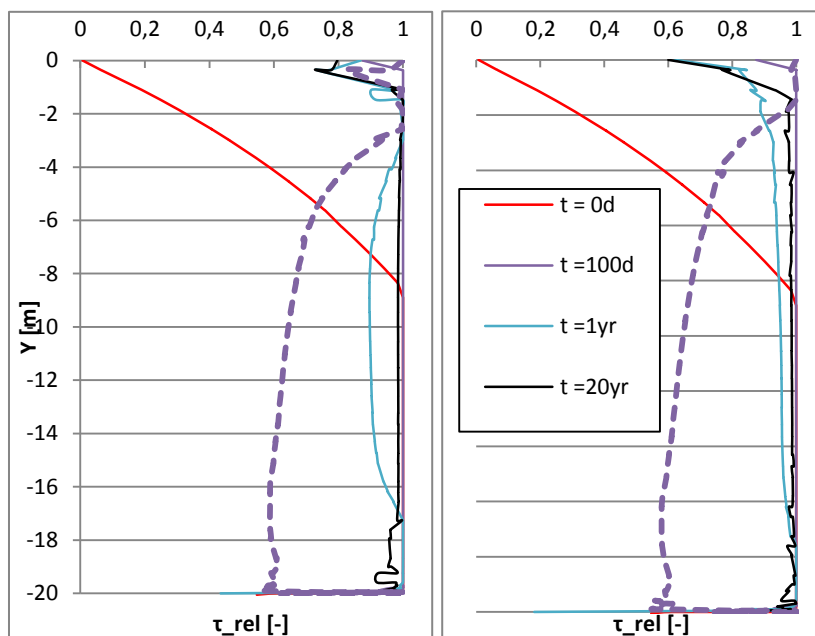
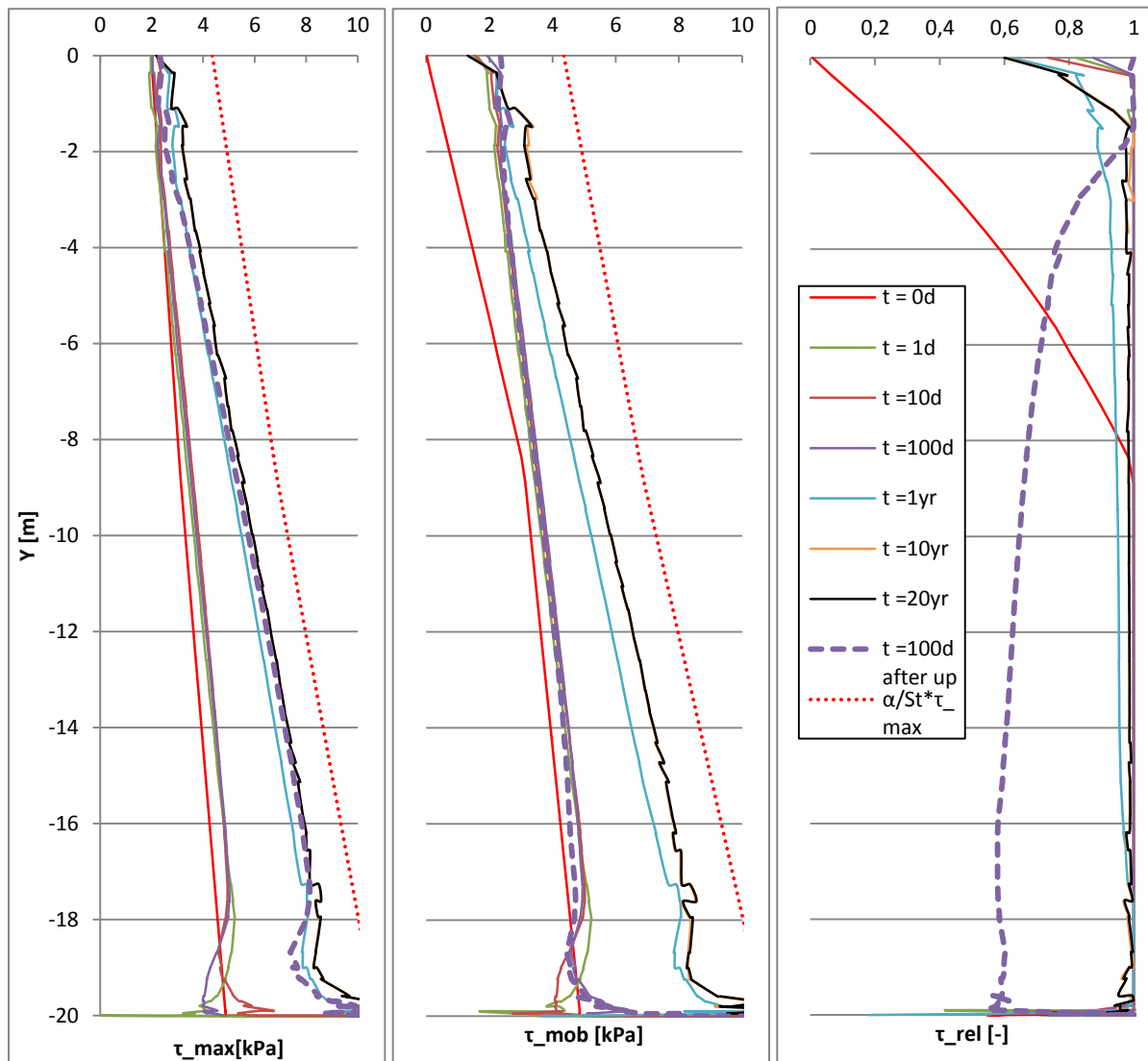


Figure 45 Relative mobilized shear strength after updating friction angle in the remolded zones and further development

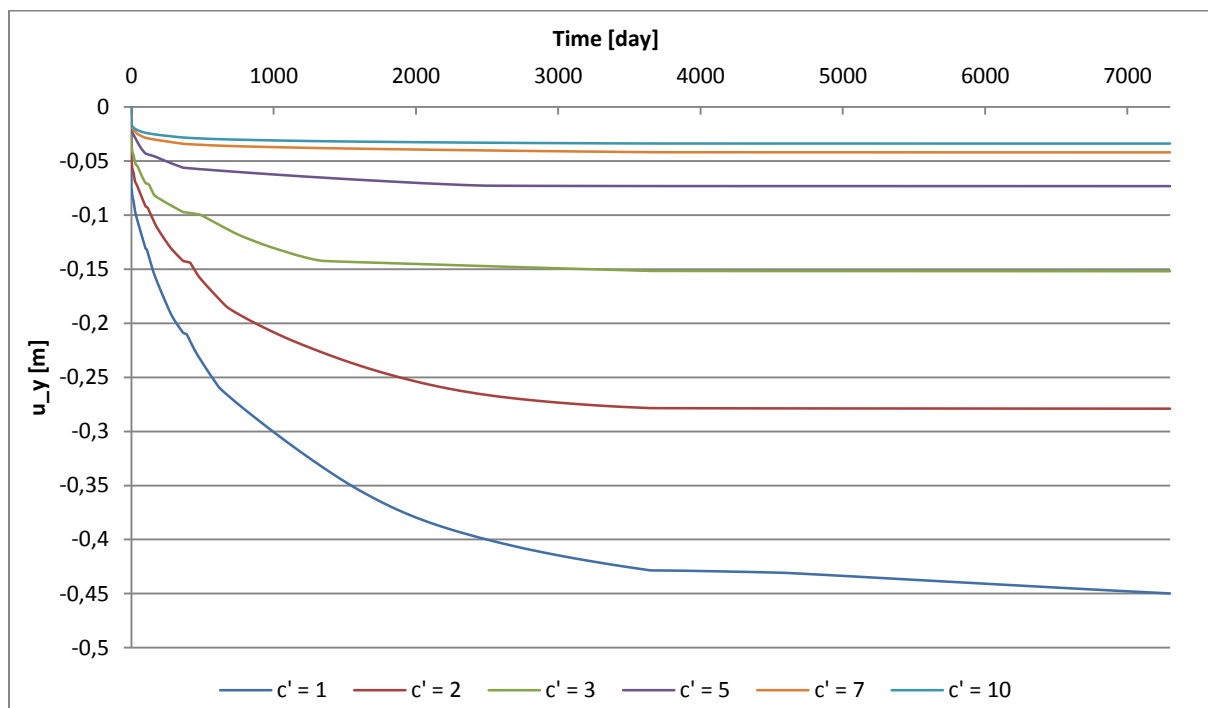


**Figure 46** Maximal shear strength, mobilized shear strength and relative mobilized shear strength at different time intervals in the outer interface zone ( $x = 2.52$  m) for Case 5 with updated friction angle and  $K_0^{NC}$

Figure 46 show development of shear strength with time before and after updating friction angle in the interface zones at  $t = 100$  days. The adjusted friction angle gives potential for higher mobilized shear strength in the interface zone. Since the increase in effective stresses in the interface zones is limited, adjusting the friction angle will be necessary to sufficiently take into account the increasing undrained shear strength. However it is still conservative compared to the proposed set-up factor in literature (denoted  $\alpha/S_t * \tau_{max}$ ). Additional adjustment (increase) and evaluation of the friction angle could improve the fit. Prior to the update at  $t = 100$  days maximal shear strength is mobilized ( $\tau_{rel} \approx 1.0$ ). After the increase in shear strength relative mobilized shear strength is gradually changed towards the initial tendency. With exception of the upper parts of the skirt wall most parts are fully mobilized by the end of consolidation. The reduced mobilization in the upper parts is a response to the general increased skirt wall friction. Gradually increasing the friction angle in several steps according to set-up theory could contribute to a smoother transition, and help avoid the large leap in relative mobilized friction ( $1.0 \rightarrow 0.6$  at  $t = 100$  days). Consolidation settlement development and further assessment is given in Chapter 5.2.

### 5.1.4 Cohesion ( $C'$ )

During the initial FEM analyses cohesion ( $c'$ ) in the remolded interface zones was found to have surprising impact on the final consolidation settlements. To avoid numerical issues during the beginning of consolidation a small cohesion ( $c' = 1$  kPa in the clay plug,  $c' = 2$  kPa in the remolded zones) was required. The numerical issue is related to equilibrium in upper most parts of the clay plug where a small suction is generated when applying the load. As indicated by Figure 24 the soft soil material model uses a preconsolidation stress ( $p_p$ ) of minimum  $c' \cot(\phi)$ . In other words specifying cohesion could result in a state of overconsolidation depending on the value and the initial stress state. Additionally the cohesion related undrained shear strength contribution ( $c' \cos(\phi)$ ) in the Mohr-Coulomb criterion will be dominant for the interface zones as the initial effective stresses are very low (or zero in case of the inner interface zone). Figure 47 illustrates the huge impact different assumptions regarding cohesion in the interface zones have on final consolidation settlements. The extreme value ( $c' = 10$  kPa) is not realistic with respect to the evaluated soil properties, but a factor of difference of 1.8 between  $c' = 3$  kPa and  $c' = 1$  kPa is still somewhat disturbing.



**Figure 47** Development of consolidation settlements with time for different cohesion values in the interface zones (Case 5)

The cohesion has negligible effect on the compressibility in the normally consolidated stress range, but increasing the cohesion significantly decreases compressibility in the overconsolidated stress range. Combined with the increasing ability to mobilize friction (Figure 49) in the interface zones this could partially explain the difference in consolidation settlements. Figure 48 show vertical displacement profile just below seabed after consolidation for 20 years. It is evident that increasing the cohesion also enhances the



mobilization of the surrounding soil, reducing final settlement for the suction caisson. Smaller cohesion enhance the modeling effect of installing the suction caisson in a “pre drilled” hole with a thin and very weak interface zone between the skirt wall and surrounding soil. Evaluating vertical displacement profiles compared to modeled undrained shear strength and remolded compressibility is important to achieve the expected results with respect to believed soil structure interaction.

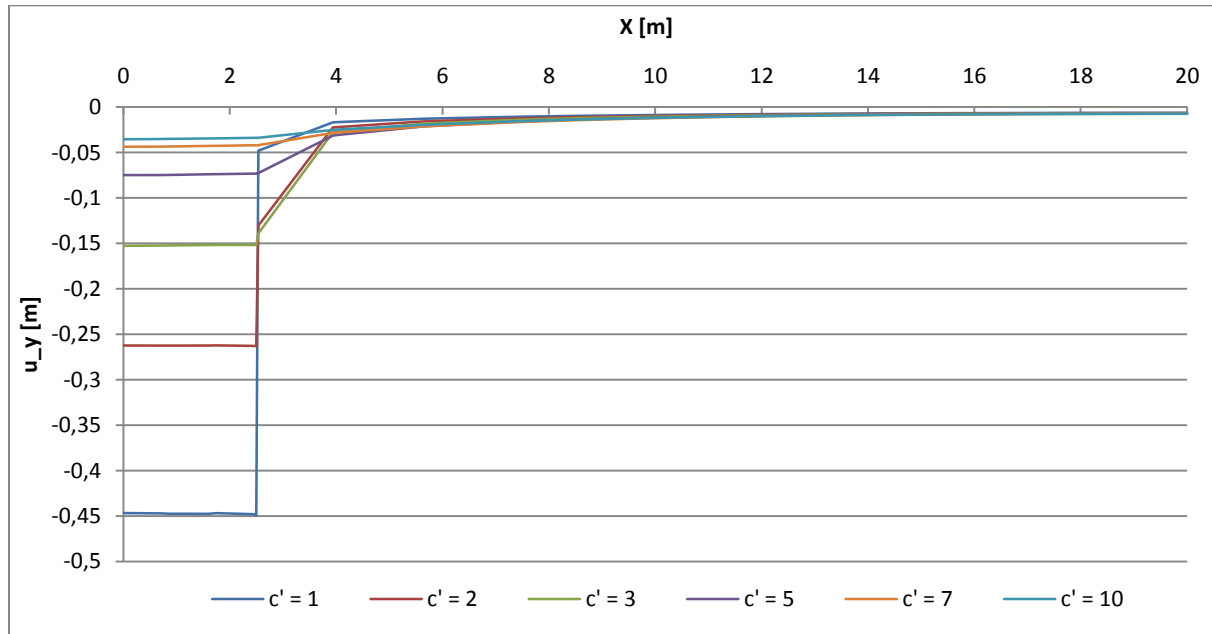


Figure 48 Vertical displacement profile after consolidation (t = 20 years, depth = 0.1 m)

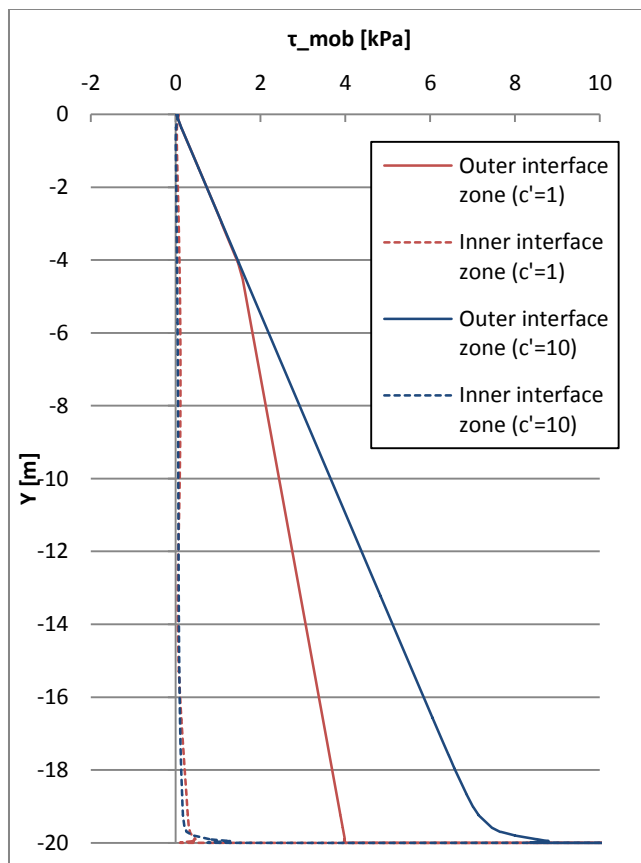


Figure 49 Mobilized friction in the interface zones after equilibrium phase (phase 2)

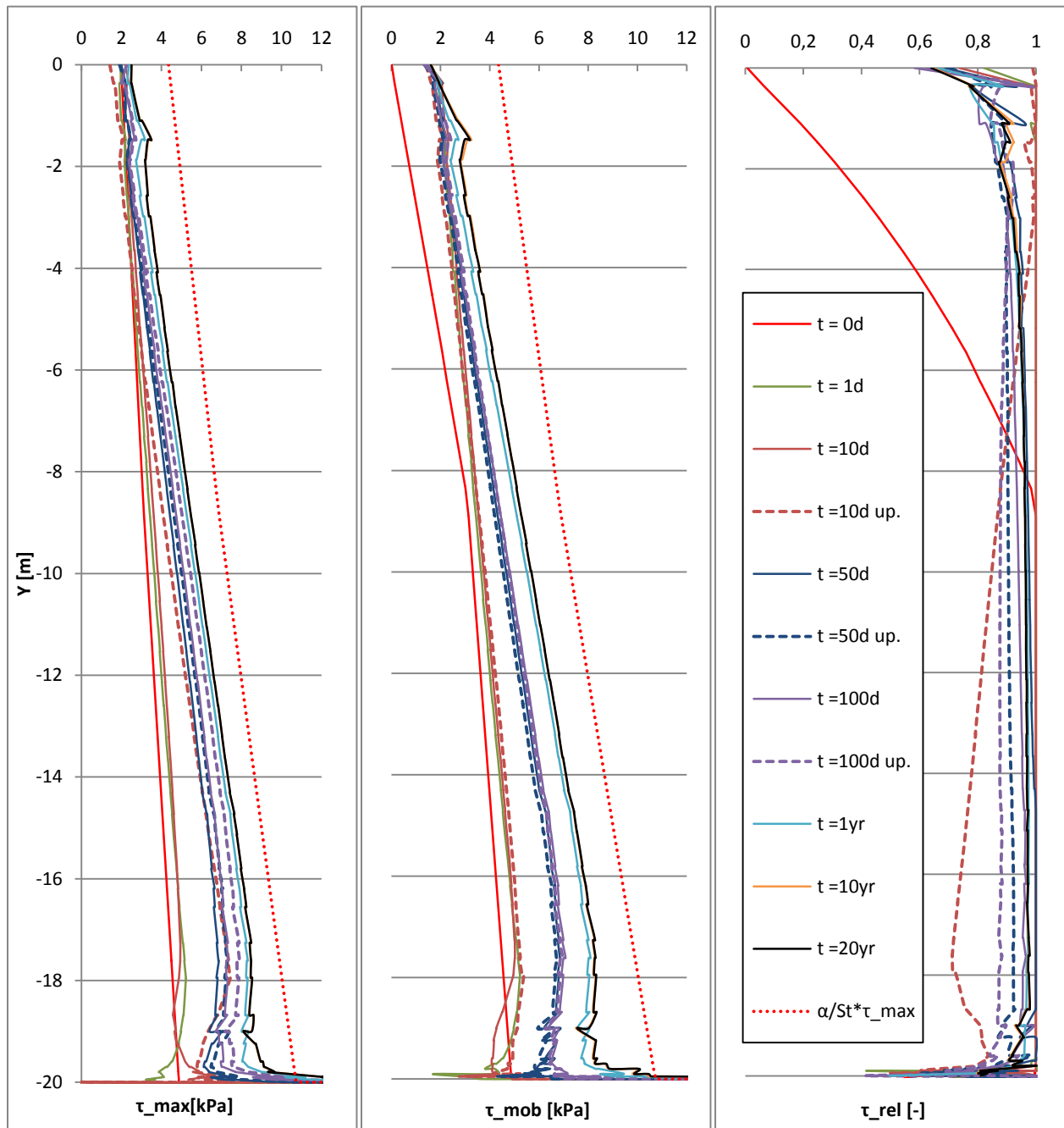
## 5.2 Adjusted FEM analysis

Based on the findings and discussion in Chapter 5.1 an updated simulation procedure is described in Table 10. The adjusted FEM analysis is denoted Case 6.

#	Identification	Calculation type (PLAXIS)	Comment
1	Initial phase	$K'_0$ -procedure	User defined pore pressure (p.p.)
2	Equilibrium phase	Plastic, staged construction	User defined pore pressure (p.p.)
3	Add load	Plastic, staged construction	General phreatic level p.p.
4	Consolidation 1	Consolidation, staged construction	Time interval = 10 days
5	Adjusting $\phi' 1$	Plastic, staged construction	Set-up factor ( $\alpha$ ) for 10 days
6	Consolidation 2	Consolidation, staged construction	Time interval = 40 days
7	Adjusting $\phi' 2$	Plastic, staged construction	Linearly interpolated set-up factor
8	Consolidation 3	Consolidation, staged construction	Time interval = 50 days
9	Adjusting $\phi' 2$	Plastic, staged construction	Set-up factor ( $\alpha$ ) for 2-/3-months
10	Consolidation 4	Consolidation, staged construction	Sufficient time interval

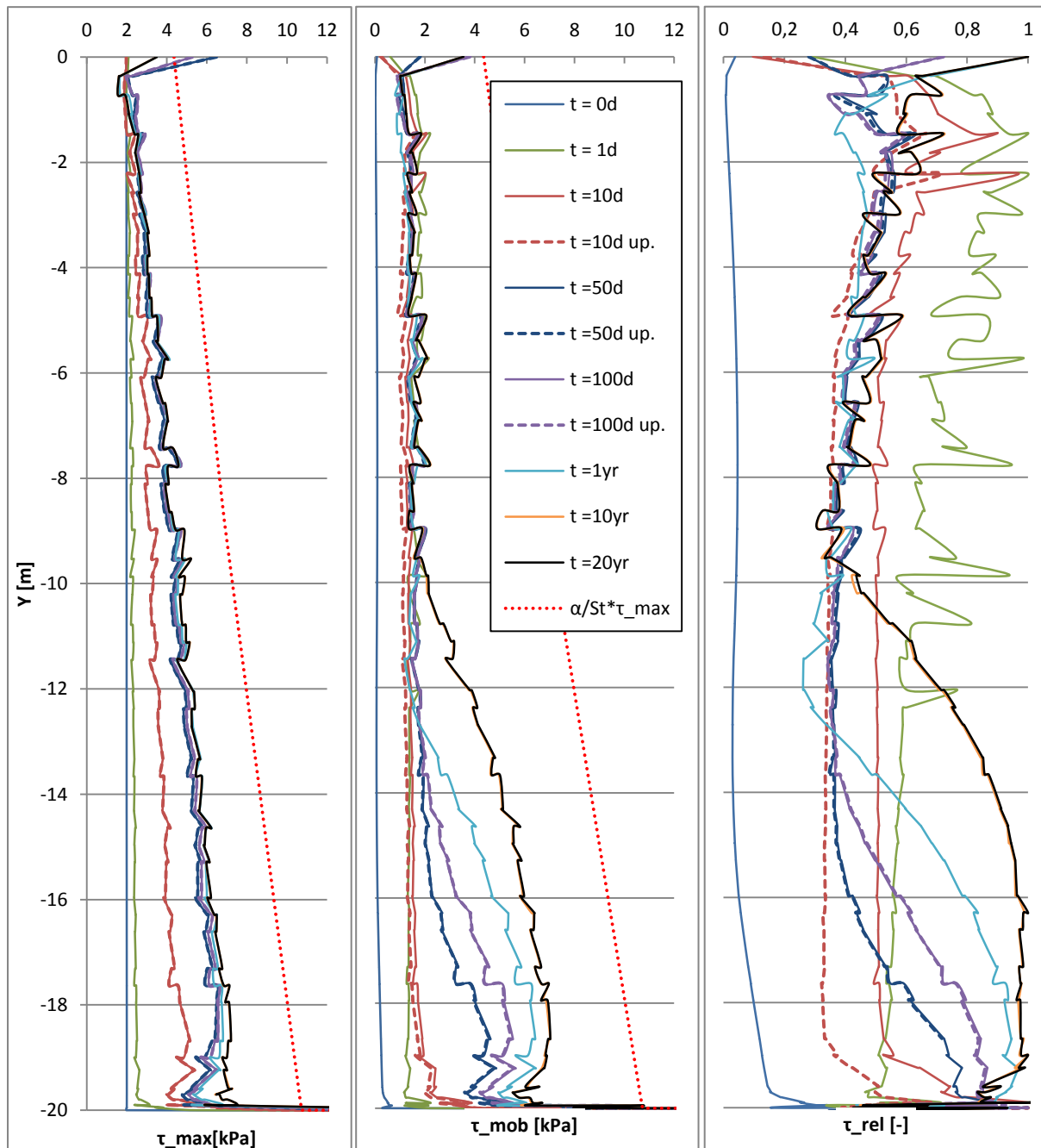
**Table 10 Adjusted FEM analysis procedure**

Adjusting the friction angle according to the simplified formula was found to model too conservative undrained shear strength in Chapter 5.1.3. Nevertheless the same friction angle was kept to avoid interfering with the basis of comparison. Further adjustment of the friction angle and evaluation of the maximal shear strength would ensure a better fit (not the scope of this section). Figure 50 show development of shear strength and mobilized shear strength at the different time intervals in the adjusted FEM analysis. The undrained shear strength ( $\tau_{max}$ ) is unaffected by the shorter updating intervals. Compared to Figure 46 relative mobilized shear strength has less significant leaps during adjustment of the friction angle. Consequently the modeled soil response after adjusting the friction angle is believed to be more realistic. Incremental increase of shear strength with time reduces the final relative mobilized shear strength along the skirt wall with approximately 5% along the skirt wall. Still final consolidation settlement is within expected limits and the average reduction along the outside of the skirt wall seems negligible.



**Figure 50** Maximal shear strength, mobilized shear strength and relative mobilized shear strength at different time intervals in the outer interface zone ( $x = 2.52$  m) for Case 6

Evaluation of undrained shear strength profiles has primarily focused on the outer interface zone. The inner interface zone is not less important, but the impact of installation on the soil volume is more complex within the suction caisson. Hence the development in maximal and mobilized shear strength with time is less intuitive, especially since the generated excess pore pressure in this FEM analysis reduced effective stresses to zero within the inner interface zone. From Figure 51 the combination of numerical interference and uneven effective stress increase in the slender interface elements may be observed. Nevertheless the undrained shear strength is not exceeded, nor is the potential strength fully mobilized. In theory additional increase in undrained shear strength for the inner interface zone should have negligible impact on the analysis results.



**Figure 51** Maximal shear strength, mobilized shear strength and relative mobilized shear strength at different time intervals in the inner interface zone ( $x = 2.48$  m) for Case 6

Final consolidation settlement is (as expected) between the upper and lower bound analyses for all of the analyses with updated shear strength (Figure 52). Incremental adjustment of friction angle according to Case 6 increases final consolidation settlement compared to the sudden adjustment in the updated Case 5 analyses. The final value for Case 6 is probably conservative due to somewhat conservative modeled shear strength profiles, but exact final consolidation settlement results has not been the aim for this subsection. However the development of relative mobilized shear strength was found to be acceptable according to the assumed response of increasing shear strength with time. In-situ records of stress development are required for final validation of the FEM analysis.

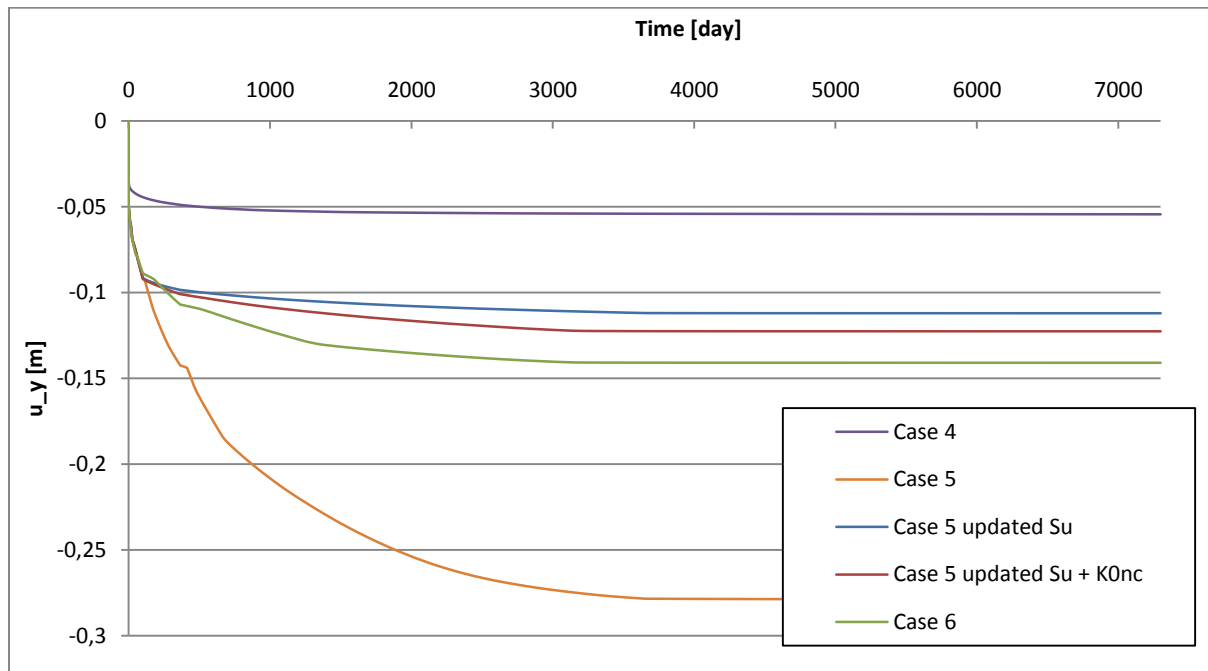


Figure 52 Consolidation settlement development for adjusted FEM analysis (Case 6) compared with initial analyses

### 5.3 Model test

Table 11 give an overview of the installation and test procedure as executed. Due to the delays described in Chapter 4.2 and some further complications only five plate arrays was installed. Peak force at failure was mainly recorded within approximately 7-15 seconds after test start. The recorded deformation (pulling distance manually observed at the rig) was approximately 2.5-4.0 cm for all tests. The average pulling speed is therefore estimated in the range of 0.15-0.45 cm/sec. If the newest test rig had been available it would be possible to accurately record force, deformation and time. Additionally it was not possible to record the installation force for comparison between undisturbed resistance (first time installation at  $t = 0$ ), remolded resistance (testing at  $t = 0$ ) and reconsolidated resistance (testing at  $t > 0$ ).

Plate id.	Installation date	Test date	Time interval	Comment
P1 & Pw1	30.05.12	08.06.12	9 days	Test results from P1 was inconclusive due to mounting error
P2 & Pw2	30.05.12	06.01.12	7 days	
P3 & Pw3	30.05.12	01.06.12	2 days	
P4 & Pw4	01.06.12	08.06.12	7 days (denoted with*)	P4 was hit with the rig during testing of P2, no visible disturbance or influence on test results noticed
P5 & Pw5	01.06.12	01.06.12 06.01.12	0 days 5 days	Reference value test at $t = 0$ , plates were then reinstalled to original depth.

Table 11 Executed installation and test procedure

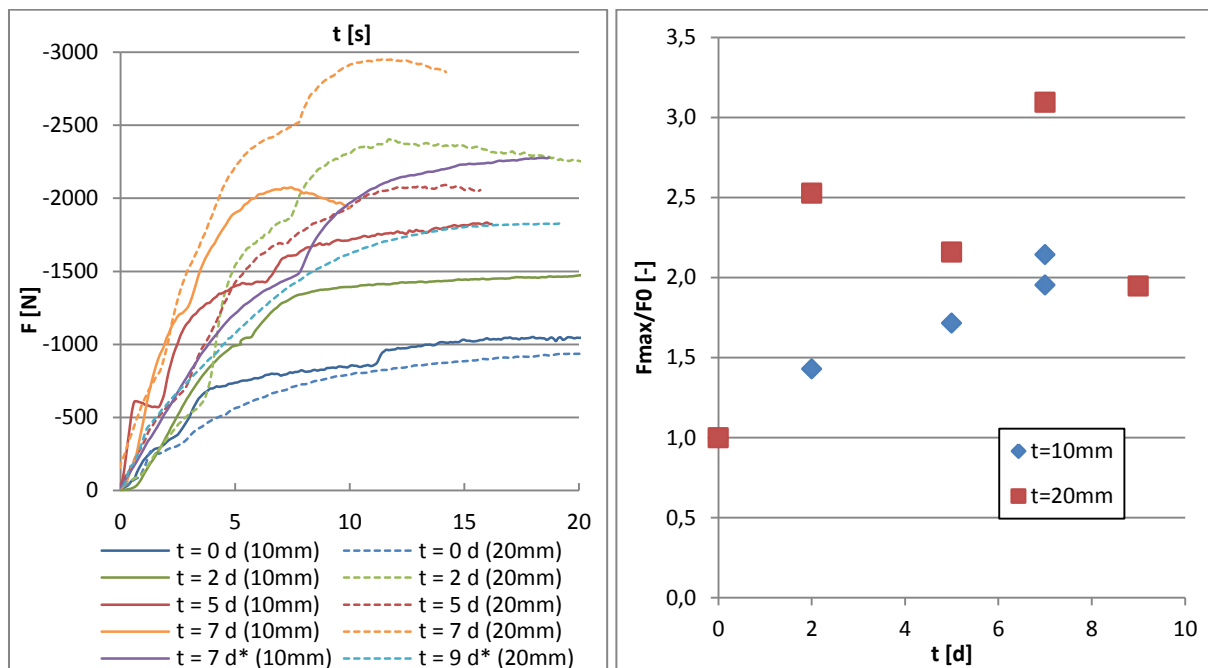


Figure 53 Model test results

From Figure 53 it is evident that the resistance increases substantially within a short time period after installation. Considering a lower bound increase after 10 days for both plate thicknesses a resistance increase ratio ( $F_{max}/F_0$ ) in the range of 1.5-2.0 is representative. The force versus time pattern is gradually changing towards quicker and more brittle failure with time. Recorded leaps in the force-time plot are mainly due to halts and uneven vertical test speed.

The hypotheses raised in Chapter 4.2 is not confirmed nor denied by the model test results. Unfortunately the reduction in available data points and time intervals due to the delays render it impossible to draw many conclusions. However there is evidently some resemblance between the increasing pulling resistance and thixotropy values (further discussed in Chapter 5.3.1). Maximum consolidation time of 9 days is insufficient to discuss relative contribution of consolidation and thixotropy on the resistance increase.

Plate thickness does seem to significantly impact the set-up factor at given time intervals. However it is somewhat surprising that the largest increase in resistance during early stages of reconsolidation is registered for the thickest plates. Despite some uncertainty related with the reference resistance (few data points) more than 50% increase in initial resistance for the thickest plate is needed to compensate for the difference between the two plate thicknesses.

Increased remolding of soil close to the steel plate tends to be beneficial for design at an early stage in the model test as the thickest plates experience the largest set-up effect. Early stage set-up is often assumed to be dominated by thixotropy. Since the model test translates to the self-weight penetration of the suction caisson, larger skirt wall thickness could increase early phase set-up.

Further testing and more data is needed before concluding; nevertheless the model test indicates some potential effect of self-weight penetration and soil displacement that could be beneficial for future suction caisson design.

Figure 54 show deep-seated clay on the steel plate after testing the pull resistance and removing the plate from the ground. Even after a short period of time ( $t = 7$  days) an approximately 2 cm thick layer of clay was stuck to the steel plate. The 3 cm thick layer along the centerline of the plate is explained by the larger cavity left above from the casing. Along the plate sides there was some clay deposits, although significantly less than 2 cm thick it indicates some deviation from the ideal plain strain assumption. For the plates the least influenced by impurities in the overburden clay the effect of pre-lifting the casing is visible (right hand side of Figure 54). Pre-lifting the casing is believed to reduce rod-casing interference on the measured resistance. Any clay along the rod had much softer and weaker behavior compared to the deposits at the plate.



**Figure 54 Deep-seated clay on steel plate (left hand side) and clay behavior in the transition zone from plate to rod (right hand side)**

### 5.3.1 Thixotropy test

The thixotropy test results (Figure 55) corresponds relatively well with the model test results. Despite quite large scatter, a lower bound estimate of increasing remolded undrained shear strength ratio of 2.0-3.0 after 10 days seem legit. Comparison against the ratio from the model test (1.5-2.0) indicates that the model test results do not dramatically overshoot an expected increase from thixotropy. Care should be taken to not overestimate the value of the simple fall cone test, but at least it links thixotropy and early stage regeneration of resistance in the model test closer together.

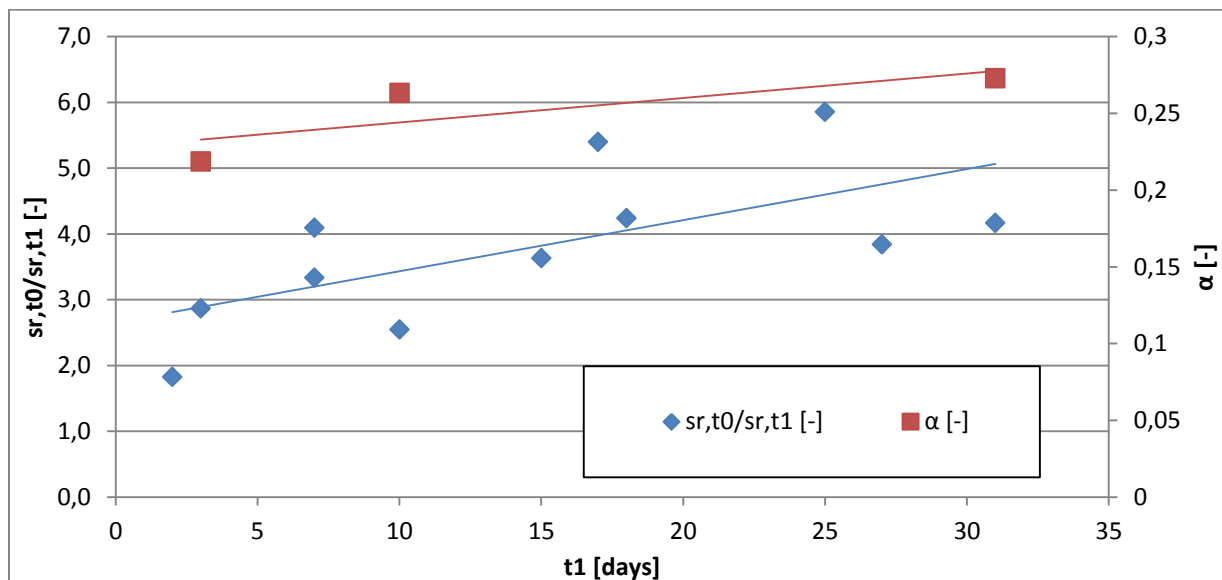


Figure 55 Thixotropy test results

Unfortunately the set-up factor ( $\alpha$ ) could not be calculated for all tests since undisturbed undrained shear strength values were missing. In addition to this the variation between different samples was too large in order to use average estimated values. Comparing the test results with reported thixotropy related strength increase in literature is therefore impossible. However the tendency of increasing undrained shear strength with time despite no volume change is underlined. Testing of water content after 25 and 27 days did not reveal any substantial change from the original values at  $t=0$  days (Appendix H).



## 6 Summary and future work

The FEM analyses presented in this MSc have several limitations. Among the most important are:

- a. Only a simplified installation procedure assuming constant applied underpressure has been evaluated
- b. Potential cyclic load situation has been neglected
- c. Only static vertical load has been applied (no moment or horizontal forces considered)
- d. Remolded stiffness in the interface zones was neglected due to absence of CRS oedometer tests on remolded soil in the available soil investigation data
- e. Final consolidation settlements could not be verified due to lack of field measurements

The simple physical model test also has several limitations that are important to take into account when evaluating the test results:

- a. Limited number of completed model tests
- b. Uncertain reference value for initial resistance due to a very limited number of tests and lack of undisturbed resistance
- c. Manually controlled vertical movement speed during tests
- d. No record of deformation combined with force
- e. Uncertain contribution of tip and rod-casing resistance
- f. Missing record of undisturbed undrained shear strength from all fall cone tests

A series of FEM analyses founded the basis for evaluating the effect of reconsolidation of suction caissons installed with applied underpressure. During consolidation dissipation of excess pore pressures and increase in effective stress result in an increase in undrained shear strength. However the increase is smaller than expected compared with set-up factors in literature. Despite buildup of effective stresses the FEM model is not able to account for the total set-up contribution. An adjusted simulation procedure including incremental increase of friction angle in the interface zones has been suggested. The results were found to be reasonable with respect to final consolidation settlements and development of mobilized shear strength with time. Further correlation of in-situ records and monitored settlements is recommended for validation of the analyses.

Modeled undrained shear strength with time proved to have huge influence on final consolidation settlements. Mobilization of soil around the suction caisson is closely related to shear strength. Higher shear strength leads to decreasing final consolidation settlement for the suction caisson. However the settlement of the surrounding seabed simultaneously increases. Appropriate evaluation of soil structure interaction is important to assess the

reliability of the analysis. The FEM model was found to be surprisingly sensitive to small adjustments to soil properties, underlining the importance of sufficient evaluation of the model behavior. Taking into account the soil volume (strength and stiffness) changes in the interface zones along the skirt wall is essential for determining long term settlements.

The simple physical model test suffered from delays and other set-backs, consequently the test results were limited. Discussing the assumptions in the FEM analyses based on the available results was not viable. Nevertheless the model test underlined the importance of considering short term set-up effects on steel body embedded into soft clay. During consolidation for less than 10 days significant increase in resistance and deep-seated clay on the steel plates was recorded. Physical observations in the field also indicate significant influence of deep-seated clay deposits on the steel plates. The increase in resistance recorded for the model test corresponded relatively well with a simple thixotropy test. A somewhat surprising trend in the model test result was larger increase in resistance for the thickest plate. This could indicate potential beneficial effects of thicker skirt walls with respect to short term set-up and increased resistance. However further testing and significantly larger basis of comparison is needed to confirm or invalidate this result.

Future work could include back calculation and correlation between FEM analyses and in-situ records of suction caissons. Development of a material model including an option for the user to specify an increase in shear strength with time would be beneficial. An intuitive relation between soil stiffness and soil strength is vital for such material model. Finally there is lot of unused potential in the simple physical model test that could be useful for future project and master thesis at the Geotechnical Division at NTNU. More test results in combination with more advanced soil tests could form the basis for comparison with numerical calculations. This could also prove applicable for FEM analyses of suction caissons, especially in relation with self-weight penetration and soil behavior outside the skirt wall.

## 7 Bibliography

- Andersen, K. H., & Jostad, H. P. (2004). Shear Strength Along Inside of Suction Anchor Skirt Wall in Clay. *Offshore Technology Conference* (ss. 1-13). Houston, Texas: OTC.
- Andersen, K. H., Andresen, L., H.P., J., & Clukey, E. C. (2004). Effect of Skirt Tip Geometry on Set-up Outside Suction Anchors in Soft Clay. *24th International Conference on Offshore Mechanics and Arctic Engineering* (ss. 1-10). Vancouver: ASME.
- Andersen, K., & Jostad, H. (1999). Foundation Design of Skirted Foundations and Anchors in Clay. *Offshore Technology Conference* (ss. 1-2). Houston: OTC.
- Andersen, K., & Jostad, H. (2002). Shear Strength Along Outside Wall of Suction Anchors in Clay. *12th ISOPE Conference*, (ss. 1-10). Kyushu.
- Baligh, M., Azzouz, A., & Chin, C.-T. (1987). Disturbances Due to "Ideal" Tube Sampling. *Journal of Geotechnical Engineering*, 739-757.
- Chen, W., & Randolph, M. F. (2007, April 3). External radial stress changes and axial capacity for suction caissons in soft clay. *Géotechnique*, 57(6), 499-511.
- DNV. (2005). *Geotechnical Design and Installation of Suction Anchors in Clay (DNV-RP-E303)*. Høvik: Det Norske Veritas (DNV).
- Hernandez-Martinez, F., Rahim, A., Strandvik, S., Jostad, H., & Andersen, K. (2009). Consolidation settlement of skirted foundations for subsea structures in soft clay. *International Conference on Soil Mechanics and Geotechnical Engineering* (ss. 1167-1172). Alexandria: IOS Press.
- Jaky, J. (1948). Pressure in Soils. *International Conference of Soil Mechanics and Foundation Engineering* (ss. 103-107). London: ICSMFE.
- Karlsrud, K. (2012). *Prediction of load-displacement behaviour and capacity of axially loaded piles in clay based on analyses and interpretation of pile load test results*. Trondheim: NTNU - trykk.
- Karlsrud, K., & Nadim, F. (1990). Axial Capacity of Offshore Piles in Clay. *Offshore Technology Conference* (ss. 405-416). Houston, Texas: OTC.
- Norsk Standard. (2007). *Petroleums- og naturgassindustri Faste offshorekonstruksjoner av stål (NS-EN ISO 19902)*. Brussel: Standard Norge.
- PLAXIS. (2012). *PLAXIS 2D 2011*. Hentet January 16, 2012 fra PLAXIS: <http://www.plaxis.nl/shop/135/info//PLAXIS+2D+2011/>
- PLAXIS Manual. (u.d.). *PLAXIS*. Hentet March 2, 2012 fra PLAXIS Material Model Manual: <http://www.plaxis.nl/files/files/GiD1-3-Material-Models.pdf>
- Renzi, R., Maggioni, W., Smits, F., & Manes, V. (1991). A Centrifugal Study on the Behavior of Suction Piles. *Internatiol Conference Centrifuge 91* (ss. 169-176). Boulder, Colorado: Balkema, Rotterdam.
- Sandven, R. (1990). *Strength and Deformation Properties of Fine Grained Soils Obtained from Piezocone Tests*. Trondheim: Norges Tekniske Høgskole.

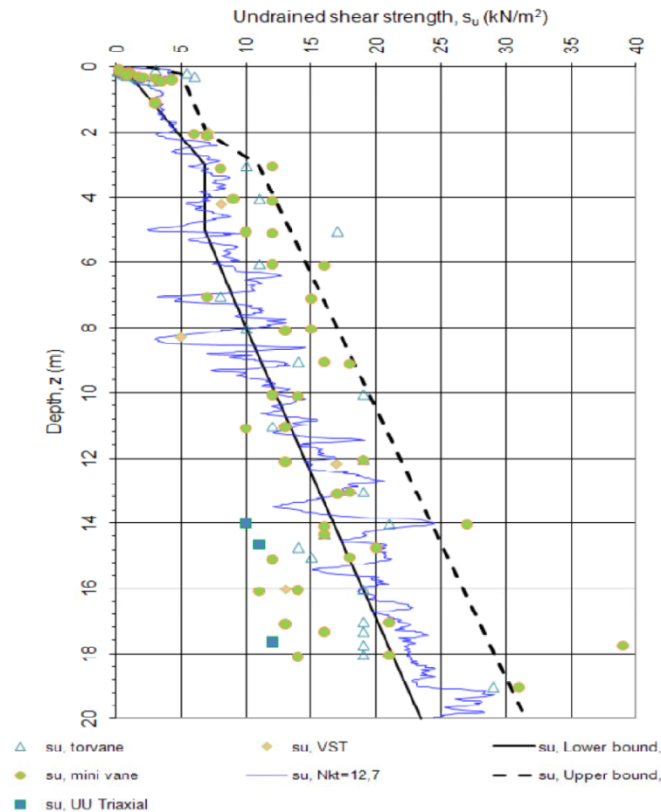


# Appendix

## Appendix A. Soil investigation data (west coast of Africa)

Stratum	Depth Below Seafloor (z)	Submerged Unit Weight ( $\gamma'$ )	Undisturbed Undrained Shear Strength ( $s_u$ )		Sensitivity ( $s_r$ )	Strain at Half-Peak Deviator Stress ( $\epsilon_{50}$ )
			Lower Bound	Upper Bound		
	[m]	[kN/m <sup>3</sup> ]	[kPa]			[%]
	0.0	2.0	0.6	2.4	2.0	2.0
	0.2	(2.1)	(1.0)	5.0	(2.0)	(2.0)
	2.0	2.9	(4.7)	7.0	(2.3)	(2.0)
	3.0	(2.9)	6.8	11.0	2.5	(2.0)
	5.0	(2.8)	6.8	(13.4)	3.2	(2.0)
	6.0	2.7	(7.9)	(14.6)	(3.6)	(2.0)
	8.0	(2.8)	10.0	(17.0)	4.4	(2.0)
	10.0	(3.0)	(12.3)	(19.4)	(4.4)	2.0
	13.5	(3.2)	(16.2)	(23.7)	(4.4)	1.0
	18.0	3.5	(21.3)	(29.1)	(4.5)	(1.0)
	20.0	(2.9)	23.5	31.5	4.5	(1.0)
	20.5	2.7	(24.1)	(32.2)	(4.5)	(1.0)
	24.0	3.1	(28.3)	(36.7)	4.7	1.0
	40.0	(3.1)	47.5	57.5	5.1	(1.0)

- Notes:
1. Values presented in parenthesis are interpolated between closest values not in parenthesis or extrapolated;
  2.  $\epsilon_{50}$  is strain at half-peak deviator stress from unconsolidated-undrained triaxial compression tests; and
  3. Depths in shaded background indicate depth below STACOR recovery.



**SUMMARY OF 1-D CONSTANT-RATE-OF-STRAIN (CRS) CONSOLIDATION TESTS**

Series &/or Test No.	Boring Sample or Spec. No.	Penetration or Depth (m)	Index Properties:				At Preconsol. Stress:		Compression Ratios:			Coeff. of Consol., $c_v$ Virgin Loading (m <sup>2</sup> /yr)	Remarks: SB-Sharp Break RSB-Relatively SB MR-Mod. Rounded R-Rounded	
			$G_s$	$S_o$ (%)	LL PI	$W_o$ (%) $LI_o$	$\gamma_{t,o}$ (kN/m <sup>3</sup> ) $e_o$	Casagrande Method Becker Method <sup>(1)</sup>	$\sigma'_p$ (kPa)	$\epsilon_s$ (%)	Virgin CR CR by LL (CR <sub>LL</sub> ) <sup>(2)</sup>			Recomp. RR Swell (SR)
1		6.82	2.774	99.0		182.4	12.5	39.4	4.9	0.380	0.034		0.61 - 1.61	SB-Sharp Break
							5.113	40.8			0.028	11.299		
2		13.82	2.785	99.8		163.5	12.9	58.8	5.5	0.455			0.02 - 2.96	SB-Sharp Break
							4.562	60.8			0.023			
3		21.82	2.759	98.7		136.9	13.3	101.6	6.7	0.439	0.025		0.92 - 6.66	SB-Sharp Break
							3.828	105.8			0.025	17.925		

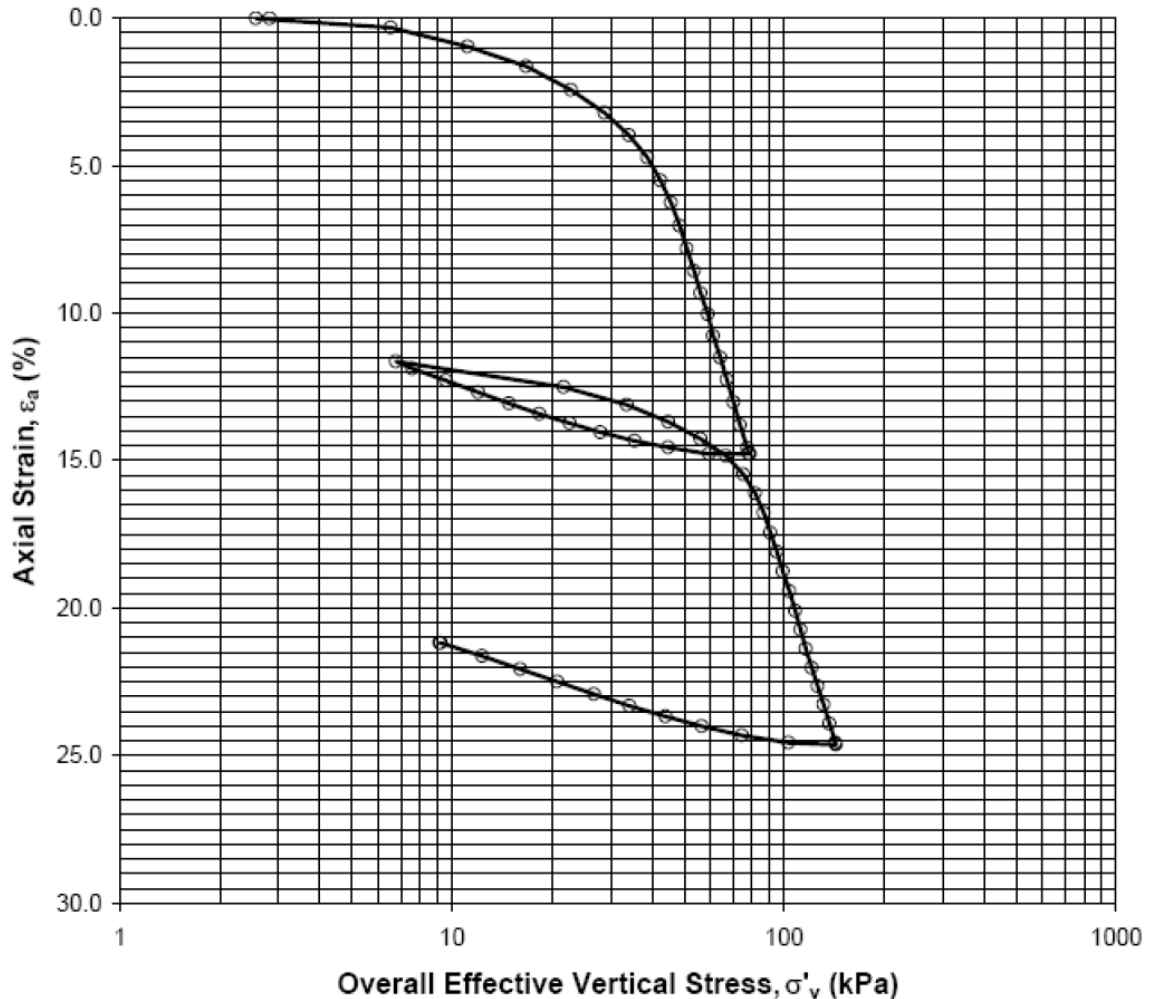
No.	Description of Tested Soil, Test Remarks, and Supplemental Data:	Plate Number
1	clay, dark gray with traces of organic matter	
2	clay, dark gray with silt seams and traces of organic matter	
3	clay, dark gray with traces of organic matter	

Notes:   Indicates value was copied from adjacent test specimen or assumed.

<sup>(1)</sup> Estimated preconsolidation stress using the Work per Unit Volume method, as described by Becker, et al. (1987).

<sup>(2)</sup>  $CR_{LL} = ((LL - 10) \times 0.009) / (1 + e_o)$

**Series 1 - depth 6.82 m**



**SUMMARY OF STATIC TRUEPATH  $K_0$  TRIAXIAL TESTS**  
Compression and Extension Tests

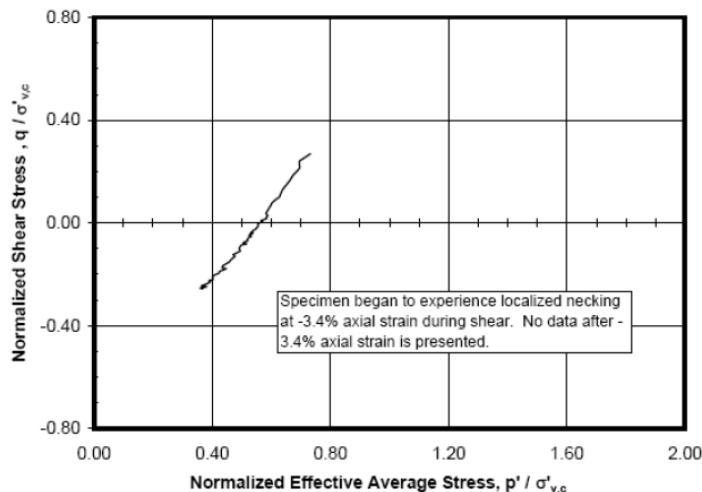
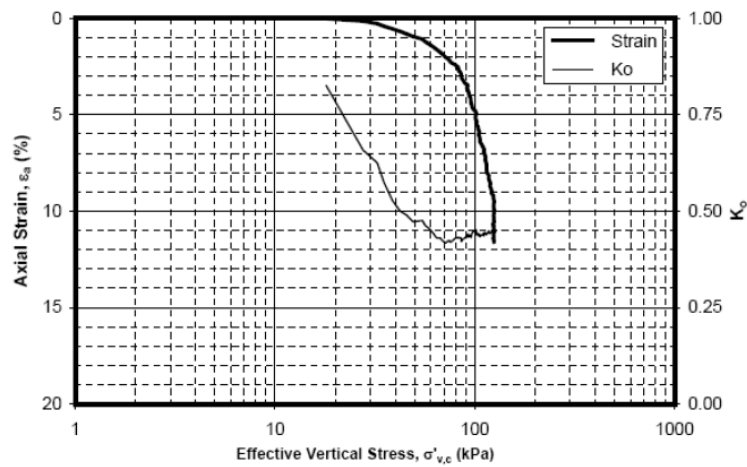
Series &/or Test No.	Boring - Sample Spec. No.	Penetration or Depth (m)	$G_e$	Index Properties:						$\sigma'_{v,c}$ (kPa)	$K_0 = \sigma'_{h,c}/\sigma'_{v,c}$	$\epsilon_{a,c}$ (%)	$\epsilon_{v,rate}$ (%/hr)	at Peak Shear Stress						$c_u/\sigma'_{v,c}$ [2]			
				LL	$w_c$	$\gamma_{t,c}$	$S_c$	LI <sub>c</sub>	Induced OCR					B-Value (%)	$\epsilon_{v,c}$ (%)	$t_c$ (days)	at Peak Stress Ratio (Obliquity)						
																	PI	$w_c$ (%)	$\gamma_{t,c}$ (kN/m <sup>3</sup> )		$S_c$	LI <sub>c</sub>	$\epsilon_a$ (%)
1-1		6.48	2.774	195.2	12.6	101.4		53.86	0.47	15.2	0.5	0.3	0.368	0.750	0.096	2.924	0.257						
				149.1	13.4	102.1		1.00	84.00	20.3	3.1	5.8	0.318	0.538	0.259	3.889	36.2						
1-2		6.73	2.774	185.2	12.7	100.9		66.517	0.43	16.3	-0.5	-1.8	-0.216	0.312	-0.130	5.476	-0.156						
				145.8	13.4	101.3		1.00	99.00	18.1	3.1	-1.8	-0.216	0.312	-0.130	5.476	-43.7						
1-3		21.51	2.791	184.8	12.8	99.0		109.091	0.50	12.2	0.5	0.8	0.333	0.708	0.128	2.783	0.252						
				141.0	13.4	100.9		1.00	100.00	13.2	3.9	4.8	0.296	0.562	0.235	3.229	31.8						
1-4		21.63	2.791	154.0	12.9	98.5		123.824	0.46	12.3	-0.5	-3.4	-0.255	0.368	-0.158	5.511	-0.179						
				130.8	13.6	100.7		1.00	98.00	13.7	3.1	-3.3	-0.254	0.358	-0.156	5.898	-45.2						

Test No.	Description of Tested Soil , Test Remarks, and Supplemental Data	Back Pressure (kPa)
1-1	Clay, olive gray	338.05
1-2	Clay, olive gray	345.90
1-3	Clay, dark gray with traces of organic matter	342.66
1-4	Clay, olive gray	343.22

Notes:   Indicates value was copied from adjacent test specimen or assumed.  
 (1) Axial strain rate during consolidation (%/h) = 0.20  
 (2)  $c_u = q_{ult} \times \cos \psi'_{-c}$

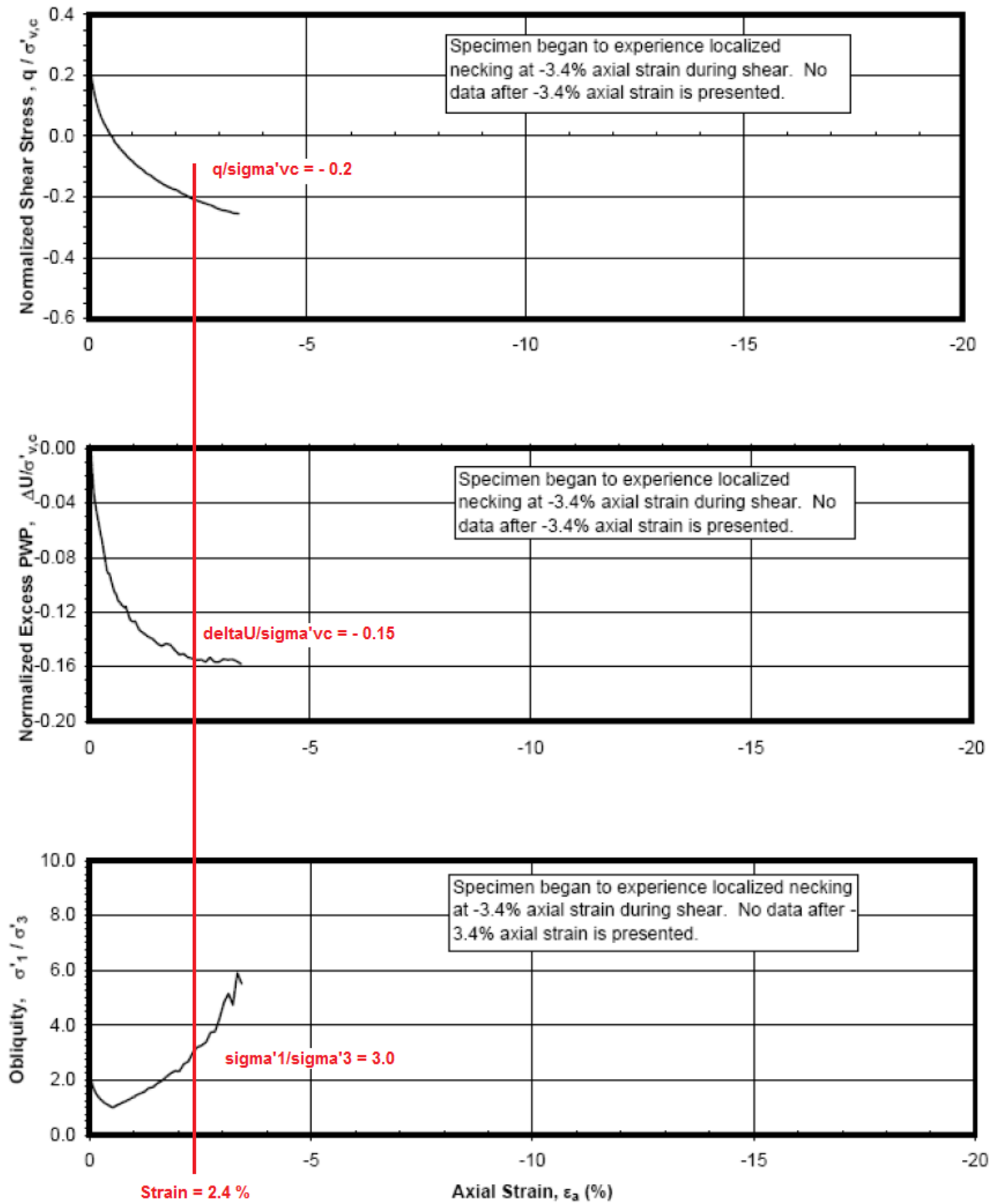
**STATIC TRUEPATH TRIAXIAL TEST - EXTENSION ( $CK_0$ UTE)**

Depth: 21.63 m



### STATIC TRUETH PATH TRIAXIAL TEST - EXTENSION (CK<sub>0</sub>UTE)

Depth: 21.63 m





**Correction of shear induced excess pore pressure ( $U_\gamma$ )** to account for change in octahedral stress in the triaxial test is derived below:

$$\sigma'_{oct} = \frac{1}{3}(\sigma'_1 + 2\sigma'_3)$$

$$q = \sigma'_1 - \sigma'_3 = X \cdot \sigma'_{v,c}$$

where X is the value of normalized shear stress at correct strain level (from graph)

$$\sigma'_1 = Y \cdot \sigma'_3$$

where Y is the value of obliquity at correct strain level (from graph)

$$Y \sigma'_3 - \sigma'_3 = X \cdot \sigma'_{v,c}$$

$$\sigma'_3 = \frac{X}{(Y - 1)} \cdot \sigma'_{v,c}$$

$$\Delta\sigma'_{oct} = \sigma'_{oct,1} - \sigma'_{oct,0} = \frac{1}{3}[(\sigma'_{1,1} + 2\sigma'_{3,1}) - (\sigma'_{1,0} + 2\sigma'_{3,0})]$$

where

$\sigma'_{oct,1}$  is octahedral stress at desired strain level (from suction caisson geometry)

$\sigma'_{oct,0}$  is octahedral stress at initial strain level (beginning of shear,  $\epsilon=0$ )

$$\frac{u_\gamma}{\sigma'_{v,0}} = \frac{\Delta U}{\sigma'_{v,c}} - \frac{\Delta\sigma'_{oct}}{\sigma'_{v,c}}$$

where

$\Delta U / \sigma'_{v,c}$  is normalized excess PWP at final strain level due to penetration (from graph)

$\Delta\sigma'_{oct} / \sigma'_{v,c}$  is normalized change in octahedral stress in triaxial test by given vertical consolidation stress

SUMMARY OF  $K_0$ -CONSOLIDATED STATIC DSS TESTS

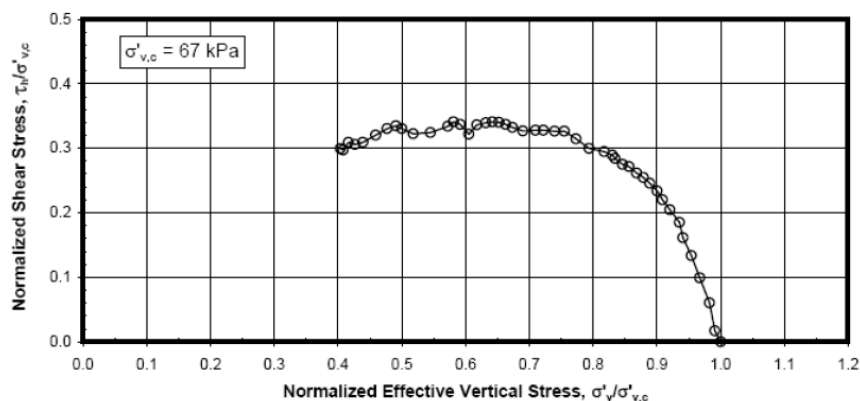
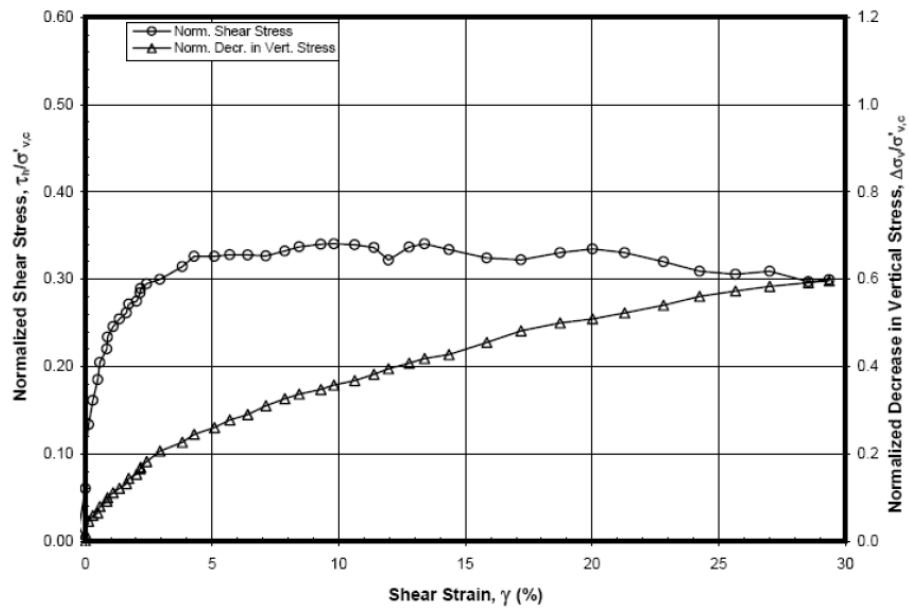
Series &/or Test No.	Boring - Sample - Spec. No.	Penetration or Depth (m)	$G_s$	Index Properties:							at Peak Shear Stress					$\frac{C_u}{\sigma'_{v,c}}$ $\Psi_{DSS}$ (degrees)
				LL	$W_o$	$\gamma_{lo}$	$S_o$	$LI_o$	$\sigma'_{v,c}$ (kPa)	$\epsilon_{a,max}$	$\gamma_{rate}$ (%/hr)	at Peak Stress Ratio - High Strain			$\frac{\Delta U}{\sigma'_{v,c}}$	
												PI	$W_c$ (%)	$\gamma_{lc}$ ( $kN/m^3$ )		
1-1		3.00	2.770	189.3	12.4	98.5		46.1	16.06	4.9	28.5	16.6	0.672	0.462	0.361	
				155.5	13.1	100.0		1.00	16.06	2.2	29.5	16.6	0.692	0.481	0.3470	
1-2		6.77	2.774	176.3	12.7	99.3		66.8	10.06	4.8	9.8	22.7	0.531	0.358	0.341	
				156.1	13.0	100.0		1.00	10.06	2.1	29.4	20.0	0.742	0.596	0.3658	
1-3		13.77	2.785	166.9	12.8	98.8		151.2	20.48	4.6	7.5	42.8	0.421	0.328	0.283	
				127.0	13.6	100.0		1.00	20.48	0.5	29.3	37.3	0.606	0.593	0.3120	
1-4		21.77	2.791	152.1	13.1	99.9		188.9	18.72	4.9	10.3	52.3	0.482	0.426	0.277	
				117.1	13.9	100.0		1.00	18.72	0.7	29.7	43.0	0.675	0.663	0.3403	
Average value (at peak stress ratio - high strain) used for remolding induced p.p.																

Test No.	Description of Tested Soil, Test Remarks, and Supplemental Data:	Plate No.
1-1	clay, olive gray	
1-2	clay, olive gray	
1-3	clay, dark gray	
1-4	clay, gray and olive gray	

Indicates value was copied from adjacent test specimen or assumed.

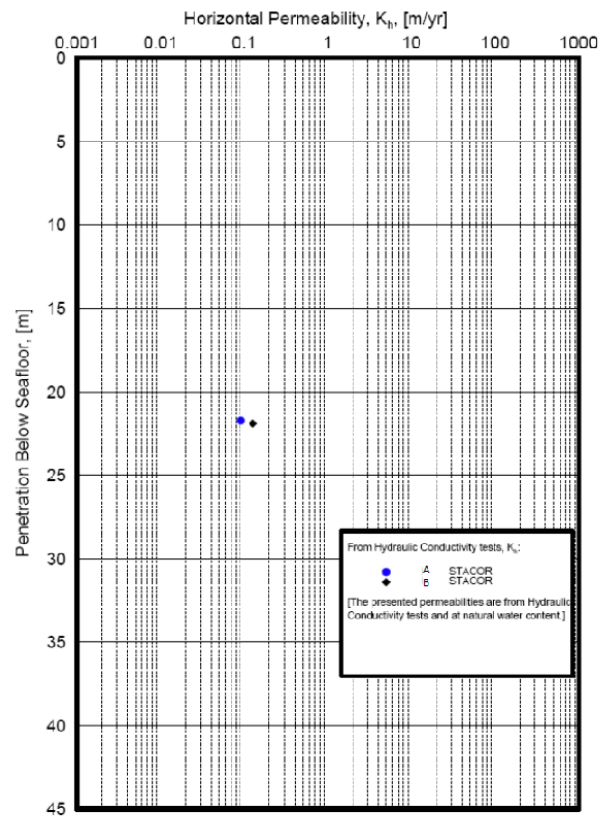
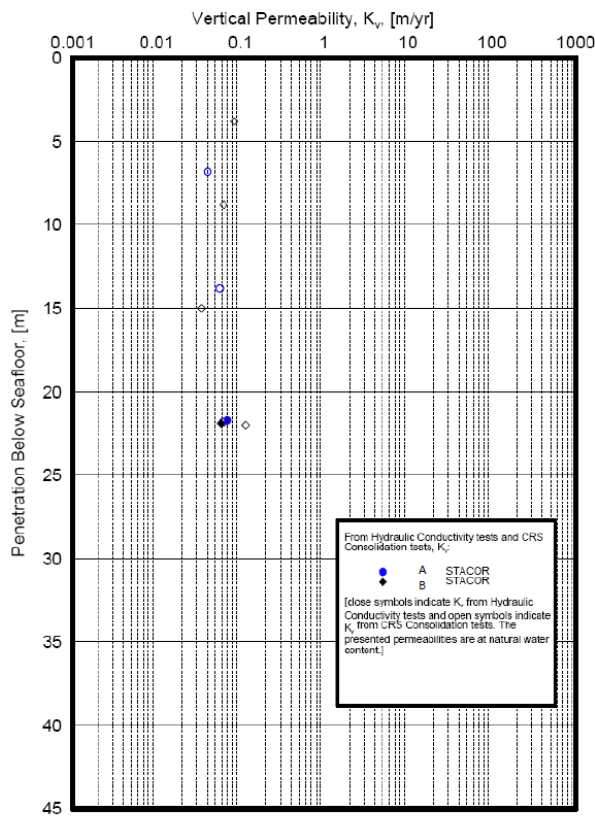
$K_0$ -CONSOLIDATED STATIC DSS TEST

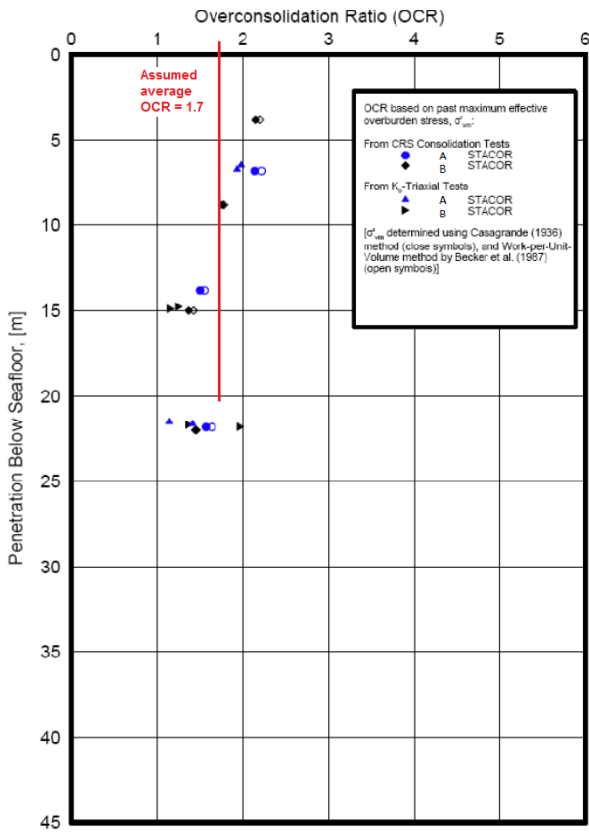
Depth: 6.77 m



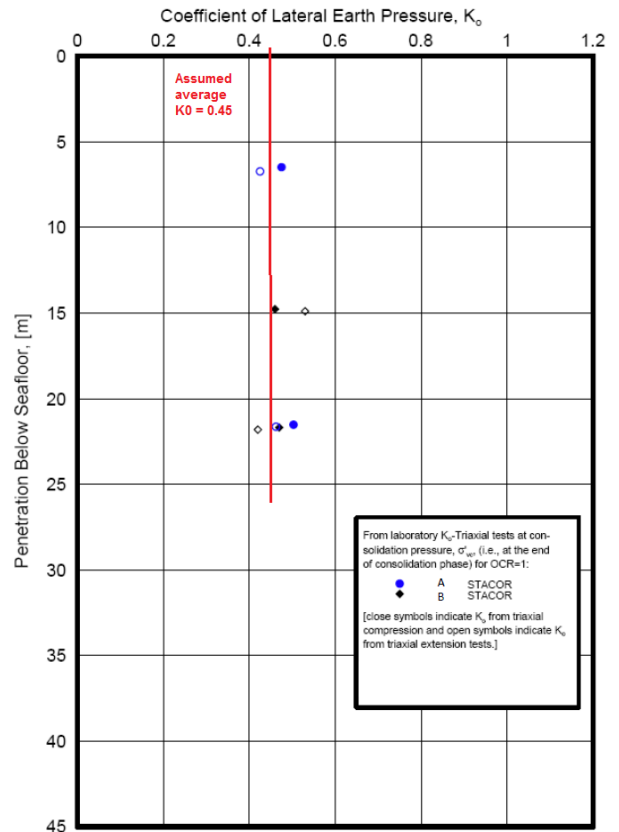
**Table II-2. Hydraulic Conductivity Test Results**

Depth (m)	$k_v$ (m/yr)	$k_h$ (m/yr)	$k_r$ (m/yr)	$k_h/k_v$	$k_r/k_v$
6.82 (CRS)	4.07E-02	Average value utilized (horizontal/vertical permeability ratio at depth = 21.73 m assumed for all depths)	-	-	-
13.82 (CRS)	5.62E-02		-	-	-
21.82 (CRS)	6.19E-02		-	-	-
21.73 (PER)	6.97E-02	9.09E-02	1.17E-01	1.30	1.68

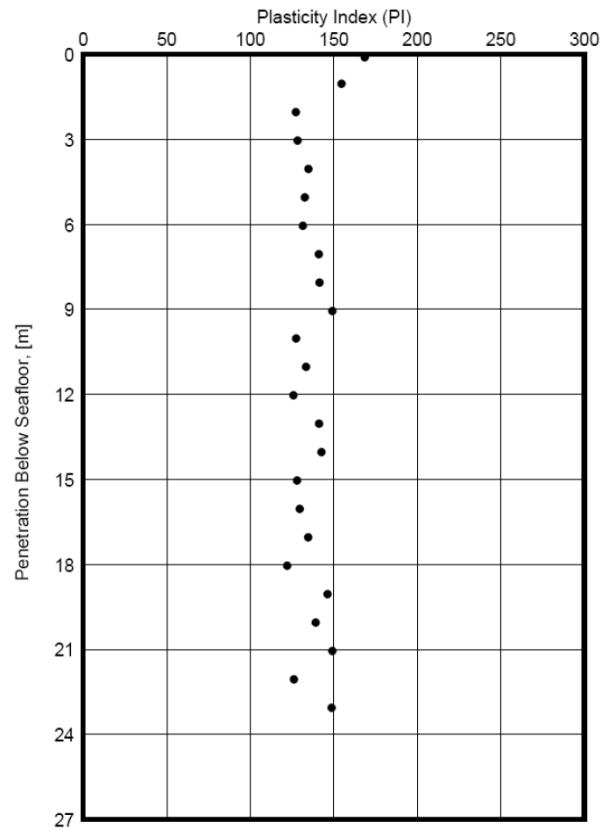
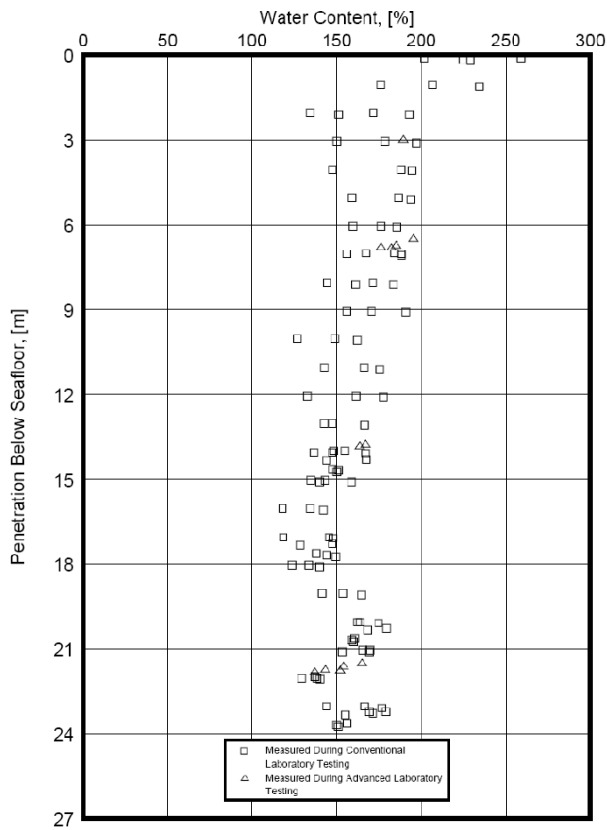




APPARENT OVERCONSOLIDATION RATIO (OCR)



COEFFICIENT OF AT-REST LATERAL EARTH PRESSURE DATA



Interpreted soil data

S <sub>v</sub> - active	
Z [m]	S <sub>v</sub> <sup>a</sup> [kPa]
0,000	1,5
0,200	3,0
2,000	5,9
3,000	8,9
5,000	10,1
6,000	11,3
8,000	13,5
10,000	15,9
13,500	20,0
18,000	25,2
20,000	27,5
20,500	28,2
24,000	32,5
40,000	52,5

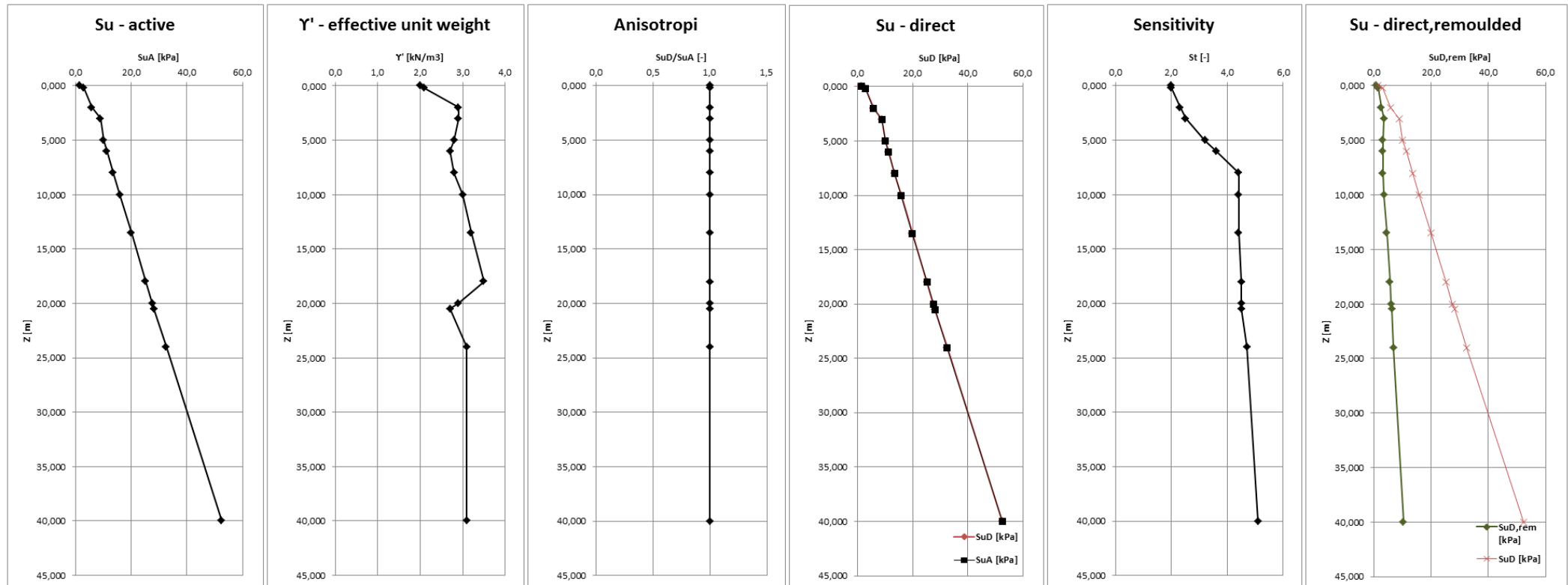
Y' - effective unit weight	
Z [m]	Y' [kN/m <sup>3</sup> ]
0,000	2,0
0,200	2,1
2,000	2,9
3,000	2,9
5,000	2,8
6,000	2,7
8,000	2,8
10,000	3,0
13,500	3,2
18,000	3,5
20,000	2,9
20,500	2,7
24,000	3,1
40,000	3,1

Anisotropi	
Z [m]	S <sub>v</sub> <sup>o</sup> /S <sub>v</sub> <sup>a</sup> [-]
0,000	1,0
0,200	1,0
2,000	1,0
3,000	1,0
5,000	1,0
6,000	1,0
8,000	1,0
10,000	1,0
13,500	1,0
18,000	1,0
20,000	1,0
20,500	1,0
24,000	1,0
40,000	1,0

S <sub>v</sub> - direct	
Z [m]	S <sub>v</sub> <sup>o</sup> [kPa]
0,000	1,5
0,200	3,0
2,000	5,9
3,000	8,9
5,000	10,1
6,000	11,3
8,000	13,5
10,000	15,9
13,500	20,0
18,000	25,2
20,000	27,5
20,500	28,2
24,000	32,5
40,000	52,5

Sensitivity	
Z [m]	S <sub>t</sub> [-]
0,000	2,0
0,200	2,0
2,000	2,3
3,000	2,5
5,000	3,2
6,000	3,6
8,000	4,4
10,000	4,4
13,500	4,4
18,000	4,5
20,000	4,5
20,500	4,5
24,000	4,7
40,000	5,1

S <sub>v</sub> - direct,remoulded	
Z [m]	S <sub>v</sub> <sup>o</sup> <sub>rem</sub> [kPa]
0,000	0,8
0,200	1,5
2,000	2,5
3,000	3,6
5,000	3,2
6,000	3,1
8,000	3,1
10,000	3,6
13,500	4,5
18,000	5,6
20,000	6,1
20,500	6,3
24,000	6,9
40,000	10,3



## Appendix B. Input data FEM model

## Input data clay + clay plug

<b>Suction anchor</b>	
Design load, L [kN]	1831
Maximum penetration depth, $Z_{max}$ [m]	20,0
Anchor diameter, D [m]	5,0
Skirt width, t [m]	0,03
Axial modulus, EA [kN/m]	3,19E+12
Rigidity modulus, EI [kN/m <sup>2</sup> /m]	2,58E+08
Distributed weight, w [kN/m/m]	0
Distributed load, a [kN/m <sup>2</sup> ]	127,3
<b>Soil parameters (installation)</b>	
Clay sensitivity, $S_y/\sigma'_{v,0}$ [1/(kN/m <sup>3</sup> )]	0,042
Clay sensitivity   Z=0, $S_t$ [-]	2
Undrained shear strength, $S_u/\sigma'_{v,0}$ [m]	0,43
Undrained shear strength   Z=0, $S_u$ [kPa]	1,5
Bearing capacity factor, $N_c$ [-]	7,5
<b>Soil parameters (stress, strain, ex.pp)</b>	
Effective unit weight soil, $\gamma'$ [kN/m <sup>3</sup> ]	3
OCR [-]	1,7
$K_{0,0}$ [-]	0,45
Shear stress at maximum vertical strain, $\tau/\sigma'_{v,0}$ [kPa]	-0,1
Shear strain induced pore pressure, $U_\gamma/\sigma'_{v,0}$ [kPa]	-0,05
Remoulding induced pore pressure, $\Delta U/\sigma'_v$ [kPa]	0,58
<b>Soil parameters (soft soil material model)</b>	
Virgin compression ratio, $\lambda^*$ , $\lambda^*$ [-]	0,148
Recompression ratio, $\kappa^*$ , $\kappa^*$ [-]	0,014
Cohesion, $C'_{ref}$ [kPa]	1
Friction angle, $\phi'$ [°]	39,5
Dilation angle, $\psi$ [°]	0
Poisson ratio unloading-reloading, $\nu'_{ur}$ [-]	0,15
Lateral earth pressure coefficient (NC), $K_0^{nc}$ [-]	0,36
Horizontal permeability, $k_x$ [m/day]	2,01E-04
Vertical permeability, $k_y$ [m/day]	1,54E-04

## Updated input data clay plug

<b>Input</b>		
Anchor radius, r [m]	2,50	
Skirt width, t [m]	0,030	
Effective unit weight soil, $\gamma'$ [kN/m <sup>3</sup> ]	3,00	
Shear stress at maximum vertical strain, $\tau/\sigma'_{v,0}$ [kPa]	-0,10	
Shear strain induced pore pressure, $U_\gamma/\sigma'_{v,0}$ [kPa]	-0,05	
OCR [-]	1,70	
$K_{0,0}$ [-]	0,45	
<b>Output, soil plug</b>		
Radial strain, $E_r$ [%]	1,20	
Vertical strain, $E_v$ [%]	-2,40	
Octahedral total stress change, $\Delta\sigma_{oct}/\sigma'_{v,0}$ [kPa]	0,50	
Shear strain induced pore pressure change, $\Delta U_\gamma/\sigma'_{v,0}$ [kPa]	-0,05	
Excess pore pressure, $\Delta U/\sigma'_{v,0}$ [kPa]	0,45	
Updated $K_0$ , $K_{0,up}$ [-]	1,36	
Updated OCR, $OCR_{up}$ [-]	3,09	
Depth, Z [m]	Excess pore pressure, $\Delta U$ [kPa]	Pore pressure, $U_{up}$ [kPa]
1,0	1,4	11,4
2,0	2,7	22,7
3,0	4,1	34,1
4,0	5,4	45,4
5,0	6,8	56,8
6,0	8,1	68,1
7,0	9,5	79,5
8,0	10,8	90,8
9,0	12,2	102,2
10,0	13,5	113,5
11,0	14,9	124,9
12,0	16,2	136,2
13,0	17,6	147,6
14,0	18,9	158,9
15,0	20,3	170,3
16,0	21,6	181,6
17,0	23,0	193,0
18,0	24,3	204,3
19,0	25,7	215,7
20,0	27,0	227,0
$U_{inc}$ [kPa]	1,4	11,4

**Input data remolded zones**

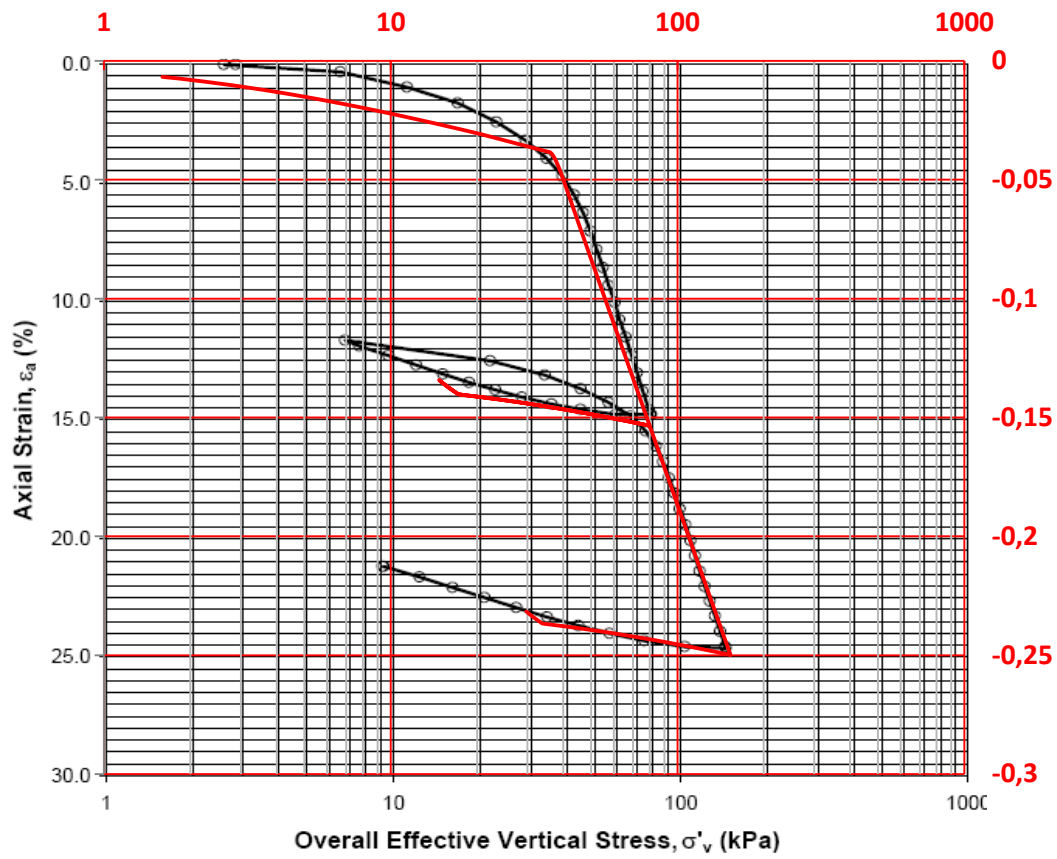
Soil parameters (soft soil material model)	
Virgin compression ratio, lambda*, λ* [-]	0,136
Recompression ratio, kappa*, κ* [-]	0,019
Cohesion, C' <sub>ref</sub> [kPa]	2
Friction angle, φ' [°]	8
Dilation angle, ψ [°]	0
Poisson ratio unloading-reloading, ν' <sub>ur</sub> [-]	0,15
Lateral earth pressure coefficient (NC), K <sub>0</sub> <sup>nc</sup> [-]	0,86
Horizontal permeability, k <sub>x</sub> [m/day]	2,01E-04
Vertical permeability, k <sub>y</sub> [m/day]	1,54E-04

**Updated input data remolded zones**

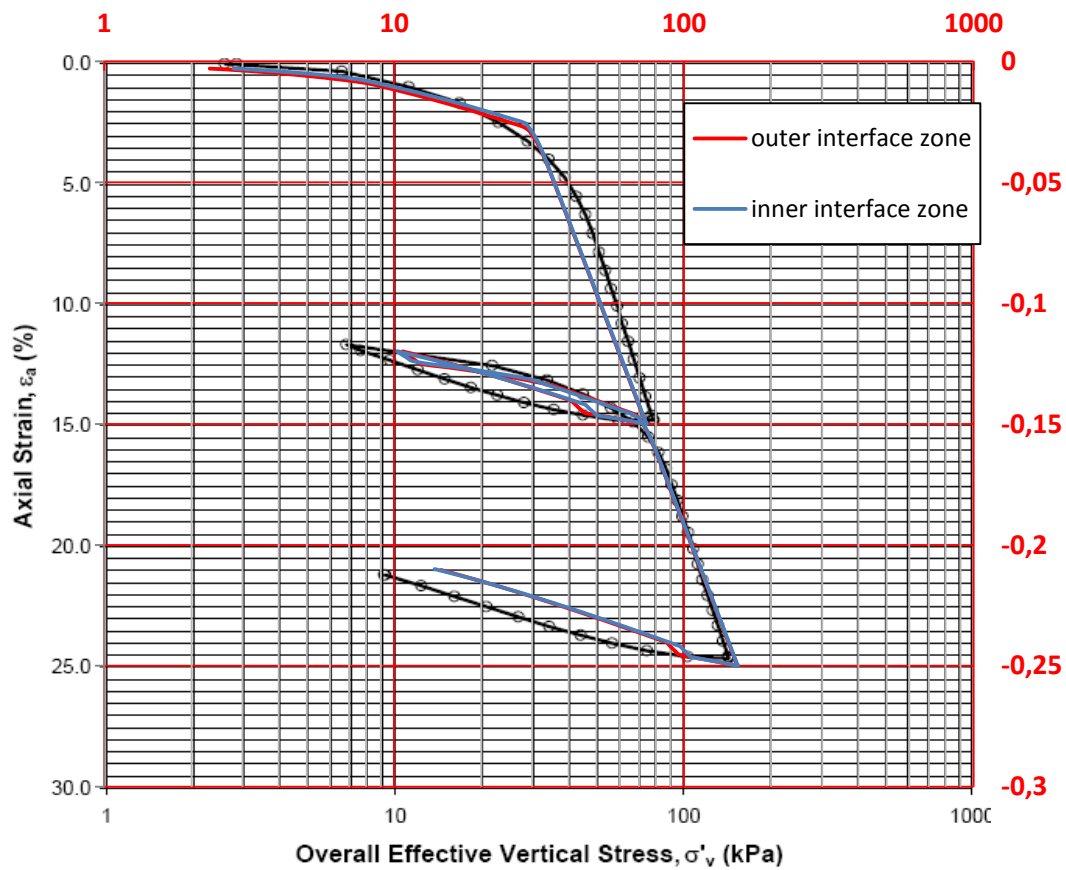
Input	
Anchor radius, r [m]	2,50
Skirt width, t [m]	0,030
Effective unit weight soil, γ' [kN/m <sup>3</sup> ]	3,00
Shear stress at maximum vertical strain, τ/σ' <sub>v,0</sub> [kPa]	-0,10
Shear strain induced pore pressure, U <sub>γ</sub> /σ' <sub>v,0</sub> [kPa]	-0,05
Remoulding induced pore pressure, ΔU/σ' <sub>oct</sub> [kPa]	0,58
OCR [-]	1,70
K <sub>0,0</sub> [-]	0,45
<b>Output, remoulded zone 2+3</b>	
Radial strain, Er [%]	1,20
Vertical strain, Ev [%]	-2,40
Octahedral total stress change, Δσ <sub>oct</sub> /σ' <sub>v,0</sub> [kPa]	0,50
Shear strain induced pore pressure change, ΔU <sub>γ</sub> /σ' <sub>v,0</sub> [kPa]	-0,05
Remoulding induced pore pressure, ΔU/σ' <sub>v</sub> [kPa]	0,58
Excess pore pressure, ΔU/σ' <sub>v,0</sub> [kPa]	1,03
Updated K <sub>0</sub> , K <sub>0,up</sub> [-]	0,78
Updated OCR, OCR <sub>up</sub> [-]	1,00

Depth, Z [m]	Inside anchor		Outside anchor	
	Excess pore pressure, ΔU [kPa]	Pore pressure, U <sub>up</sub> [kPa]	Excess pore pressure, ΔU [kPa]	Pore pressure, U <sub>up</sub> [kPa]
1,0	3,1	13,1	1,7	11,7
2,0	6,2	26,2	3,5	23,5
3,0	9,3	39,3	5,2	35,2
4,0	12,4	52,4	7,0	47,0
5,0	15,5	65,5	8,7	58,7
6,0	18,5	78,5	10,4	70,4
7,0	21,6	91,6	12,2	82,2
8,0	24,7	104,7	13,9	93,9
9,0	27,8	117,8	15,7	105,7
10,0	30,9	130,9	17,4	117,4
11,0	34,0	144,0	19,1	129,1
12,0	37,1	157,1	20,9	140,9
13,0	40,2	170,2	22,6	152,6
14,0	43,3	183,3	24,4	164,4
15,0	46,4	196,4	26,1	176,1
16,0	49,4	209,4	27,8	187,8
17,0	52,5	222,5	29,6	199,6
18,0	55,6	235,6	31,3	211,3
19,0	58,7	248,7	33,1	223,1
20,0	61,8	261,8	34,8	234,8
U <sub>inc</sub> [kPa]	3,1	13,1	1,7	11,7

**Clay plug**



**Interface zones**





Appendix C. Penetration analysis

				z [m]	Su [kPa]	St[-]	Su,rem [kPa]	Qs [kN]	Qp [kN]	$\sigma_{v,und,pres.}$ [kPa]	$\sigma'_v$ [kPa]	$\Delta u$ [kPa]	Driving force [-]
				0,0	1,5	2,0	0,8	0,0	0,0	-108,1	0	-108,1	Self-weight
				0,5	2,1	2,1	1,0	16,3	0,0	-106,5	1,5	-108,0	Self-weight
				1,0	2,8	2,1	1,3	36,9	0,0	-104,8	3	-107,8	Self-weight
				1,5	3,4	2,2	1,6	61,6	0,0	-103,1	4,5	-107,6	Self-weight
				2,0	4,1	2,3	1,8	90,1	0,0	-101,4	6	-107,4	Self-weight
				2,5	4,7	2,3	2,0	122,1	0,0	-99,6	7,5	-107,1	Self-weight
				3,0	5,4	2,4	2,3	157,6	0,0	-97,7	9	-106,7	Self-weight
				3,5	6,0	2,4	2,5	196,3	0,0	-95,9	10,5	-106,4	Self-weight
				4,0	6,7	2,5	2,7	238,1	0,0	-94,0	12	-106,0	Self-weight
				4,5	7,3	2,6	2,8	282,8	0,0	-92,0	13,5	-105,5	Self-weight
				5,0	8,0	2,6	3,0	330,3	0,0	-90,1	15	-105,1	Self-weight
				5,5	8,6	2,7	3,2	380,4	0,0	-88,1	16,5	-104,6	Self-weight
<b>General input</b>				6,0	9,2	2,8	3,4	433,1	0,0	-86,1	18	-104,1	Self-weight
Effective unit weight soil, $\gamma'$ [kN/m <sup>3</sup> ]	3			6,5	9,9	2,8	3,5	488,1	0,0	-84,0	19,5	-103,5	Self-weight
Clay sensitivity, $S_u/\sigma'_{v,0}$ [1/kPa]	0,042			7,0	10,5	2,9	3,7	545,5	0,0	-82,0	21	-103,0	Suction
Clay sensitivity   Z=0, $S_t$ [-]	2			7,5	11,2	2,9	3,8	605,1	0,0	-79,9	22,5	-102,4	Suction
Undrained shear strength, $S_u/\sigma'_{v,0}$ [-]	0,43			8,0	11,8	3,0	3,9	666,9	0,0	-77,8	24	-101,8	Suction
Undrained shear strength   Z=0, $S_u$ [kPa]	1,5			8,5	12,5	3,1	4,1	730,6	0,0	-75,7	25,5	-101,2	Suction
OCR [-]	1,70			9,0	13,1	3,1	4,2	796,3	0,0	-73,6	27	-100,6	Suction
Maximum penetration depth, $Z_{max}$ [m]	20			9,5	13,8	3,2	4,3	863,9	0,0	-71,4	28,5	-99,9	Suction
Anchor diameter, D [m]	5			10,0	14,4	3,3	4,4	933,3	0,0	-69,3	30	-99,3	Suction
Skirt width, t [m]	0,030			10,5	15,0	3,3	4,5	1004,4	0,0	-67,1	31,5	-98,6	Suction
Bearing capacity factor, $N_c$ [-]	7,5			11,0	15,7	3,4	4,6	1077,2	0,0	-64,9	33	-97,9	Suction
				11,5	16,3	3,4	4,7	1151,6	0,0	-62,7	34,5	-97,2	Suction
<b>Output</b>				12,0	17,0	3,5	4,8	1227,5	0,0	-60,5	36	-96,5	Suction
Effective anchor weight, $W'$ [kN]	669			12,5	17,6	3,6	4,9	1305,0	0,0	-58,3	37,5	-95,8	Suction
Skirt wall area, $A_{wall}$ [m <sup>2</sup> ]	628,3			13,0	18,3	3,6	5,0	1383,9	0,0	-56,0	39	-95,0	Suction
Skirt tip area, $A_{tip}$ [m <sup>2</sup> ]	0,47			13,5	18,9	3,7	5,1	1464,1	0,0	-53,8	40,5	-94,3	Suction
Side friction resistance, $Q_{side}$ [kN]	2616			14,0	19,6	3,8	5,2	1545,8	0,0	-51,5	42	-93,5	Suction
Tip resistance, $Q_{tip}$ [kN]	125			14,5	20,2	3,8	5,3	1628,7	0,0	-49,3	43,5	-92,8	Suction
Total penetration resistance, $Q_{tot}$ [kN]	2741			15,0	20,9	3,9	5,4	1712,9	0,0	-47,0	45	-92,0	Suction
Required underpressure, $\Delta u_{top}$ [kPa]	108			15,5	21,5	4,0	5,4	1798,3	0,0	-44,7	46,5	-91,2	Suction
Allowable underpressure, $U_{allow}$ [kPa]	357	OK		16,0	22,1	4,0	5,5	1884,9	0,0	-42,5	48	-90,5	Suction
				16,5	22,8	4,1	5,6	1972,7	0,0	-40,2	49,5	-89,7	Suction
				17,0	23,4	4,1	5,7	2061,5	0,0	-37,9	51	-88,9	Suction
				17,5	24,1	4,2	5,7	2151,4	0,0	-35,6	52,5	-88,1	Suction
				18,0	24,7	4,3	5,8	2242,4	0,0	-33,2	54	-87,2	Suction
				18,5	25,4	4,3	5,9	2334,4	0,0	-30,9	55,5	-86,4	Suction
				19,0	26,0	4,4	5,9	2427,4	0,0	-28,6	57	-85,6	Suction
				19,5	26,7	4,5	6,0	2521,3	0,0	-26,3	58,5	-84,8	Suction
				20,0	27,3	4,5	6,0	2616,2	124,8	-23,9	60	-83,9	Suction
							<b>Sum</b>	<b>2616</b>	<b>125</b>				

## Appendix D. Input data FEM model (self-weight penetration)

**Updated input data clay plug**

Input			Depth, Z [m]	Excess pore pressure, $\Delta U$ [kPa]	Pore pressure, $U_{up}$ [kPa]
Anchor radius, r [m]	2,50		0,3	0,4	3,6
Skirt width, t [m]	0,030		0,7	0,7	7,2
Effective unit weight soil, $\gamma'$ [kN/m <sup>3</sup> ]	3,00		1,0	1,1	10,9
Shear stress at maximum vertical strain, $\tau/\sigma'_{v,0}$ [kPa]	-0,05		1,3	1,5	14,5
Shear strain induced pore pressure, $U_{\gamma}/\sigma'_{v,0}$ [kPa]	-0,05		1,6	1,9	18,1
OCR [-]	1,70		2,0	2,2	21,7
$K_{0,0}$ [-]	0,45		2,3	2,6	25,4
			2,6	3,0	29,0
<b>Output, soil plug</b>			2,9	3,4	32,6
Radial strain, $E_r$ [%]	0,60		3,3	3,7	36,2
Vertical strain, $E_v$ [%]	-1,20		3,6	4,1	39,9
Octahedral total stress change, $\Delta\sigma_{oct}/\sigma'_{v,0}$ [kPa]	0,43		3,9	4,5	43,5
Shear strain induced pore pressure change, $\Delta U_{\gamma}/\sigma'_{v,0}$ [kPa]	-0,05		4,2	4,9	47,1
Excess pore pressure, $\Delta U/\sigma'_{v,0}$ [kPa]	0,38		4,6	5,2	50,7
Updated $K_0$ , $K_{0,1}$ [-]	1,16		4,9	5,6	54,4
Updated OCR, $OCR_1$ [-]	2,76		5,2	6,0	58,0
			5,5	6,4	61,6
<b>Transition zone (6.5 - 11.5 m)</b>			5,9	6,7	65,2
Self weight penetration depth	6,5		6,2	7,1	68,9
Suction anchor diameter	5,0		6,5	7,5	72,5
$U_{ref}$ at self weight penetration depth	72,5				
Applied underpressure penetration $\Delta u$	1,4		$U_{inc}$ [kPa]	1,2	11,2
$U_{ref}$ at applied underpressure penetration depth	131,1				
Linearly excess pore pressure transition $U_{inc}$	11,7				

## Updated input data remoulded zones

Input			
Anchor radius, $r$ [m]		2,50	
Skirt width, $t$ [m]		0,030	
Effective unit weight soil, $\gamma'$ [kN/m <sup>3</sup> ]		3,00	
Shear stress at maximum vertical strain, $\tau/\sigma'_{v,0}$ [kPa]		-0,05	
Shear strain induced pore pressure, $U_v/\sigma'_{v,0}$ [kPa]		-0,05	
Remoulding induced pore pressure, $\Delta U/\sigma'_{oct}$ [kPa]		0,58	
OCR [-]		1,70	
$K_{0,0}$ [-]		0,45	
<b>Output, remoulded zone 2+3</b>			
Radial strain, $E_r$ [%]		1,20	
Vertical strain, $E_v$ [%]		-2,40	
Octahedral total stress change, $\Delta\sigma_{oct}/\sigma'_{v,0}$ [kPa]		0,43	
Shear strain induced pore pressure change, $\Delta U_v/\sigma'_{v,0}$ [kPa]		-0,05	
Remoulding induced pore pressure, $\Delta U/\sigma'_{v,0}$ [kPa]		0,58	
Excess pore pressure, $\Delta U/\sigma'_{v,0}$ [kPa]		0,96	
Updated $K_0$ , $K_{0,1}$ [-]		0,58	
Updated OCR, $OCR_1$ [-]		1,00	
<b>Transition zone (6.5 - 11.5 m)</b>			
		<b>Inside</b>	<b>Outside</b>
Self weight penetration depth		6,5	6,5
Suction anchor diameter		5,0	5,0
$U_{ref}$ at self weight penetration depth		83,8	83,8
Applied underpressure penetration $\Delta u$		3,1	1,7
$U_{ref}$ at applied underpressure penetration depth		150,7	134,6
Linearly excess pore pressure transition $U_{inc}$		13,4	10,2

Depth, $Z$ [m]	Inside anchor		Outside anchor	
	Excess pore pressure, $\Delta U$ [kPa]	Pore pressure, $U_{up}$ [kPa]	Excess pore pressure, $\Delta U$ [kPa]	Pore pressure, $U_{up}$ [kPa]
1,0	2,9	12,9	2,9	12,9
2,0	5,8	25,8	5,8	25,8
3,0	8,7	38,7	8,7	38,7
4,0	11,6	51,6	11,6	51,6
5,0	14,5	64,5	14,5	64,5
6,0	17,3	77,3	17,3	77,3
7,0	20,2	90,2	20,2	90,2
8,0	23,1	103,1	23,1	103,1
9,0	26,0	116,0	26,0	116,0
10,0	28,9	128,9	28,9	128,9
11,0	31,8	141,8	31,8	141,8
12,0	34,7	154,7	34,7	154,7
13,0	37,6	167,6	37,6	167,6
14,0	40,5	180,5	40,5	180,5
15,0	43,4	193,4	43,4	193,4
16,0	46,2	206,2	46,2	206,2
17,0	49,1	219,1	49,1	219,1
18,0	52,0	232,0	52,0	232,0
19,0	54,9	244,9	54,9	244,9
20,0	57,8	257,8	57,8	257,8
$U_{inc}$ [kPa]	2,9	12,9	2,9	12,9

## Appendix E. Mathematical derivations

**Updated lateral earth pressure coefficient in the clay plug ( $K_{0,up,plug}$ )** is based on these assumptions:

- No change in total vertical stress
- Total horizontal stress changes according to a triaxial extension test (TxEuD)

$$K'_{0,up,plug} = \frac{\sigma'_{h,up}}{\sigma'_{v,up}} = \frac{\sigma_{h,up} - u_{up}}{\sigma_{v,up} - u_{up}} = \frac{\sigma_{v,0} - 2 \cdot \tau - u_{up}}{\sigma_{v,0} - u_{up}}$$

$\sigma_{v,0}$  is calculated from equation (2.6)

$\sigma_{h,0}$  is calculated from equation (2.7)

**Updated lateral earth pressure coefficient in the remolded zone inside the skirt wall ( $K_{0,up,rem}$ )** is based on these assumptions:

- Horizontal equilibrium between the clay plug and remolded zone after penetration

$$\sigma_{h,plug} = K_{0,up,plug} \cdot \sigma'_{v,0} + u_{up,plug}$$

$$\sigma_{h,rem} = K_{0,up,rem} \cdot \sigma'_{v,0} + u_{up,plug}$$

$$\sigma_{h,plug} = \sigma_{h,rem}$$

$$K'_{0,up,plug} \cdot \sigma'_{v,0} + u_{up,plug} = K'_{0,up,rem} \cdot \sigma'_{v,0} + u_{up,plug}$$

$$K'_{0,up,rem} = \frac{1}{\sigma'_{v,0}} (K'_{0,up,plug} \cdot \sigma'_{v,0} + u_{up,plug} - u_{up,plug})$$

$$K'_{0,up,rem} = K'_{0,up,plug} + \frac{u_{up,plug} - u_{up,rem}}{\sigma'_{v,0}}$$

**Updated overconsolidation ratio ( $OCR_{up}$ )** is based on these assumptions:

- No change in preconsolidation pressure ( $p'_c$ )

$$OCR_0 = \frac{p'_c}{\sigma'_{v,0}}$$

$$OCR_{up} = \frac{p'_c}{\sigma'_{v,up}}$$

$$\sigma'_{v,up} = \sigma_{v,up} - u_{up} = \sigma_{v,0} - u_{up} = \sigma'_{v,0} + u_0 - u_{up} = \sigma'_{v,0} + (-\Delta u) = \sigma'_{v,0} - \Delta u$$

$$p'_c = OCR_0 \cdot \sigma'_{v,0}$$

$$OCR_{up} = \frac{OCR_0 \cdot \sigma'_{v,0}}{\sigma'_{v,up}} = \frac{OCR_0 \cdot \sigma'_{v,0}}{\sigma'_{v,0} - \Delta u} = \frac{OCR_0}{1 - \frac{\Delta u}{\sigma'_{v,0}}}$$

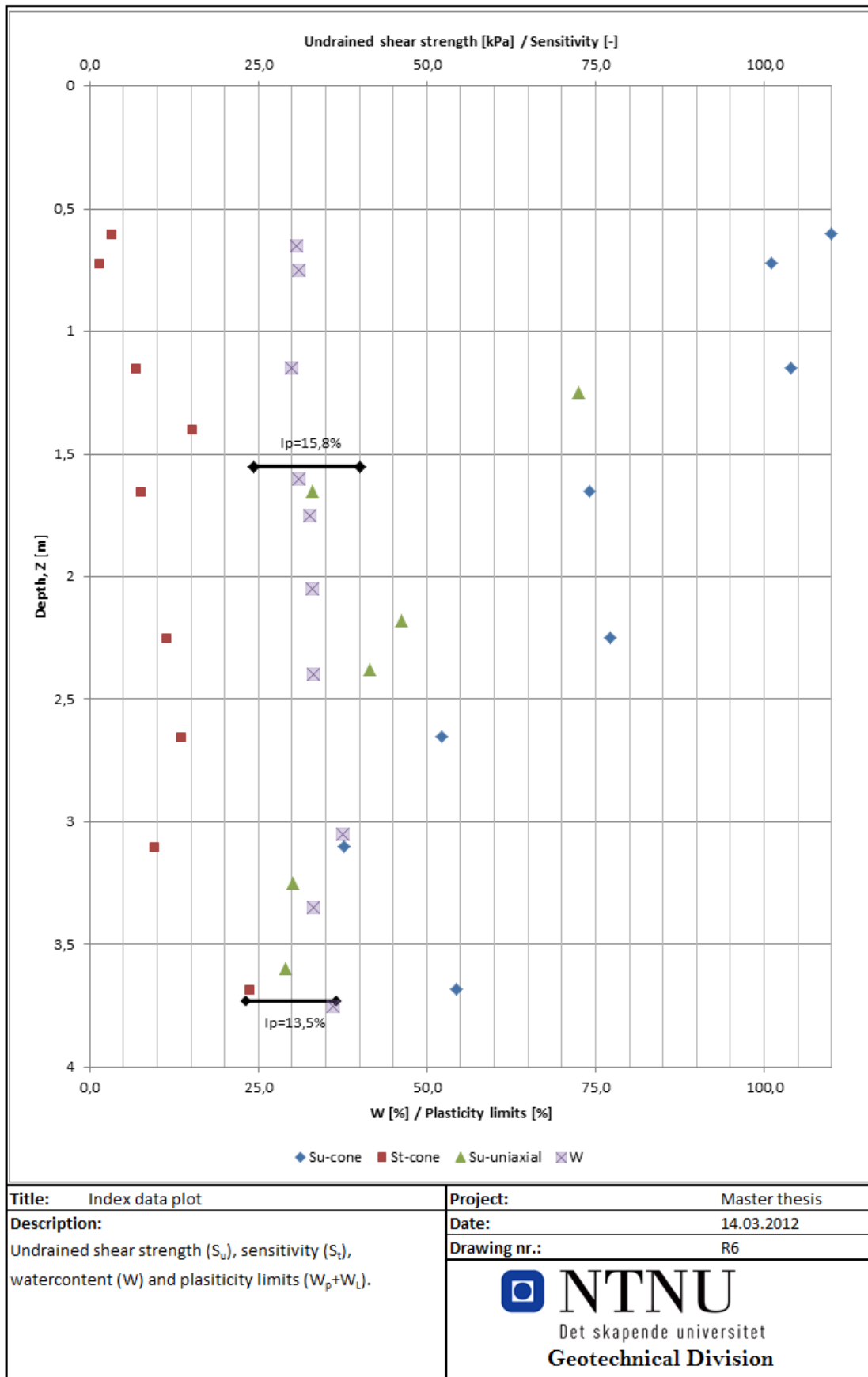
**Updated friction angle ( $\phi'$ )** is based on these assumptions:


- Negligible contribution with depth of cohesion ( $\cos(\phi) \cdot c' / \sigma_{v0}' \approx 0$ )
- Radial stress ( $\sigma_r$ ) larger than tangential stress ( $\sigma_\theta$ )
- Acceptable fit between modeled undrained shear strength ( $t = 0$ ) and original design shear strength ( $S_u / \sigma_{v0}' \cdot 1 / S_t = 0,43 \cdot 1/4 \approx 0.11$ )


$$\frac{S_u}{\sigma'_{v0}} = \frac{\cos \varphi \cdot c'}{\sigma'_{v0}} + \frac{1}{2} (1 + K'_0) \sin \varphi$$

$$\varphi = \sin^{-1} \left( \frac{2}{1 + K'_0} \cdot \frac{S_u}{\sigma'_{v0}} \right)$$

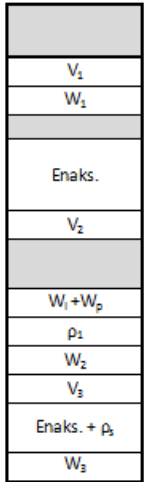

Appendix F. Soil investigation Tiller





<b>Konuforsøk</b>					<b>Vanninnhold</b>			
Z [m]	$s_u$ [kPa]	$s_v$ [kPa]	$S_c$ [-]	Z [m]	w [%]			
0,6	110,0	35,5	3,1	0,65	30,7			
0,72	101,0	74,1	1,4	0,75	31,1			
1,15	104,0	35,5	6,8	1,15	29,9			
1,4	245,0	16,2	15,1	1,60	31,1			
1,65	74,1	9,8	7,6	1,75	32,6			
2,25	77,1	6,8	11,3	2,05	33,0			
2,65	52,2	3,9	13,4	2,40	33,2			
3,1	37,8	4,0	9,5	2,75				
3,68	54,4	2,3	23,7	3,05	37,5			
				3,35	33,2			
				3,75	36,0			
<b>Enaks. Trykk</b>					<b>Plastisitetsgrenser</b>			
Z [m]	$s_u$ [kPa]	$\epsilon_a$ [%]	Z [m]			$w_l$ [%]	$w_p$ [%]	$I_p$ [%]
	-	-				-	-	-
	-	-				-	-	-
1,25	72,5	8,5	1,55	40,1	24,4	15,8		
1,65	33,1	8,0	2,75	-	-	-		
2,18	46,2	3,0	3,73	36,7	23,2	13,5		
2,38	41,5	2,0						
3,25	30,1	1,8						
3,60	29,1	1,8						
<b>Densitet liten prøve</b>					<b>Rutineparametere</b>			
Z [m]	$\rho_{\text{tørr}}$ [g/cm <sup>3</sup> ]	$\rho_{\text{våt}}$ [g/cm <sup>3</sup> ]	$\gamma_{\text{tørr}}$ [kN/m <sup>3</sup> ]	$\gamma_{\text{våt}}$ [kN/m <sup>3</sup> ]	Z [m]	n [-]	e [-]	
0,65	1,45	1,92	14,2	18,8	0,65	0,47	0,88	
1,58	1,36	1,87	13,3	18,3	1,58	0,51	1,03	
2,20	1,50	1,95	14,7	19,2	2,20	0,46	0,84	
3,15	1,46	1,97	14,3	19,4	3,15	0,52	1,07	
<b>Title:</b> Index testing					<b>Project:</b> Master thesis			
<b>Description:</b>					<b>Date:</b> 20.03.2012			
<b>Prosjekt:</b>					<b>Drawing nr.:</b> R5			
<b>Operatør/Gruppe:</b> Sjødis & Ulvestad		<b>Borested:</b>		<b>Tiller</b>				
<b>Dato prøvetaking:</b> 08.03.2012		<b>Hull nr.:</b>		1				
<b>Dato prøveåpning:</b> 14.03.2012		<b>Prøve nr.:</b>						
<b>Generell klassifisering:</b>					 <b>NTNU</b> Det skapende universitet <b>Geotechnical Division</b>			
<b>Geoteknisk betegnelse:</b> Tørrskorpe + leire								
<b>Jordart:</b> Torv/Siltig Leire/Leire								
<b>Dybde:</b> 0,0-3,8 m								
<b>Merknader:</b> Nøkkeldata samlet for borhull 1.								

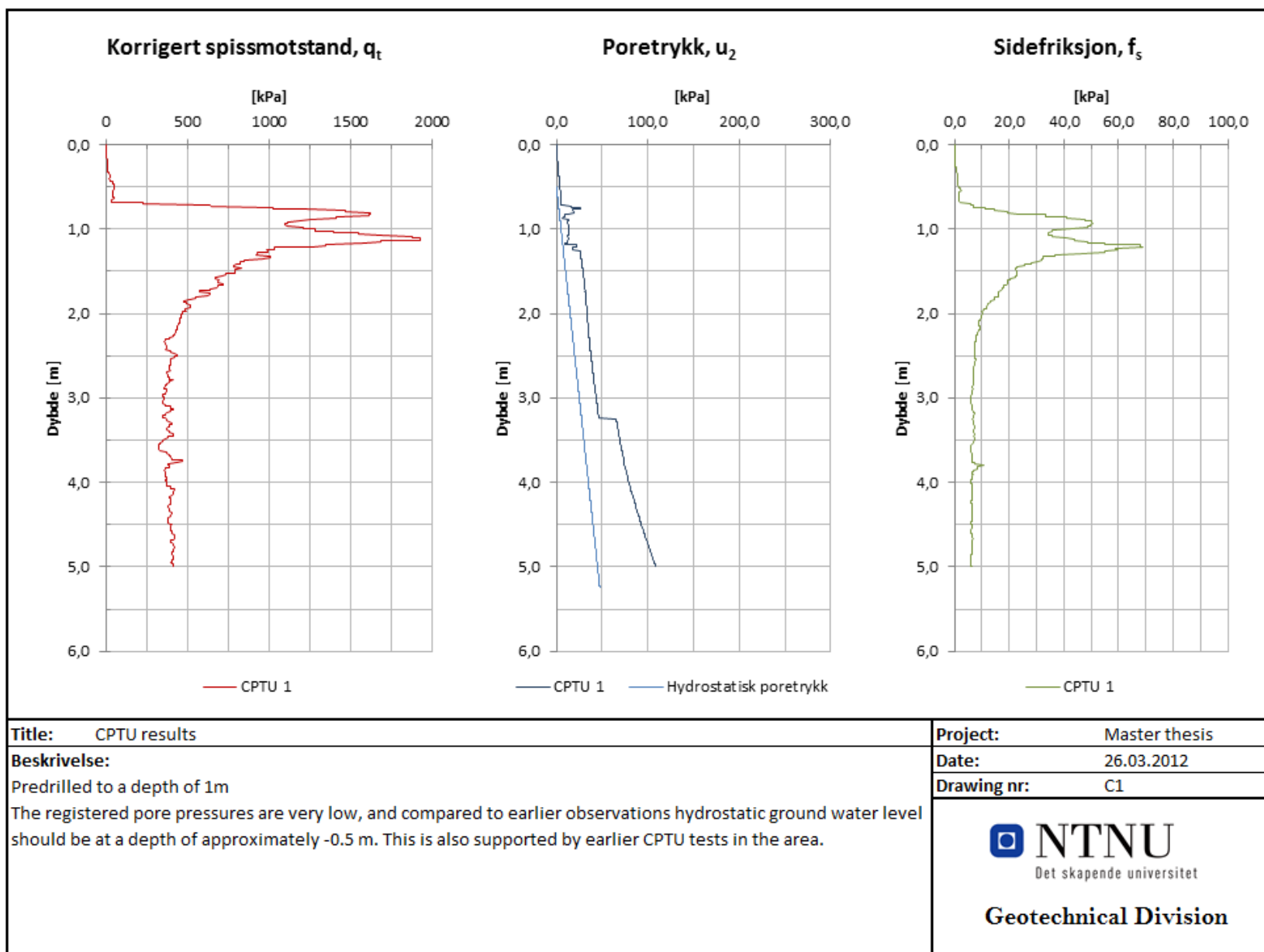
<b>Åpning av prøverør</b> Dybde, z: 0,0-0,8 m Grunnvannstand 0,5 m Lengde av prøve, L: 51 cm Volum av prøve, 23,2xL: 1183,2 cm <sup>3</sup> Masse av sylinder m/prøve 4448 g Masse tom sylinder 2046 g Masse prøve 2402,0 g Midlere densitet, $\rho$ 2,0 g/cm <sup>3</sup> Midlere tyngdetetthet, $\gamma = \rho \cdot g$ 19,9 kN/m <sup>3</sup>		<b>Korndensitet fra pyknometermåling</b> Masse pyknometer+vann (1): 148,63 g Masse pykn.+prøve+vann (2): 156,72 g Total masse tørr: 225,18 g Masse skål: 212,86 g Masse tørr (3): 12,32 g Korndensitet: $\rho_s = (3)/[(1)+(3)-(2)]\rho_w$ 2,91 g/cm <sup>3</sup>		<b>Plastisitetsgrenser</b> Test 1 Masse beger m/lokk - g Total masse våt - g Total masse tørr - g Masse vann - g Flytegrense, $w_L$ - % Masse beger m/lokk - g Total masse våt - g Total masse tørr - g Masse vann - g Rullegrense, $w_p$ - %	
<b>Konusforsøk</b> Test 1 Test 2 Test 3 $s_u$ 110 101 - kPa $s_r$ 35,5 74,1 - kPa $s_t$ 3,1 1,4 - <b>Enaks. Trykk</b> Test 1 Test 2 $s_u$ - - kPa Ea - - % <b>Vanninnhold</b> Test 1 Test 2 Test 3 Skål nr 243 111 - Tot masse våt 108,69 108,7 - g Tot masse tørr 89,58 88,29 - g Masse vann 19,11 20,41 - g Masse skål 27,34 22,57 - g Masse tørr prøve 62,24 65,72 - g Vanninnhold 30,7 31,1 - %		<b>Prøveinndeling</b> Mangler. Forstyrret torv/myr masse m/mye vann $\rho_1$ $V_1$ $\rho_2$ $W_1$ $\rho_2$ $V_2$ $W_2$		<b>Densitet liten prøve</b> Ring Ring nr 7 Masse ring 31,64 g Volum ring 34,8 cm <sup>3</sup> Skål nr 65,18 Masse skål 65,18 g Tot masse våt 163,47 g Tot masse tørr 115,53 g Masse våt prøve 66,65 g Masse tørr prøve 50,35 g Tørr densitet 1,4 g/cm <sup>3</sup> Tørr tyngdetetthet 14,2 kN/m <sup>3</sup> Våt densitet 1,9 g/cm <sup>3</sup> Våt tyngdetetthet 18,8 kN/m <sup>3</sup> <b>Rutineparametere</b> Plastisitetsindeks: $I_p = w_L - w_p$ - % Flyteindeks: $I_f = (w - w_p) / (w_L - w_p)$ - Porøsitet: $n = 1 - (\rho_d / \rho_s)$ 0,50 Porøsitet: $n = V_v / V$ 0,47 Poretall: $e = (\rho_s / \rho_d) - 1$ 1,01 Poretall: $e = n / (1 - n)$ 0,88 Metningsgrad: Sr 100 %	
<b>Title:</b> Index testing			<b>Project:</b> Master thesis		
<b>Description:</b> Prosjekt: Tiller Operatør/Gruppe: Sjødals & Ulvestad Dato prøvetaking: 08.03.2012 Dato prøveåpning: 12.03.2012 Borested: Tiller Hull nr: 1 Prøve nr: U87			<b>Date:</b> 20.03.2012 <b>Drawing nr.:</b> R1		
<b>Generell klassifisering:</b> Geoteknisk betegnelse: Torv, myr, leire Jordart: Beskrivelse: Øvre del er komprimert/smeltet. Noe røtter og organiske partikler. Merknader: Mangler ca. 35 cm av prøven.			 <b>NTNU</b> Det skapende universitet <b>Geotechnical Division</b>		

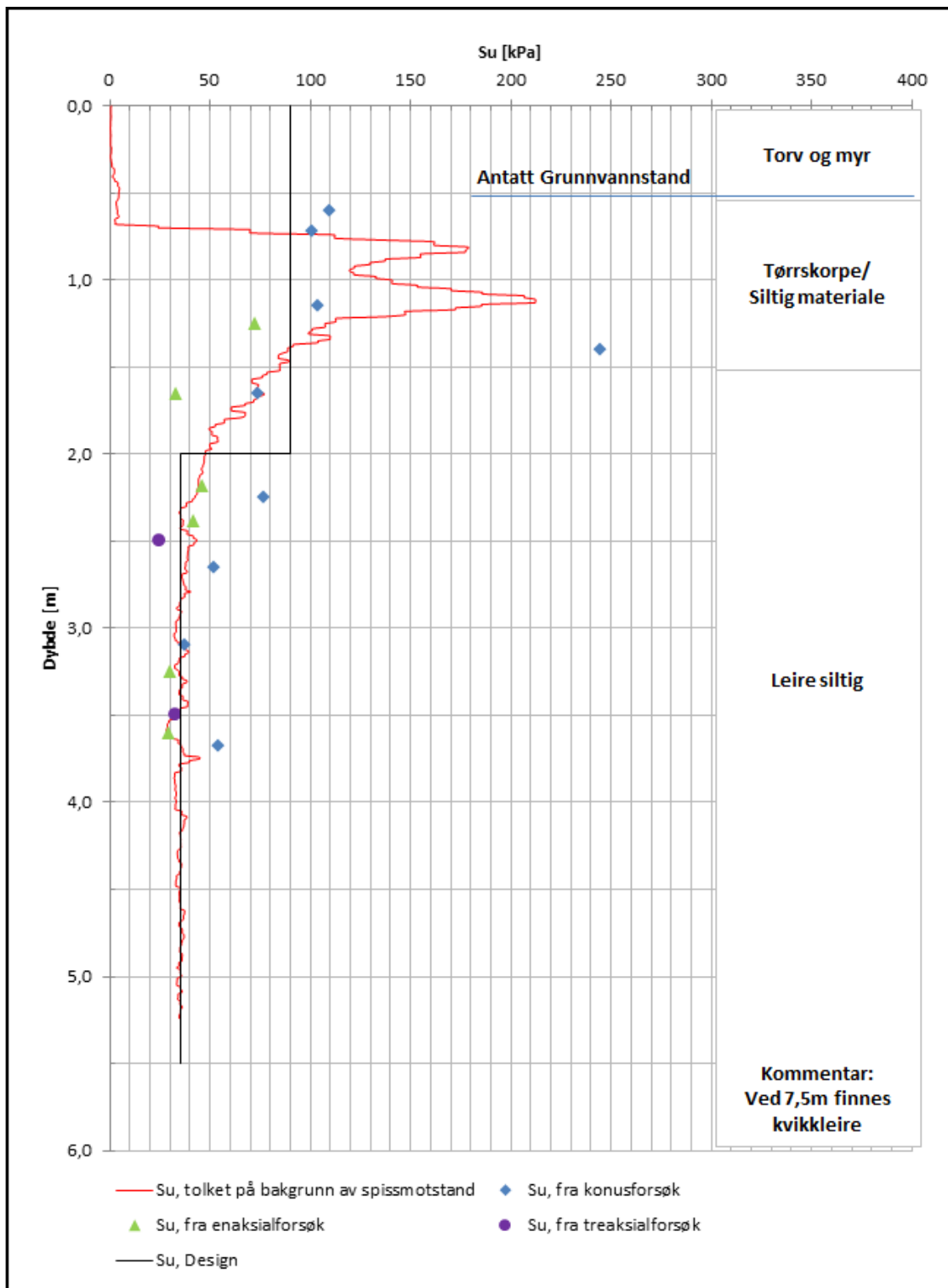



<b>Åpning av prøverør</b> Dybde, z: 1,0-1,8 m Grunnvannstand 0,5 m Lengde av prøve, L: 79,1 cm Volum av prøve, 23,2xL: 1835,1 cm <sup>3</sup> Masse av sylinder m/prøve 5330,3 g Masse tom sylinder 1730 g Masse prøve 3600,3 g Midlere densitet, $\rho$ 2,0 g/cm <sup>3</sup> Midlere tyngdetetthet, $\gamma = \rho \cdot g$ 19,2 kN/m <sup>3</sup>		<b>Korndensitet fra pyknometermåling</b> Masse pyknometer+vann (1): 148,35 g Masse pykn.+prøve+vann (2): 158,63 g Total masse tørr: 318,26 g Masse skål: n/a g Masse tørr (3): - g Korndensitet: - g/cm <sup>3</sup> $\rho_s = (3)/[(1)+(3)-(2)] \cdot \rho$		<b>Plastisitetsgrenser</b> Masse beger m/lokk 27,68 g Total masse våt 61,65 g Total masse tørr 51,92 g Masse vann 9,73 g Flytegrense, $w_L$ 40,1 % Masse beger m/lokk 25,47 g Total masse våt 41,28 g Total masse tørr 38,18 g Masse vann 3,10 g Rullegrense, $w_p$ 24,4 %	
<b>Konussforsøk</b> Test 1 Test 2 Test 3 $s_u$ 104 245 74,1 kPa $s_v$ 15,2 16,2 9,8 kPa $s_t$ 6,8 15,1 7,6		<b>Prøveinndeling</b> 		<b>Densitet liten prøve</b> Ring nr 7 Masse ring 31,64 g Volum ring 34,8 cm <sup>3</sup> Skål nr 54 Masse skål 25,22 g Tot masse våt 121,8 g Tot masse tørr 72,48 g Masse våt prøve 64,94 g Masse tørr prøve 47,26 g Tørr densitet 1,4 g/cm <sup>3</sup> Tørr tyngdetetthet 13,3 kN/m <sup>3</sup> Våt densitet 1,9 g/cm <sup>3</sup> Våt tyngdetetthet 18,3 kN/m <sup>3</sup>	
<b>Enaks. Trykk</b> Test 1 Test 2 $s_u$ 72,5 33,1 kPa Ea 8,5 8 %		<b>Vanninnhold</b> Test 1 Test 2 Test 3 Skål nr 85 65,18 78 Tot masse våt 129,07 127,1 111,14 g Tot masse tørr 110,67 112,41 96,06 g Masse vann 18,40 14,69 15,08 g Masse skål 49,07 65,18 49,83 g Masse tørr prøve 61,60 47,23 46,23 g Vanninnhold 29,9 31,1 32,6 %		<b>Rutineparametere</b> Plastisitetsindeks: $I_p = w_L - w_p$ 15,8 % Flyteindeks: $I_f = (w - w_p)/(w_L - w_p)$ 0,3 Porøsitet: $n = 1 - (\rho_d/\rho_s)$ - Porøsitet: $n = V_v/V$ 0,51 Poretall: $e = (\rho_s/\rho_d) - 1$ - Poretall: $e = n/(1-n)$ 1,03 Metningsgrad: Sr 100 %	
<b>Title:</b> Index testing				<b>Project:</b> Master thesis	
<b>Description:</b> Prosjekt: Tiller Operatør/Gruppe: Søjdis & Ulvestad Dato prøvetaking: 08.03.2012 Dato prøveåpning: 13.03.2012 Borested: Tiller Hull nr: 1 Prøve nr: T100				<b>Date:</b> 20.03.2012 <b>Drawing nr.:</b> R2	
<b>Generell klassifisering:</b> Geoteknisk betegnelse: Tørrskorpe Jordart: Siltig leire / leire? Beskrivelse: Øvre del består av humusholdig tørrskorpe (øvre 57 cm). Nedre del leire. Merknader:				 <b>NTNU</b> Det skapende universitet <b>Geotechnical Division</b>	

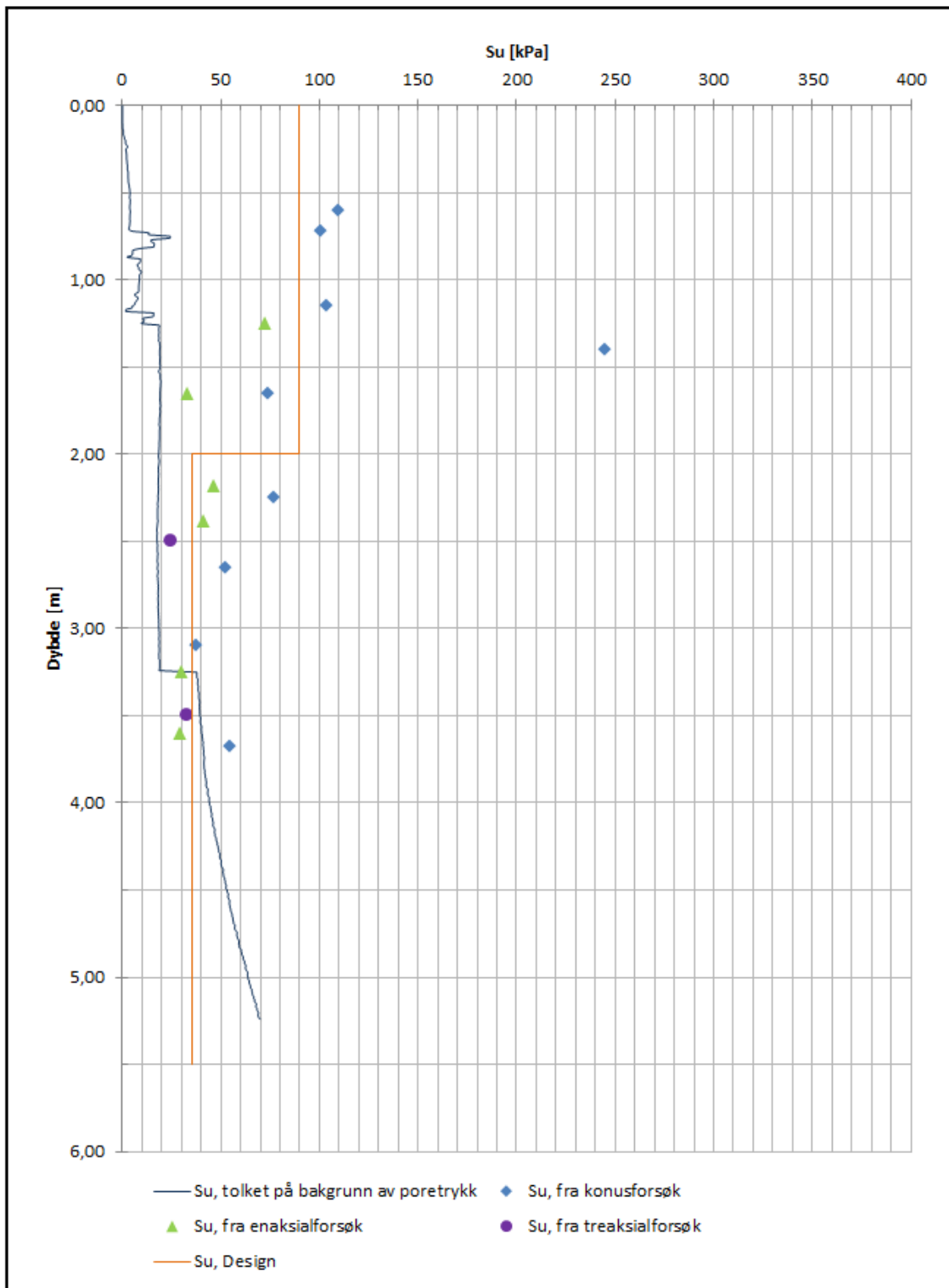
<b>Åpning av prøverør</b>		<b>Korndensitet fra pyknometermåling</b>		<b>Plastisitetsgrenser</b>		<b>Test 1</b>
Dybde, z:	2,0-2,8 m	Masse pyknometer+vann (1):	148,35 g	Masse beger m/lokk		21,29 g
Grunnvannstand	0,5 m	Masse pykn.+prøve+vann (2):	159,31 g	Total masse våt		46,6 g
Lengde av prøve, L:	79,3 cm	Total masse tørr:	146,98 g	Total masse tørr		33,62 g
Volum av prøve, 23,2xL	1839,8 cm <sup>3</sup>	Masse skål:	129 g	Masse vann		12,98 g
Masse av sylinder m/prøve	5321,1 g	Masse tørr (3):	17,98 g	Flytegrense, w <sub>l</sub>		105,3 %
Masse tom sylinder	1726,4 g	Korndensitet:		Masse beger m/lokk		29,63 g
Masse prøve	3594,7 g	$\rho_s = (3)/[(1)+(3)-(2)] \cdot \rho$	2,56 g/cm <sup>3</sup>	Total masse våt		36,34 g
Midlere densitet, $\rho$	2,0 g/cm <sup>3</sup>			Total masse tørr	n/a?	g
Midlere tyngdetetthet, $\gamma = \rho \cdot g$	19,2 kN/m <sup>3</sup>			Masse vann	-	g
				Rullegrense, w <sub>p</sub>	-	%
<b>Konusforsøk</b>	Test 1	Test 2	Test 3	<b>Prøveinndeling</b>	<b>Densitet liten prøve</b>	<b>Ring</b>
s <sub>u</sub>	77,1	52,2	-	0	Ring nr	3
s <sub>r</sub>	6,8	3,9	-	W <sub>1</sub>	Masse ring	32,61 g
s <sub>t</sub>	11,3	13,4	-	Enaks. 1	Volum ring	35,3 cm <sup>3</sup>
				10	Skål nr	213,05
<b>Enaks. Trykk</b>	Test 1	Test 2		ρ <sub>1</sub>	Masse skål	213,65 g
s <sub>u</sub>	46,2	41,5	kPa	V <sub>1</sub>	Tot masse våt	315,21 g
ε <sub>a</sub>	3	2	%	Enaks. 2	Tot masse tørr	266,47 g
				30	Masse våt prøve	68,95 g
<b>Vanninnhold</b>	Test 1	Test 2	Test 3	W <sub>2</sub>	Masse tørr prøve	52,82 g
Skål nr	201	63,61	60,79	40	Tørr densitet	1,5 g/cm <sup>3</sup>
Tot masse våt	97,42	111,64	133,32 g	Ødo.	Tørr tyngdetetthet	14,7 kN/m <sup>3</sup>
Tot masse tørr	79,48	99,68	99,68 g	Triax.	Våt densitet	2,0 g/cm <sup>3</sup>
Masse vann	17,94	11,96	33,64 g	60	Våt tyngdetetthet	19,2 kN/m <sup>3</sup>
Masse skål	25,14	63,61	60,79 g	ρ <sub>s</sub>		
Masse tørr prøve	54,34	36,07	38,89 g	V <sub>2</sub>	<b>Rutineparametere</b>	
				W <sub>1</sub> +W <sub>p</sub>	Plastisitetsindeks: I <sub>p</sub> =w <sub>l</sub> -w <sub>p</sub>	- %
<b>Vanninnhold</b>				W <sub>2</sub>	Flyteindeks: I <sub>f</sub> =(w-w <sub>p</sub> )/(w <sub>l</sub> -w <sub>p</sub> )	-
	33,0	33,2	86,5 %	80	Porøsitet: n=1-(ρ <sub>s</sub> /ρ <sub>2</sub> )	0,42
					Porøsitet: n=V <sub>v</sub> /V	0,46
					Poretall: e=(ρ <sub>s</sub> /ρ <sub>d</sub> )-1	0,71
					Poretall: e=n/(1-n)	0,84
					Metningsgrad: Sr	100 %
<b>Title:</b>	Index testing			<b>Project:</b>	Master thesis	
<b>Description:</b>				<b>Date:</b>	20.03.2012	
Operatør/Gruppe:	Søjdås & Ulvestad	Borested:	Tiller	<b>Drawing nr.:</b>	R3	
Dato prøvetaking:	08.03.2012	Hull nr:	1	 <b>NTNU</b> Det skapende universitet <b>Geotechnical Division</b>		
Dato prøveåpning:	14.03.2012	Prøve nr:	NTH120			
<b>Generell klassifisering:</b>						
Geoteknisk betegnelse:	Leire					
Jordart:	Leire					
Beskrivelse:	Fin prøve. Noe organisk materiale (rester av røtter).					
Merknader:	Observert en liten stein i overflaten ved utskyvning (30-50 cm ned fra topp).					


<b>Åpning av prøverør</b> Dybde, z: 3,0-3,8 m Grunnvannstand: 0,5 m Lengde av prøve, L: 79,1 cm Volum av prøve, 23,2xL: 1835,1 cm <sup>3</sup> Masse av sylinder m/prøve: 5265,4 g Masse tom sylinder: 1727,4 g Masse prøve: 3538,0 g Midlere densitet, ρ: 1,9 g/cm <sup>3</sup> Midlere tyngdetetthet, γ=ρ·g: 18,9 kN/m <sup>3</sup>			<b>Korndensitet fra pyknometermåling</b> Masse pyknometer+vann (1): 148,35 g Masse pykn.+prøve+vann (2): 163,39 g Total masse tørr: 314,90 g Masse skål: 290,36 g Masse tørr (3): 24,54 g Korndensitet: ρ <sub>s</sub> =(3)/[(1)+(3)-(2)] ρ: 2,58 g/cm <sup>3</sup>			<b>Plastisitetsgrenser</b> Masse beger m/lokk: 22,43 g Total masse våt: 40,51 g Total masse tørr: 35,66 g Masse vann: 4,85 g Flytegrense, w <sub>l</sub> : 36,7 % Masse beger m/lokk: 20,66 g Total masse våt: 33,52 g Total masse tørr: 31,10 g Masse vann: 2,42 g Rullegrense, w <sub>p</sub> : 23,2 %					
<b>Konusforsøk</b> Test 1: s <sub>u</sub> 37,8 kPa Test 2: s <sub>r</sub> 4,0 kPa Test 3: s <sub>t</sub> 23,7 kPa			<b>Prøveinndeling</b> 0 W <sub>1</sub> 10 V <sub>1</sub> 20 ρ <sub>1</sub> Enaks. 1 30 Ødometer W <sub>2</sub> 40 Triax. 50 60 Enaks. 2 ρ <sub>2</sub> 70 W <sub>1</sub> +W <sub>p</sub> V <sub>2</sub> 80 W <sub>3</sub>			<b>Densitet liten prøve</b> Ring nr: 7 Masse ring: 31,64 g Volum ring: 34,80 cm <sup>3</sup> Skål nr: 57 Masse skål: 24,98 g Tot masse våt: 125,31 g Tot masse tørr: 75,68 g Masse våt prøve: 68,69 g Masse tørr prøve: 50,70 g Tørr densitet: 1,5 g/cm <sup>3</sup> Tørr tyngdetetthet: 14,3 kN/m <sup>3</sup> Våt densitet: 2,0 g/cm <sup>3</sup> Våt tyngdetetthet: 19,4 kN/m <sup>3</sup>					
<b>Enaks. Trykk</b> Test 1: s <sub>u</sub> 30,1 kPa Test 2: E <sub>a</sub> 1,8 %			<b>Vanninnhold</b> Test 1: Skål nr 79 Test 2: Tot masse våt 96,31 g Test 3: Tot masse tørr 82,36 g Masse vann: 13,95 g Masse skål: 45,13 g Masse tørr prøve: 37,23 g Vanninnhold: 37,5 %			<b>Rutineparametere</b> Plastisitetsindeks: I <sub>p</sub> =w <sub>l</sub> -w <sub>p</sub> : 13,5 % Flyteindeks: I <sub>f</sub> =(w-w <sub>p</sub> )/(w <sub>l</sub> -w <sub>p</sub> ): 1,1 Porøsitet: n=1-(ρ <sub>s</sub> /ρ <sub>2</sub> ): 0,44 Porøsitet: n=V <sub>2</sub> /V: 0,52 Poretall: e=(ρ <sub>s</sub> /ρ <sub>2</sub> )-1: 0,77 Poretall: e=n/(1-n): 1,07 Metningsgrad: S <sub>r</sub> : 100 %					
<b>Title:</b> Index testing						<b>Project:</b> Master thesis					
<b>Description:</b> Prosjekt: Tiller Operatør/Gruppe: Sjødis & Ulvestad Dato prøvetaking: 08.03.2012 Dato prøveåpning: 14.03.2012						<b>Date:</b> 20.03.2012 <b>Drawing nr.:</b> R4					
Borested: Tiller Hull nr: 1 Prøve nr: 700						 <b>NTNU</b> Det skapende universitet <b>Geotechnical Division</b>					
Generell klassifisering: Geoteknisk betegnelse: Leire Jordart: Leire Beskrivelse: Ren og fin prøve. Konturerer til noe uklar lagdeling (forskjellig fargenyanser). Merknader:											

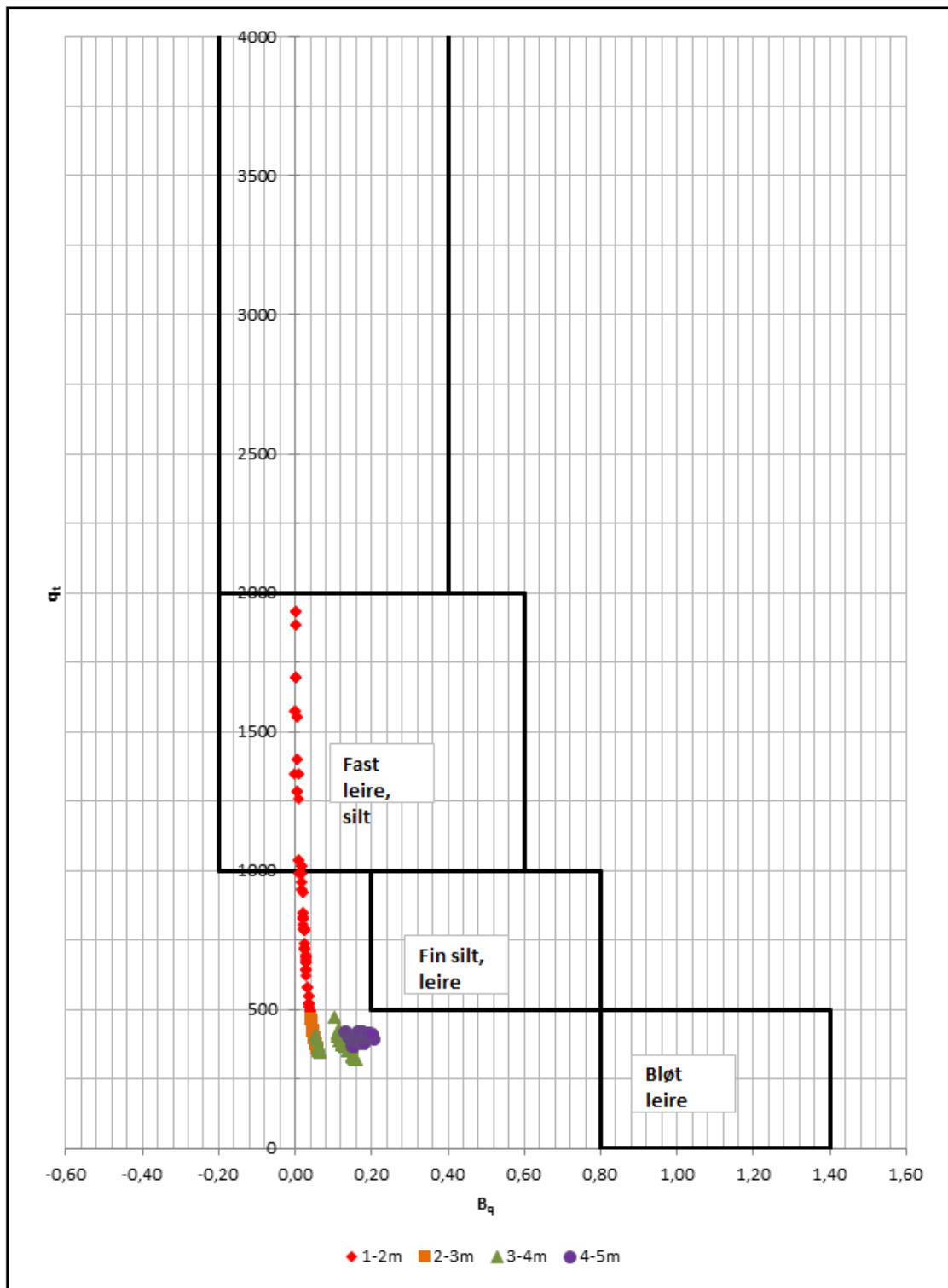





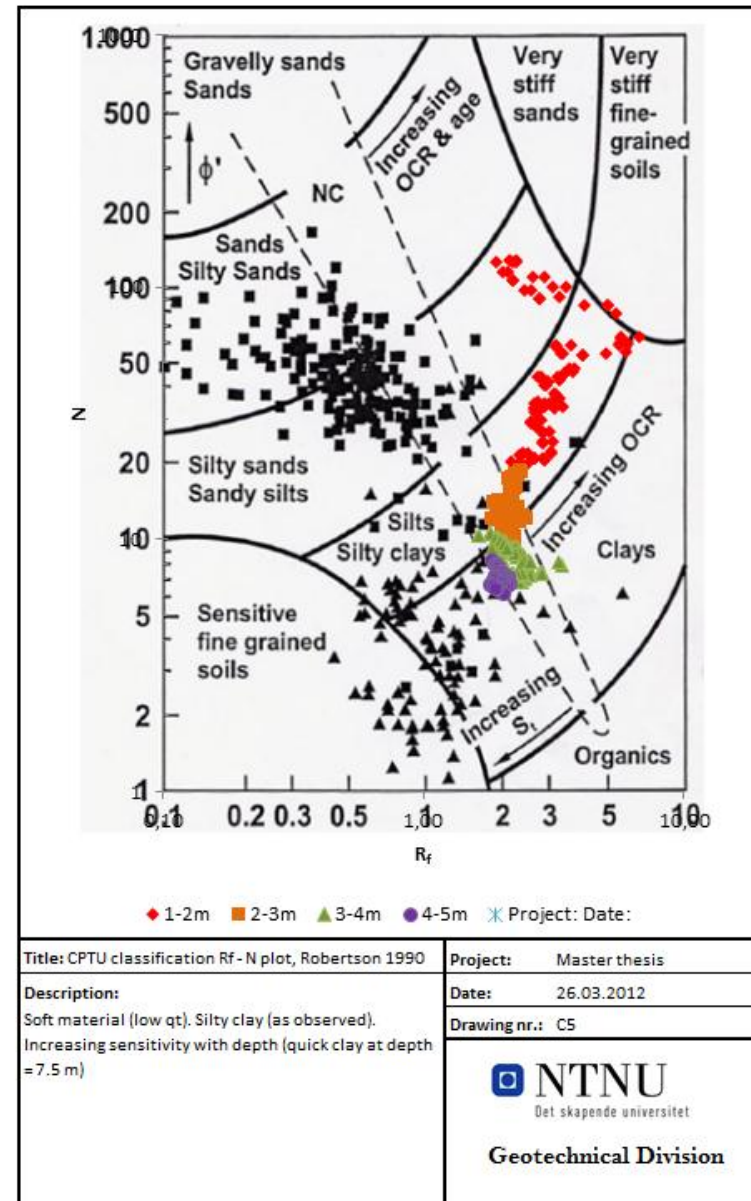
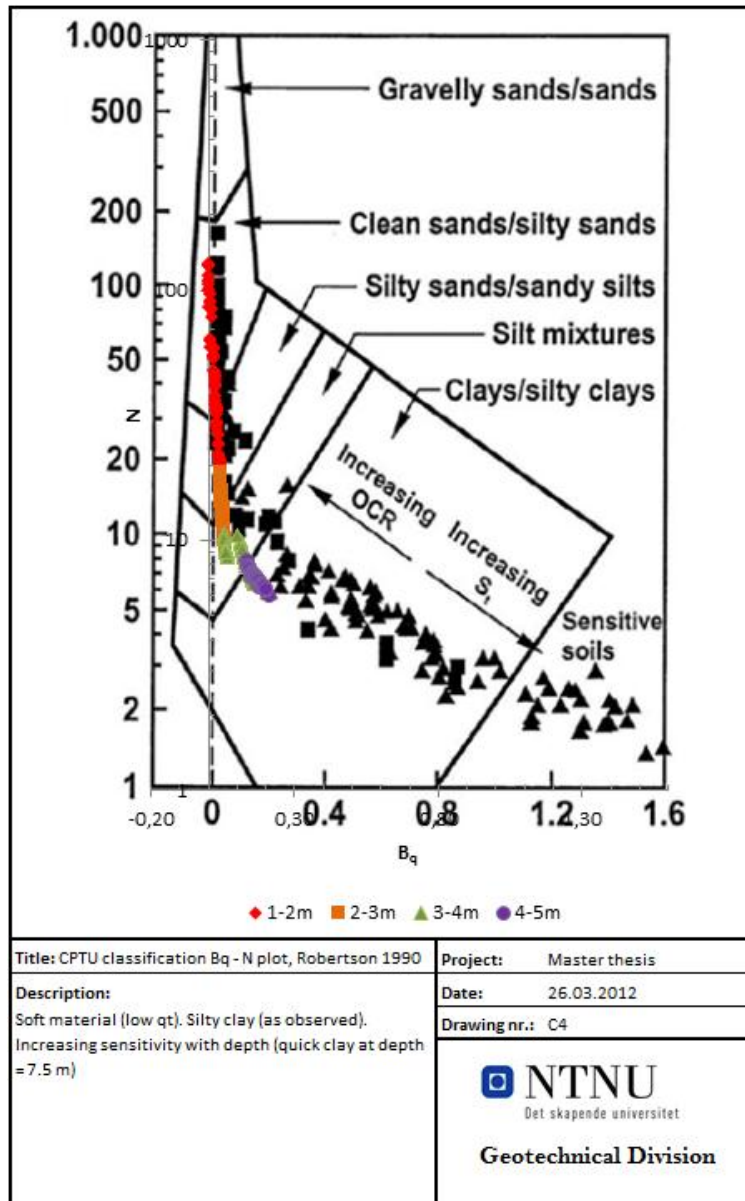
<b>Title:</b> Interpreted $S_u$ -profile based on tip resistance	<b>Project:</b> Master thesis
<b>Description:</b> Su 0-2m: 90 kPa Su 2-5m: 35kPa Nkt=9,0 Classification based on chart by Robertson and Senneset in addition to earlier soil investigation in the area.	<b>Date:</b> 26.03.2012
	<b>Drawing nr.:</b> C2
 <b>NTNU</b> Det skapende universitet <b>Geotechnical Division</b>	



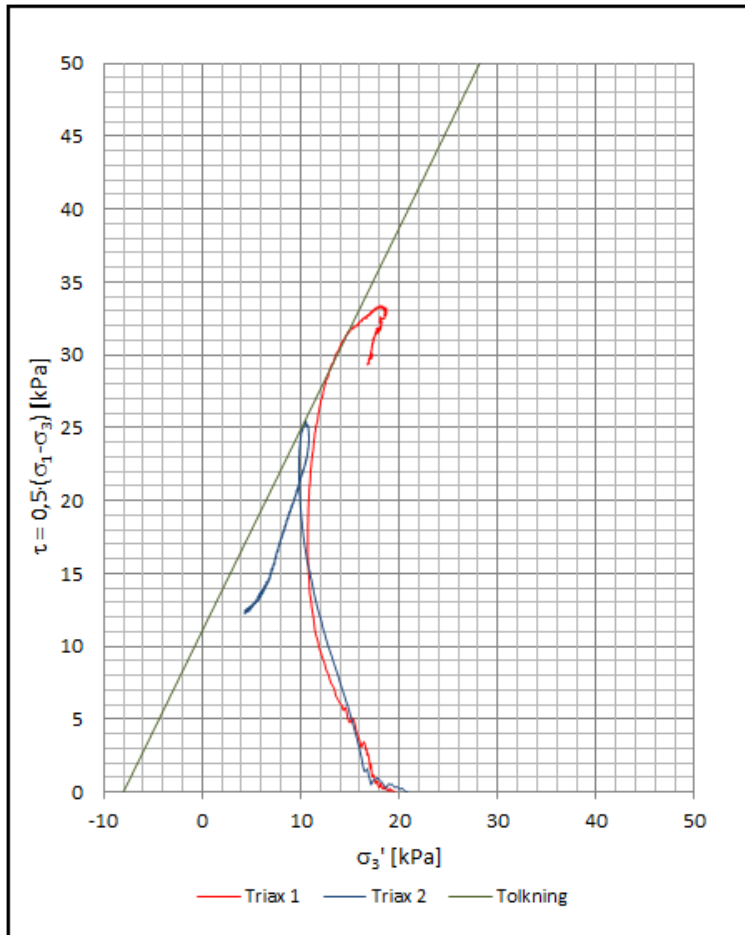
<b>Title:</b> Interpreted $S_u$ profile based on pore pressures	<b>Project:</b> Master thesis
<b>Description:</b>	<b>Date:</b> 26.03.2012
Nu = 1	<b>Drawing nr.:</b> C3
Expected Nu between 6-9, $U_2$ is probably too low.	 Det skapende universitet  <b>Geotechnical Division</b>



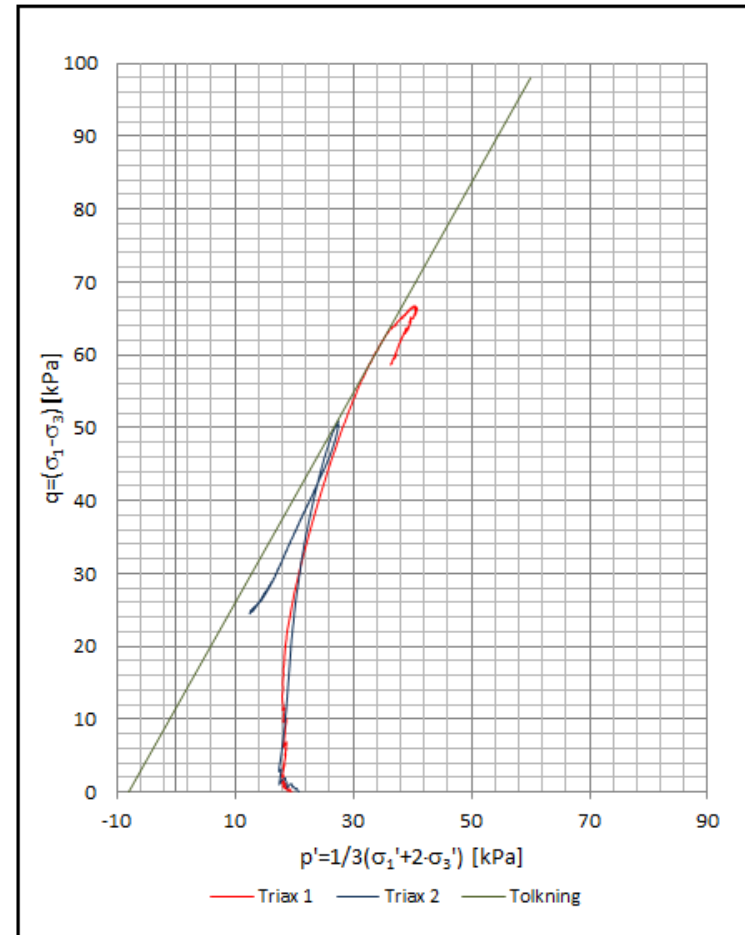
<b>Title:</b> CPTU classification $B_q - N$ plot, Senneset et al. 1989	<b>Project:</b> Master thesis
<b>Description:</b> Soft material (low $q_t$ ). Silty clay (as observed). Increasing sensitivity with depth (quick clay at depth = 7.5 m)	<b>Date:</b> 26.03.2012
	<b>Drawing nr.:</b> C6
 <p><b>NTNU</b> Det skapende universitet</p> <p><b>Geotechnical Division</b></p>	



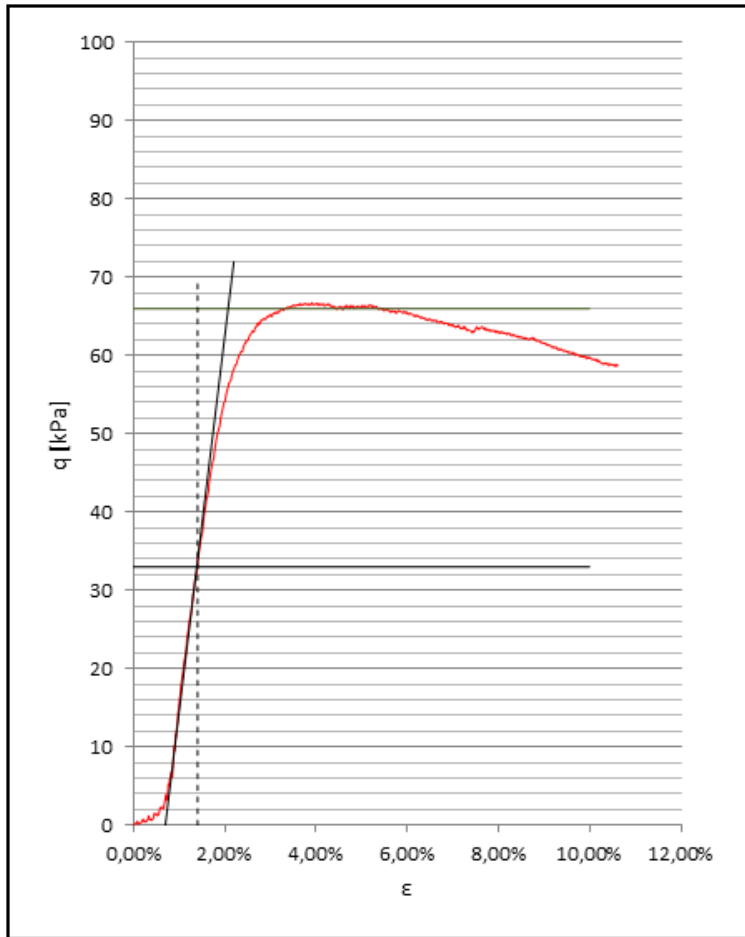




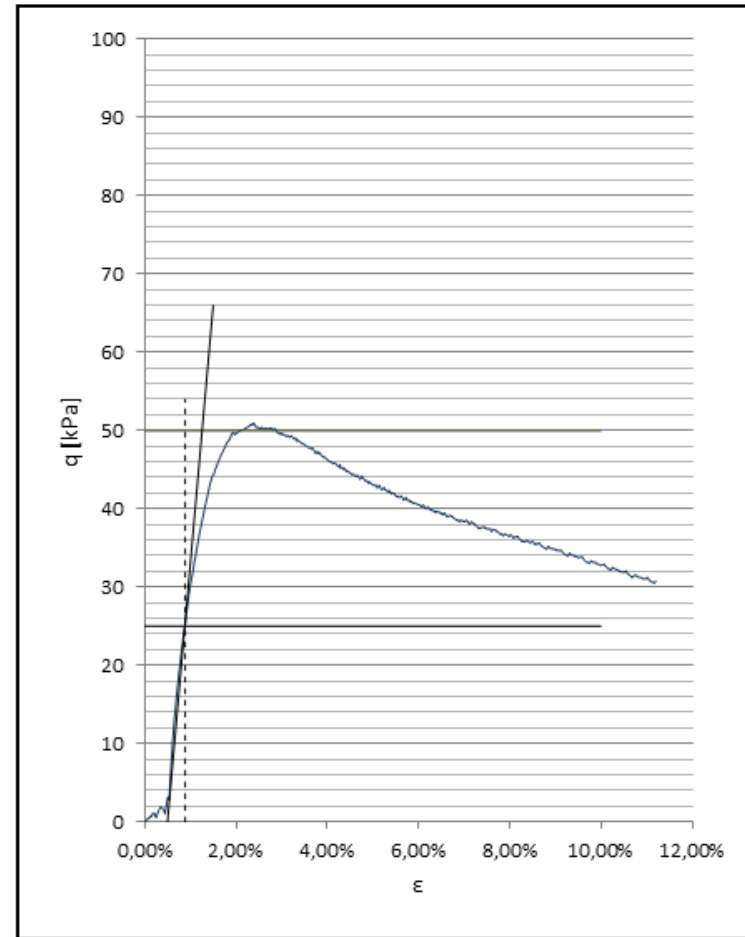
<b>Tittel:</b> Triaxial test - NTNU plot	<b>Prosjekt:</b> Master thesis
<b>Beskrivelse:</b>	<b>Dato:</b> 26.03.2012
a 8 kPa	<b>Tegningsnr.:</b> T1
S 1,3823529 -	 <b>Geotechnical Division</b>
φ 35,467911 °	
tanφ 0,7124484 -	
Triax 1: Sample quality = acceptable	
Triax 2: Sample quality = disturbed	



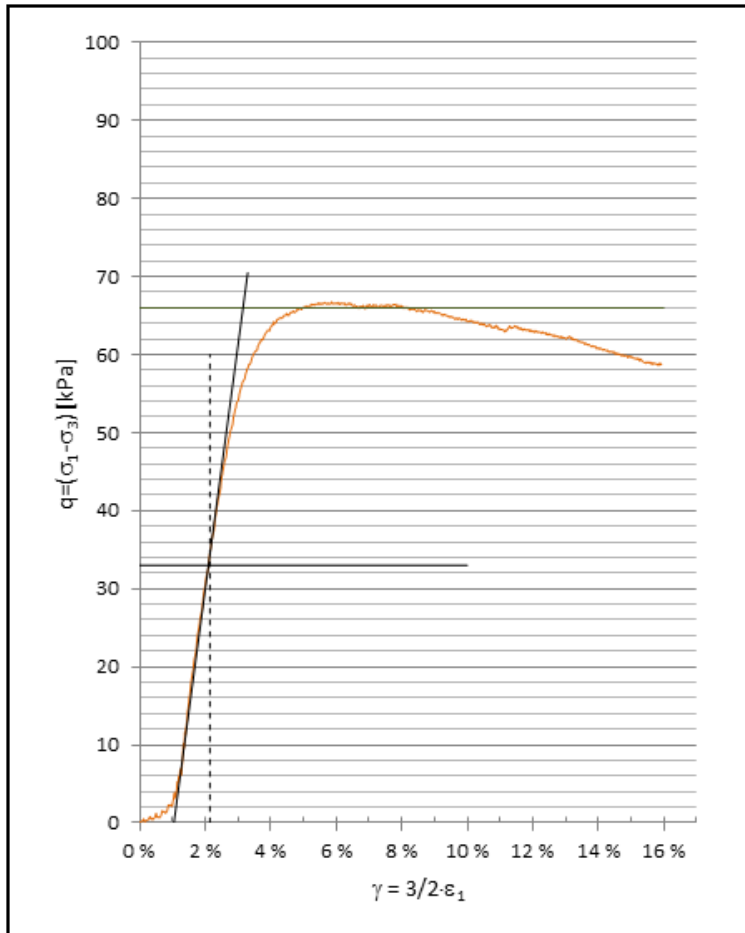
<b>Tittel:</b> Triaxial test - NTNU plot	<b>Prosjekt:</b> Master thesis
<b>Beskrivelse:</b>	<b>Dato:</b> 26.03.2012
a 8 kPa	<b>Tegningsnr.:</b> T2
M 1,4411765 -	 <b>Geotechnical Division</b>
φ 35,522856 °	
tanφ 0,7138951 -	
Triax 1: Sample quality = acceptable	
Triax 2: Sample quality = disturbed	



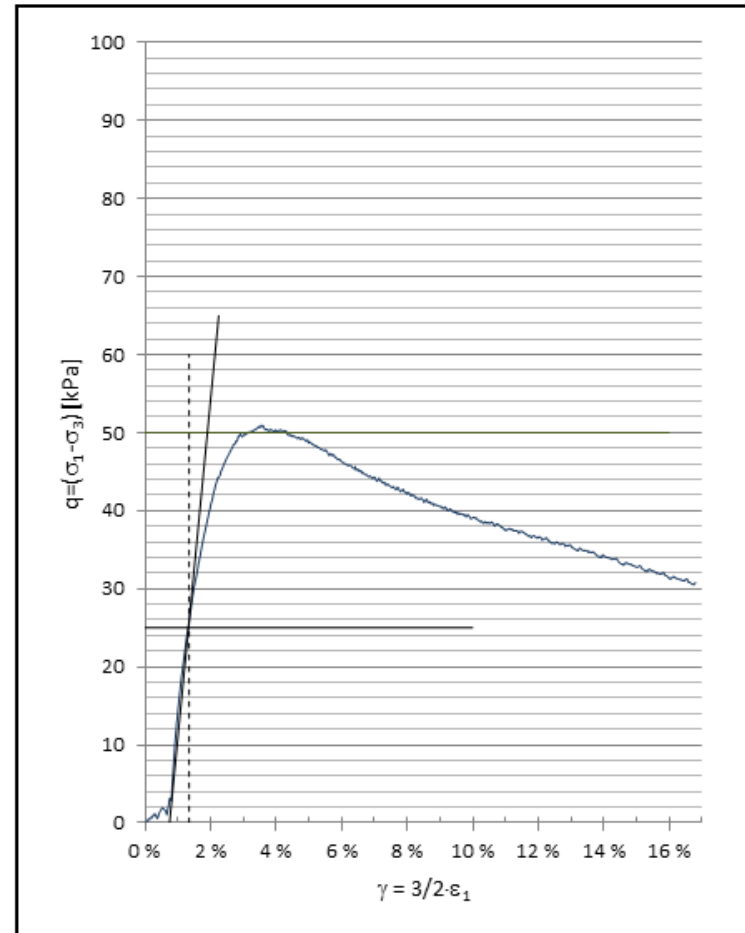
<b>Titel:</b> Triax 1 - deformation vs. deviatoric stress	<b>Prosjekt:</b>
<b>Beskrivelse:</b>	<b>Dato:</b> 26.03.2012
Su1 33 kPa	<b>Tegningsnr.:</b> T3
50 % 16,5 kPa	 <b>Geotechnical Division</b>
eps50 0,0071 -	
E50 4800 kN/m2	
Triax 1: Sample quality = acceptable	
Triax 2: Sample quality = disturbed	



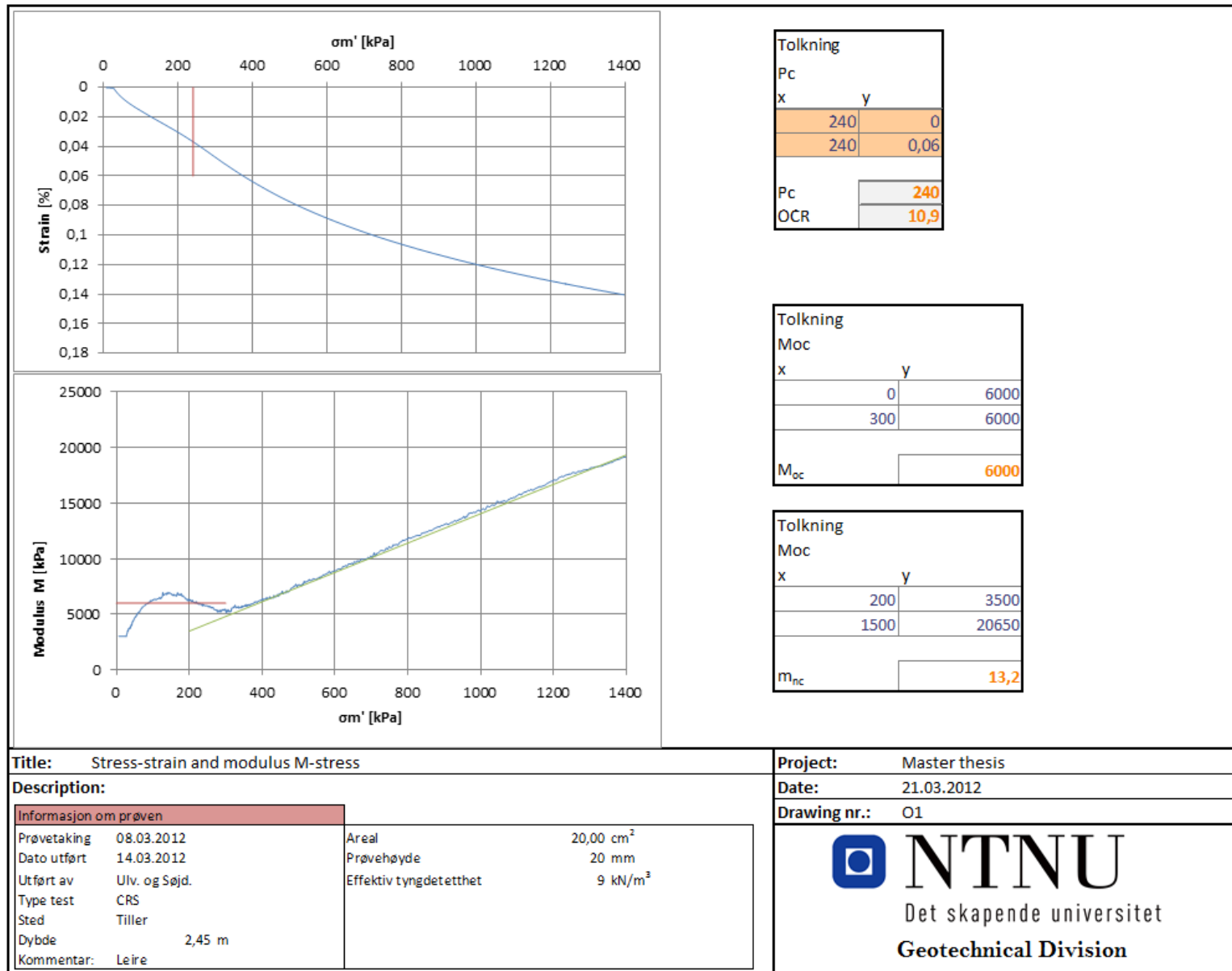
<b>Titel:</b> Triax 2 - deformation vs. deviatoric stress	<b>Prosjekt:</b>
<b>Beskrivelse:</b>	<b>Dato:</b> 26.03.2012
Su2 25 kPa	<b>Tegningsnr.:</b> T4
50 % 12,5 kPa	 <b>Geotechnical Division</b>
eps50 0,0039 -	
E50 6600 kN/m2	
Triax 1: Sample quality = acceptable	
Triax 2: Sample quality = disturbed	



<b>Tittel:</b> Triax 1 - shear strain vs. deviatoric stress		<b>Prosjekt:</b>	
<b>Beskrivelse:</b>		<b>Dato:</b> 26.03.2012	
Max	66 kPa	<b>Tegningsnr.:</b> T5	
50 %	33 kPa	 <b>Geotechnical Division</b>	
gamma50	0,0110 -		
G50	1567 kN/m2		
Triax 1: Sample quality = acceptable			
Triax 2: Sample quality = disturbed			



<b>Tittel:</b> Triax 2 - shear strain vs. deviatoric stress		<b>Prosjekt:</b>	
<b>Beskrivelse:</b>		<b>Dato:</b> 26.03.2012	
Max	50 kPa	<b>Tegningsnr.:</b> T6	
50 %	25 kPa	 <b>Geotechnical Division</b>	
gamma50	0,0060 -		
G50	2167 kN/m2		
Triax 1: Sample quality = acceptable			
Triax 2: Sample quality = disturbed			



**Title:** Stress-strain and modulus M-stress

**Description:**

Informasjon om prøven			
Prøvetaking	08.03.2012	Areal	20,00 cm <sup>2</sup>
Dato utført	14.03.2012	Prøvehøyde	20 mm
Utført av	Ulv. og Sjøjd.	Effektiv tyngdetetthet	9 kN/m <sup>3</sup>
Type test	CRS		
Sted	Tiller		
Dybde	2,45 m		
Kommentar:	Leire		

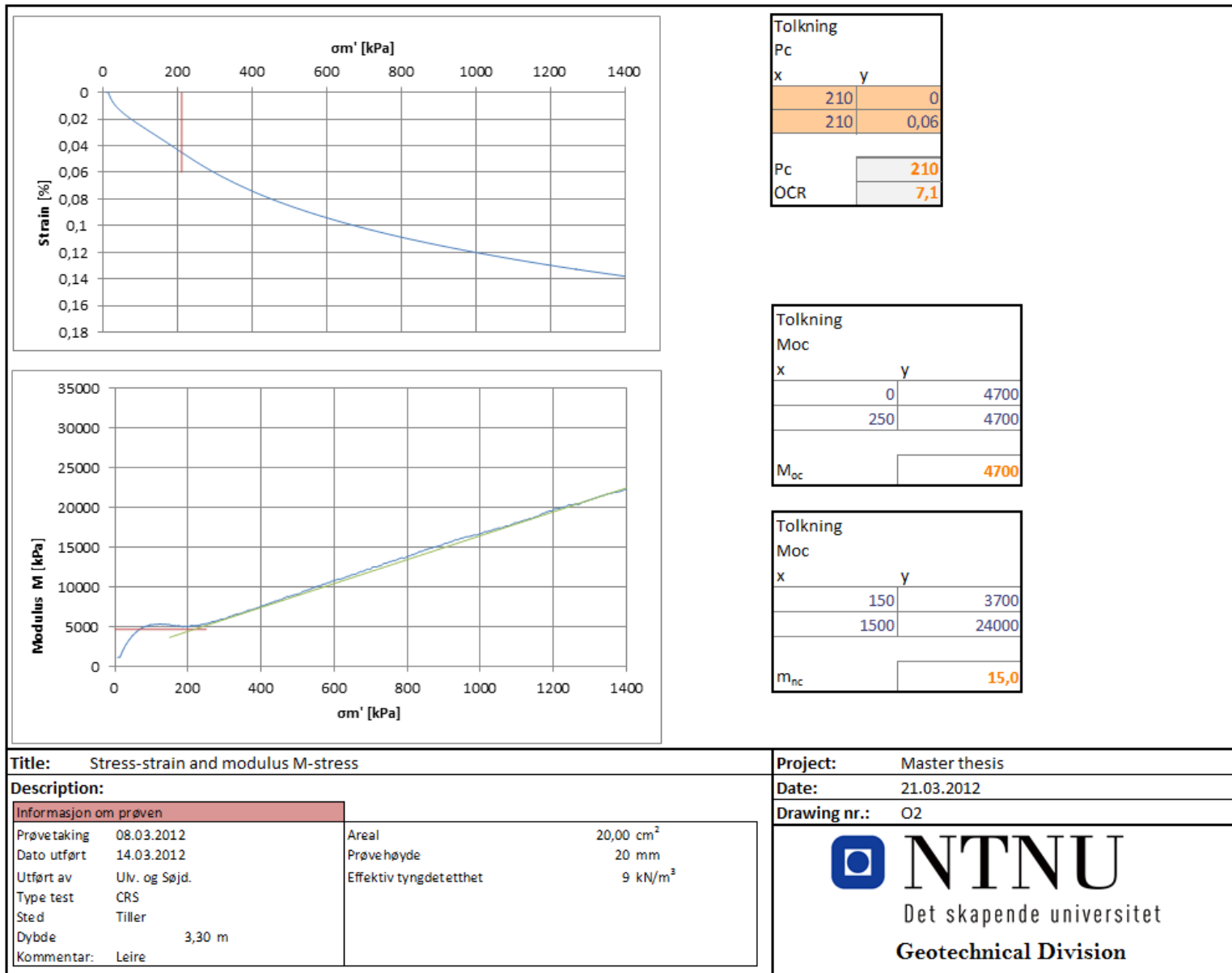
**Project:** Master thesis

**Date:** 21.03.2012

**Drawing nr.:** O1



**NTNU**  
Det skapende universitet  
Geotechnical Division



**Title:** Stress-strain and modulus M-stress

**Description:**

Informasjon om prøven	
Prøvetaking	08.03.2012
Dato utført	14.03.2012
Utført av	Ulv. og Sjøjd.
Type test	CRS
Sted	Tiller
Dybde	3,30 m
Kommentar:	Leire

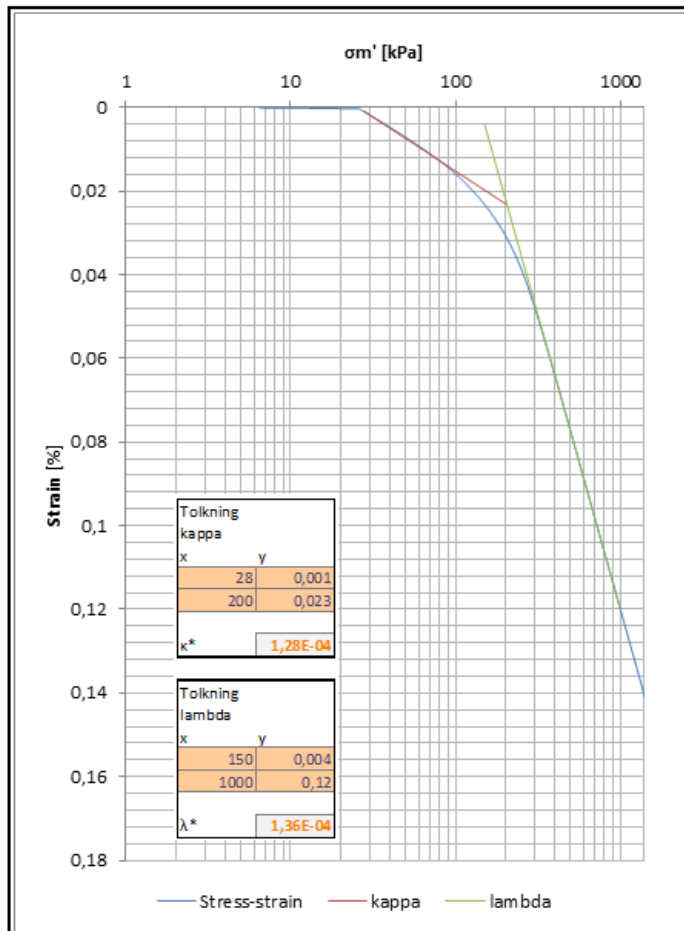
Areal	20,00 cm <sup>2</sup>
Prøvehøyde	20 mm
Effektiv tyngdetetthet	9 kN/m <sup>3</sup>


**Project:** Master thesis

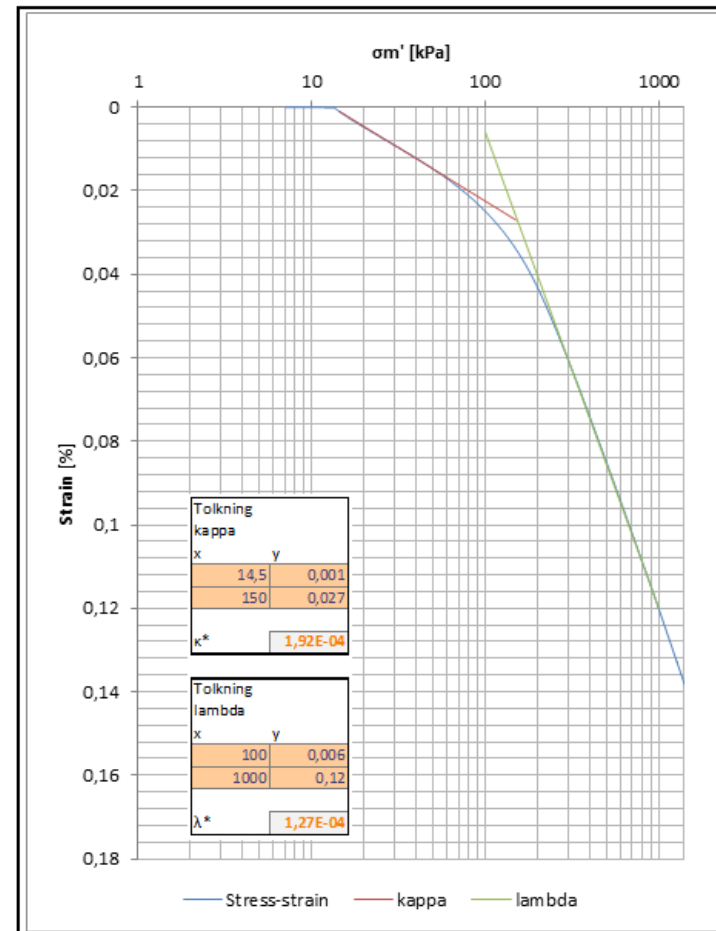
**Date:** 21.03.2012


**Drawing nr.:** O2





<b>Title:</b> Logarithmic stress-strain	<b>Project:</b> Master thesis
<b>Description:</b>	<b>Date:</b> 21.03.2012
<b>Informasjon om prøven</b>	
Prøvetaking	08.03.2012
Dato utført	14.03.2012
Utført av	Ulv. og Sjød.
Type test	CRS
Sted	Tiller
Dybde	2,45 m
Kommentar:	Leire
<b>Drawing nr.:</b> O5	
 <b>NTNU</b> Det skapende universitet <b>Geotechnical Division</b>	



<b>Title:</b> Logarithmic stress-strain	<b>Project:</b> Master thesis
<b>Description:</b>	<b>Date:</b> 21.03.2012
<b>Informasjon om prøven</b>	
Prøvetaking	08.03.2012
Dato utført	14.03.2012
Utført av	Ulv. og Sjød.
Type test	CRS
Sted	Tiller
Dybde	3,30 m
Kommentar:	Leire
<b>Drawing nr.:</b> O6	
 <b>NTNU</b> Det skapende universitet <b>Geotechnical Division</b>	

## Appendix G. Model test design

## Design input data

Input						
Effective unit weight soil, $\gamma'$ [kN/m <sup>3</sup> ]	9	z [m]	Su [kPa]	Su,rem [kPa]	Q <sub>side</sub> [kN]	Q <sub>tip</sub> [kN]
Clay sensitivity, S <sub>c</sub> [-]	13	3	33,8	2,60	0,00	0,00
Undrained shear strength, S <sub>u</sub> /σ' <sub>v,0</sub> [kPa]	1,25	3,05	34,3	2,64	0,03	0,00
Bearing capacity factor, N <sub>c</sub> [-]	2	3,1	34,9	2,68	0,05	0,00
Skirt thickness, t [m]	0,01	3,15	35,4	2,73	0,08	0,00
Skirt height, h [m]	0,5	3,2	36,0	2,77	0,11	0,00
Skirt width, b [m]	0,1	3,25	36,6	2,81	0,14	0,00
Penetration depth top, Z <sub>d</sub> [m]	3	3,3	37,1	2,86	0,16	0,00
		3,35	37,7	2,90	0,19	0,00
		3,4	38,3	2,94	0,22	0,00
Output						
Skirt wall area, A <sub>wall</sub> [m <sup>2</sup> ]	0,10	3,45	38,8	2,99	0,25	0,00
Skirt tip area, A <sub>tip</sub> [m <sup>2</sup> ]	0,001	3,5	39,4	3,03	0,28	0,11
Side friction resistance, Q <sub>side</sub> [kN]	0,281			Sum	0,28	0,11
Tip resistance, Q <sub>tip</sub> [kN]	0,1					
Total penetration resistance, Q <sub>tot</sub> [kN]	0,4					
Quota side friction resistance, Q <sub>side</sub> [%]	71,8					
Quota tip resistance, Q <sub>tip</sub> [%]	28,2					

## Buckling check installation

Load input	
Maximal average undrained shear strength (0,5 m), S <sub>u,0.5m</sub> [kPa]	60
Sensitivity for max. Undrained shear strength (0,5m), S <sub>t,0.5m</sub> [-]	10
Depth of design values, Z <sub>design</sub> [m]	2,25
Design tip resistance, Q <sub>tip,d</sub> [kN]	0,14
Design skirt side friction, Q <sub>side,d</sub> [kN]	0,60
Load factor, Y <sub>c</sub> [-]	1,50
Design total resistance, Q <sub>total</sub> [kN]	1,11
Rod	
Input	
Rod diameter, Ø [m]	0,016
Output	
Area moment of inertia, x-axis, I <sub>x</sub> [mm <sup>4</sup> ]	3,22E+03
Area, A [m <sup>2</sup> ]	2,01E-04
Buckling length, L <sub>k,x</sub> [m]	1,5
Area radius of inertia, i <sub>x</sub> [mm]	4,00E+03
Slenderness, λ <sub>k,x</sub> [-]	3,75E-04
Bucklingload, P <sub>k</sub> [kN]	2,96 OK
Plate	
Output	
Area moment of inertia, x-axis, I <sub>x</sub> [mm <sup>4</sup> ]	8,33E+03
Area, A [m <sup>2</sup> ]	0,05
Buckling length, L <sub>k,x</sub> [m]	0,35
Area radius of inertia, i <sub>x</sub> [mm]	4,08E+02
Slenderness, λ <sub>k,x</sub> [-]	8,57E-04
Bucklingload, P <sub>k</sub> [kN]	140,99 OK

## Buckling check pull test

Rod	
Input	
Rod diameter, Ø [m]	0,016
Output	
Area moment of inertia, x-axis, I <sub>x</sub> [mm <sup>4</sup> ]	3,22E+03
Area, A [m <sup>2</sup> ]	2,01E-04
Buckling length, L <sub>k,x</sub> [m]	1,5
Area radius of inertia, i <sub>x</sub> [mm]	4,00E+03
Slenderness, λ <sub>k,x</sub> [-]	3,75E-04
Bucklingload, P <sub>k</sub> [kN]	2,96 OK
Plate	
Output	
Area moment of inertia, x-axis, I <sub>x</sub> [mm <sup>4</sup> ]	8,33E+03
Area, A [m <sup>2</sup> ]	0,05
Buckling length, L <sub>k,x</sub> [m]	0,35
Area radius of inertia, i <sub>x</sub> [mm]	4,08E+02
Slenderness, λ <sub>k,x</sub> [-]	8,57E-04
Bucklingload, P <sub>k</sub> [kN]	140,99 OK

## Appendix H. Thixotropy test results

Rutineundersøkelser; Laboratorium for Geoteknikk NTNU				
<b>Prosjekt:</b>	Tiller			
Operatør/Gruppe:	Ulvestad	Borested:	Tiller	
Dato prøvetaking:	25.01.2012	Hull nr:	3	
Dato prøveåpning:	03.05.2012	Prøve nr:	205	
<b>Generell klassifisering:</b>				
Geoteknisk betegnelse:	Leire			
Jordart:	Leire			
Beskrivelse:	Ren og fin prøve.			
Merknader:				
<b>Åpning av prøverør</b>				
Dybde, z:	3,0-3,8 m			
Grunnvannstand	0,5 m			
Lengde av prøve, L:	79,3 cm			
Volum av prøve, 23,2xL	1839,8	cm <sup>3</sup>		
Masse av sylinder m/prøve	5277,1 g			
Masse tom sylinder	1728,9 g			
Masse prøve	3548,2	g		
Midlere densitet, $\rho$	1,9	g/cm <sup>3</sup>		
Midlere tyngdetetthet, $\gamma=\rho \cdot g$	18,9	kN/m <sup>3</sup>		
<b>Konussøk</b>	Test 1	Test 2	Test 3	<b>Prøveinndeling</b>
$s_u$	-	31,9	29,9 kPa	
$s_r$	-	3,3	1,9 kPa	
$s_t$	-	9,7	15,7	
<b>Vanninnhold</b>	Test 1	Test 2	Test 3	
Skål nr	72	86	-	
Tot masse våt	160,16	163,93	-	g
Tot masse tørr	134,65	140,37	-	g
Masse vann	25,51	23,56	-	g
Masse skål	48,87	45,69	-	g
Masse tørr prøve	85,78	94,68	-	g
Vanninnhold	29,7	24,9	-	%
<b>Plastisitetsgrenser</b>	Test 1	Test 2		
Masse beger m/lokk	31,55	30,50	g	
Total masse våt	51,35	57,22	g	
Total masse tørr	46,63	50,01	g	
Masse vann	4,72	7,21	g	
Flytegrense, $w_l$	31,3	37,0	%	
Masse beger m/lokk	31,21	29,10	g	
Total masse våt	41,11	38,50	g	
Total masse tørr	39,41	36,86	g	
Masse vann	1,70	1,64	g	
Rullegrense, $w_p$	20,7	21,1	%	
<b>Rutineparametere</b>				
Plastisitetsindeks: $I_p=w_l-w_p$	10,6	15,8	%	
Flyteindeks: $I_f=(w-w_p)/(w_l-w_p)$	0,9	0,2		

	0
Destroyed	
$V_a$	10
$V_b$	
$V_c$	20
$V_d$	
$V_2 + I_p$	30
$W_1$	
$V_e$	40
$V_f$	
$V_g$	50
$V_h$	
$V_i$	60
$V_j$	
$W_2$	70
$V_3 + I_p$	
	80



Test #	V <sub>d(2)</sub>	V <sub>d</sub>	V <sub>a</sub>	V <sub>b</sub>	V <sub>c</sub>	V <sub>d</sub>	V <sub>e</sub>	V <sub>f</sub>	V <sub>g</sub>	V <sub>h</sub>	V <sub>i</sub>	V <sub>j</sub>	Tid [d]	27	25
S <sub>u,ref</sub> [kPa]	30,2			31,9				27,5					Skål nr	61	61
S <sub>t,ref</sub> [-]	0,0	0,0	13,1	0,0	0,0	9,7	0,0	0,0	0,0	0,0	15,3	0,0	Tot masse våt	78,02	49,07 g
Date t0 [-]	14.mai	14.mai	04.mai	04.mai	04.mai	04.mai	04.mai	04.mai	04.mai	04.mai	04.mai	04.mai	Tot masse tørr	65,38	43,55 g
S <sub>r,t0</sub> [kPa]	4,6	4,6	2,3	2,1	2,4	3,3	2	2,1	2,5	2,1	1,8	1,9	Masse vann	12,64	5,52 g
t1 [days]	2	15	3	7	7	10	17	18	27	25	31		Masse skål	24,48	24,48 g
Date t1 [-]	16.mai	29.mai	07.mai	11.mai	11.mai	14.mai	21.mai	22.mai	31.mai	29.mai	04.jun		Masse tørr prøve	40,90	19,07 g
S <sub>r,t1</sub> [kPa]	8,4	16,7	6,6	8,6	8	8,4	10,8	8,9	9,6	12,3	7,5				
S <sub>r,t0</sub> /S <sub>r,t1</sub> [-]	1,8	3,6	2,9	4,1	3,3	2,5	5,4	4,2	3,8	5,9	4,2		Vanninnhold	30,9	28,9 %